

INSTITUTE OF EXPERIMENTAL PHYSICS  
DEPARTMENT OF PHYSICS  
WARSAW UNIVERSITY



# Analysis of sleep spindles and model of their generation

by

Jarosław Żygierewicz

Advisor

Prof. dr hab. Katarzyna J. Blinowska

A DISSERTATION SUBMITTED IN PARTIAL FULFILLMENT  
OF THE REQUIREMENTS FOR THE DEGREE OF  
DOCTOR OF PHYSICS

APRIL 2000

# Acknowledgements

I am grateful to my advisor Prof. Katarzyna Blinowska,  
for her support through all the work that led to this dissertation and for  
allowing me to taste real academic freedom.

I wish to express my gratefulness to Prof. Waldemar Szelenberger,  
M.D. Wojciech Androsiuk and Ph.D. Szymon Niemcewicz  
from Medical University of Warsaw  
for experimental data, cooperation and help.

I would also like to thank:  
Ph.D. Piotr Franaszczuk  
M.Sc. Piotr Suffczyński  
Ph.D. Piotr Durka  
M.Sc. Dobiesław Ircha  
for fruitful discussions and stimulating ideas.

# Abstract

Analysis of sleep spindles involves their detection and description of their properties. Matching Pursuit (MP) is a time-frequency analysis method that allows for robust, in respect to noise, detection of signal structures (e.g. sleep spindles). The method offers description of properties of detected structures in a natural language. A sleep spindle detector based on MP algorithm was constructed. The detector was validated against human experts scoring and against the criteria of reproducing known facts about sleep spindles properties.

The precise description of detected sleep spindles confirmed the variability in topographical distribution of spectral properties of sleep spindles. The statistical K-means clustering procedure applied for classifying spindles due to their frequency allowed to distinguish two types of sleep spindles. It was found that the two types of sleep spindles differ also in the topographical locations of appearance and in the distributions of intervals between successive occurrences. High time-frequency resolution of the MP algorithm allowed to notice the fine differences between properties of sleep spindles of normal and of insomniac subjects.

A signal analysis in itself gives a limited insight into a system that generates the signal. For the reason a model of sleep spindle generation that produces an output that can be compared with sleep spindles detected in EEG was constructed. The model accounts for the neurophysiological facts known about the system that generates them.

In terms of model parameters, possible explanations of the observed properties of sleep spindles and a possible cause of the fine differences between sleep spindles features of normal and insomniac subjects are given. The model suggests an explanation of the relation between sleep spindles and Slow Wave Activity. The model captures a wide range of experimental facts, some of them not explained by other models. It is computationally efficient and it takes the advantages of models of single neurons and neural masses.

# Contents

<b>Acknowledgements</b>	<b>i</b>
<b>Abstract</b>	<b>ii</b>
<b>List of Figures</b>	<b>iv</b>
<b>1 Introduction</b>	<b>1</b>
1.1 Definition of a sleep spindle . . . . .	1
1.2 Clinical importance of sleep spindles . . . . .	2
1.2.1 Sleep stages and sleep spindles . . . . .	2
1.2.2 Sleep spindles changes with age . . . . .	3
1.2.3 Sleep spindles in pathologies . . . . .	3
1.2.4 Relation of sleep spindles to other rhythms of EEG . .	4
1.2.5 Sleep spindles studies in pharmacology . . . . .	4
1.2.6 The hypothesis of two kinds of sleep spindles . . . . .	5
1.3 Modeling methods . . . . .	5
1.3.1 The problem of scale . . . . .	5
1.3.2 The need of models of EEG . . . . .	6
1.4 Aim of the work . . . . .	9
<b>2 Analysis of sleep spindles . . .</b>	<b>11</b>
2.1 Time-Frequency Parameterization of Time Series - the MP Method . . . . .	11
2.1.1 Adaptive approximations of time series . . . . .	11
2.1.2 Outline of Matching Pursuit algorithm . . . . .	12
2.2 Experimental Data . . . . .	14
2.3 MP-based sleep spindles detection method . . . . .	14
2.3.1 Other sleep spindles detection methods . . . . .	15
2.3.2 Implementation of MP-based sleep spindles detection .	16
2.3.3 Validation of MP-based sleep spindles detection method	17
2.4 Properties of sleep spindles of normal subjects . . . . .	22

2.4.1	Topographic distribution of sleep spindles properties . . . . .	22
2.4.2	Periodicity of sleep spindles occurrence . . . . .	26
2.4.3	Superimposed sleep spindles . . . . .	26
2.5	Sleep spindles in insomnia . . . . .	28
<b>3</b>	<b>Model of sleep spindles generation</b>	<b>32</b>
3.1	Different approaches to modeling of neuronal activity . . . . .	32
3.1.1	Biophysical models of a single neuron . . . . .	32
3.1.2	Distributed versus lumped models of neural network . . . . .	34
3.1.3	Lumped models . . . . .	35
3.2	Physiological bases of models of sleep spindles and mechanisms of their generation . . . . .	38
3.3	Existing models of spindles and similar type of oscillations . . . . .	43
3.3.1	Single neuron models . . . . .	43
3.3.2	Distributed models . . . . .	44
3.3.3	The lumped model . . . . .	45
3.4	The model of sleep spindles generation . . . . .	46
3.4.1	Assumptions . . . . .	46
3.4.2	Structure . . . . .	48
3.5	Results of the model studies . . . . .	52
3.5.1	Mechanisms of spindles generation . . . . .	52
3.5.2	How properties of generated spindles depend on model parameters . . . . .	61
3.5.3	Representation of other behavioral states in the model . . . . .	70
<b>4</b>	<b>Discussion</b>	<b>71</b>
	<b>Summary</b>	<b>77</b>
	<b>Appendices: Formulas and parameters used in the model</b>	<b>78</b>
	<b>A The sigmoid function</b>	<b>79</b>
	<b>B Synaptic currents</b>	<b>80</b>
	<b>C Values of parameters used in TC population</b>	<b>81</b>
	<b>D Values of parameters used in RE population</b>	<b>84</b>
	<b>Bibliography</b>	<b>85</b>
	<b>List of author's papers</b>	<b>94</b>

# List of Figures

1.1	Example of a sleep spindle from human EEG . . . . .	2
1.2	Schematic representation of one sleep cycle with samples of characteristic EEG signals. . . . .	2
2.1	Positions of the EEG electrodes in 10 – 20 standard. (From [53]) . . . . .	14
2.2	Comparison of automatic and visual detection of sleep spindles as a function of threshold amplitude. Presented curve is an average of nine curves describing agreement between automatic detection made by three experts for three episodes of EEG stage 2 sleep; bars indicate mean's error. . . . .	18
2.3	Energy density in time-frequency coordinates (Wigner maps) obtained from MP decomposition of simulated signals. Panels (a) components of simulated signals A - sinusoid, B - Dirac's delta, C, D, E - Gabor functions; $b$ — is a signal composed of structures A, B, C, D, E; $c$ — is a noisy version of $b$ . Panels (b): 3D and 2D Wigner maps of signal $b$ . Panels (c) - 3D and 2D Wigner maps of signal $c$ . . . . .	19
2.4	Time evolution of sleep spindles. A - hypnogram, B - spindles amplitudes, C - spindles/min. At plot B, each bar represents amplitude of one spindle. Blue markers show REM sleep episodes. . . . .	20
2.5	Relation between relative power of sleep spindles (blue) and slow waves (red). The power of each type of activity was averaged over episodes of 5 min. duration. To make the comparison of the curves easier, each of them was transformed by the normal transformation $\tilde{P}(t) = \frac{P(t) - \bar{P}(t)}{\sigma_P}$ and $\min \tilde{P}(t)$ was subtracted. . . . .	21

2.6	Topographic distribution of relation between sleep spindles amplitude and frequency. Each dot corresponds to one spindle. Positions of plots correspond to arrangement of electrodes in 10/20 system. . . . .	23
2.7	Topographical distribution of sleep spindles power spectra. Presented spectra were constructed from waveforms representing spindles, therefore they show sleep spindles power at given frequency, not the energy of whole EEG in the spindles frequency band. . . . .	24
2.8	Topographic representation of relative number of low and high frequency sleep spindles for the group of normal subjects; each bar represents one subject, blue part — fraction of LFS, red part — fraction of HFS. For each subject the distinction between LFS and HFS was based on cluster K-means analysis performed on frequencies of spindles recorded in the Cz channel.	25
2.9	A — auto-correlation of HFS for electrode Pz; B — auto-correlation of LFS calculated for electrode Fz. Horizontal scale in seconds. Grey outlines represent mean's errors. . . . .	26
2.10	Left — fragment of sleep EEG, marked fragment corresponds to structure, identified by the algorithm as a superposition of two sleep spindles. Right — topographic representation of superimposed sleep spindles energy in time-frequency coordinates. . . . .	27
2.11	A — cross-correlation of HFS from electrodes Fz and Pz; B — cross-correlation of HFS from Pz and LFS from Fz. Horizontal scale in seconds. Grey outlines represent mean's errors. . . . .	28
2.12	Normalized histograms of frequencies of sleep spindles weighted by their energy. . . . .	29
2.13	Boxplots of average frequency of HFS for normal and insomniac group of subjects. Each box has lines at the lower quartile, median, and upper quartile values. The whiskers are lines extending from each end of the box to show the extent of the rest of the data. Notches graph a robust estimate of the uncertainty about the means for box to box comparison. . . . .	30
2.14	Histograms of intervals between occurrences of successive sleep spindles. Bars indicate mean relative number of given interval, error bars show standard deviation in a group of subjects. Horizontal scale — seconds. The histograms were normalized in the range 1 – 6 s for each subject. Panel A) — normal group, B) — insomniac. . . . .	31

2.15	Boxplots of average intervals of HFS spindles for normal and insomniac group of subjects. . . . .	31
3.1	Equivalent electric circuit for active membrane . . . . .	34
3.2	Block diagram of a lumped model of interacting excitatory and inhibitory populations. Based on [89]. . . . .	37
3.3	Location of thalamus in a human brain (A) and its anatomical structure (B). Adapted from [47] . . . . .	38
3.4	The scheme of thalamic network in which spindles are generated. Sign ”+” indicates excitatory synaptic connection, ”-” — inhibitory. Adapted from [70] . . . . .	40
3.5	Two pyramidal cells A and B and a distant point P in which we measure the potential. . . . .	41
3.6	Block diagram of the lumped model (based on Lopes da Silva et al. 1974 [15]) for rhythmic activity. The system consists of two populations. TC, main cells with input and output pulse density, respectively $P(t)$ and $E(t)$ , and membrane potential $V_m(t)$ . RE, inhibitory population with membrane potential $V_i(t)$ , and output pulse density $I(t)$ . . . . .	45
3.7	Structure of the model . . . . .	49
3.8	Two mechanisms of spindle initiation. Upper traces: without external noise, lower traces: in the presence of external noise. Blue — membrane potential in TC population, red — in RE population. First marker shows the beginning of a spindle, second maker shows when the other population joins the spindle oscillations. . . . .	53
3.9	Membrane potential in TC population. Top: sequence of two spontaneously generated spindles in case of absence of external noise. Bottom: expanded fragment form the upper trace, initiation of the spindle. . . . .	54
3.10	Upper two traces: $I_{TC}$ and $I_h$ currents during initiation of a spindle (the same as in fig. 3.9) overlaid on the trace of membrane potential (gray). The lower panel: $I_{TC}$ — $I_h$ plane shows the phase relation between $I_{TC}$ and $I_h$ . In the zoom window the oscillatory behavior of the $I_{TC}$ current in the very beginning of a spindle generation is clearly seen. . . . .	55

3.11	Initiation of a spindle in the presence of external noise. a) blue — membrane potential in RE, gray — in TC population (in [mV]); b) input pulse rate for RE population (in [Hz]); c) AMPA synaptic current in RE (in [ $\mu A/cm^2$ ]); d) $I_{TRE}$ current in RE (in [ $\mu A/cm^2$ ]); e) activation variable $m$ of $I_{TRE}$ ; f) inactivation variable $h$ of $I_{TRE}$ ; . . . . .	56
3.12	One cycle of a spindle. Vertical axis in arbitrary units, horizontal axis in [ms]. Panel a) shows traces of membrane potential (red), synaptic current (green), and input pulse rate (blue) in RE neurons; panel b) — the same for TC population. . . . .	57
3.13	Termination of a spindle. a) membrane potential $V_m$ in TC population ([mV]); b) $V_m$ averaged over cycles; c) $I_h$ during spindle ([ $\mu A/cm^2$ ]); d) $I_h$ averaged over cycles; e) slow (red) and fast (blue) activation variables of the $I_h$ current; f) slow (red) and fast (blue) activation variables of the $I_h$ current in the locked form. . . . .	59
3.14	Intra spindle period. Upper set of traces corresponds to conditions without external noise, the lower — in the presence of noise. Trace a) membrane potential in TC; trace b) membrane potential averaged over time of one spindle cycle; c) activation of $I_h$ ; d) activation of $I_{TC}$ . . . . .	60
3.15	Spectral power estimate of representative signal (30 s.) generated by the model with constant time step solver: a) whole frequency range 0 – 50 kHz; b) zoomed to 0 – 2000 Hz. . . . .	62
3.16	Spindle frequency as a function of coupling strength. . . . .	64
3.17	Mechanism of frequency changes with coupling strength. Red — membrane potential in TC, blue — in RE. Panels a) and b) the same $RE \rightarrow TC$ strength, different $TC \rightarrow RE$ ; Panels c) and d) the same $TC \rightarrow RE$ strength, different $RE \rightarrow TC$ . The main difference is in the amplitude of membrane potential in RE and consequently different periods of hyperpolarization of TC. . . . .	65
3.18	Spindle frequency as a function of $I_{LK}$ in TC and RE. . . . .	66
3.19	Mechanism of frequency changes with potassium leakage. Red — membrane potential in TC, blue — in RE. . . . .	67
3.20	Shift in spindle frequency caused by increase in $I_h$ conductance. Dotted lines $\bar{g}_h = 0.2 mS/cm^2$ , solid lines $\bar{g}_h = 0.6 mS/cm^2$ . . . . .	67
3.21	Dependance of intraspindle period duration on coupling strength.	

3.22	Transition from long to short intraspindle periods with increasing input noise. Panel a) — duration of the period; panel b) — autocorrelation based measure of degree of periodicity. . . .	69
3.23	Degree of periodicity as a function of coupling strength. . . .	69
3.24	Modes of the membrane potential oscillations in the model. a) $\alpha$ -like, b) and c) sleep spindles, d) $\delta$ rhythm . . . . .	70

# Chapter 1

## Introduction

### 1.1 Definition of a sleep spindle

Since the beginning of EEG recordings, different kinds of oscillations were observed in the brain electric activity. Among them special attention was paid to "waxing and waning" wave of frequency around 13 Hz. The first commonly accepted definition of that structure — *sleep spindle* — was given by Rechtschaffen and Kales (1968) [65]:

*"The presence of a sleep spindle should not be defined unless it is of at least 0.5sec duration, i.e., one should be able to count 6 or 7 distinct waves within the half-second period. Because the term "sleep spindle" has been widely used in sleep research, this term will be retained. The term should be used only to describe activity between 12 and 14 cps."*

As the knowledge about the phenomena was increasing, the definition evolved and presently most authors agree with M. Steriade [70]:

*"Spindles are the epitome of EEG synchronization at sleep onset. This type of oscillation is defined by the association of two distinct rhythms: the waxing and waning spindle waves at 7-14 Hz with sequences lasting for 1 - 2 seconds, and the periodic recurrence of spindle sequences with a slow rhythm of 0.1 - 0.2 Hz."*

The definition is based on visual analysis of sleep spindles sequences in EEG recordings (in humans) and in recordings from implanted electrodes in animals. An example of a sleep spindle is presented in Figure 1.1

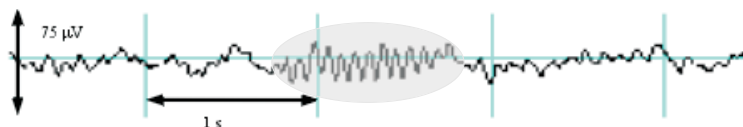


Figure 1.1: Example of a sleep spindle from human EEG

## 1.2 Clinical importance of sleep spindles

### 1.2.1 Sleep stages and sleep spindles

We spend a third part of our life sleeping. Insomnia can cause severe health disturbances, sometimes — even death. The study of electrical brain activity (EEG) can elucidate the mechanisms of sleep, wakefulness and transition between them and can help in understanding the neurophysiological basis of consciousness. Sleep is a dynamic state of an organism. It consists of stages differing in the level of synchrony of neural pools — the higher synchrony is connected with deeper sleep. The stages are grouped in cycles. Each cycle goes from desynchronized (wakefulness or Rapid Eye Movement - REM) brain activity through deeper levels of synchronization (NREM) and back to desynchronized state. This process is schematically shown in fig. 1.2.

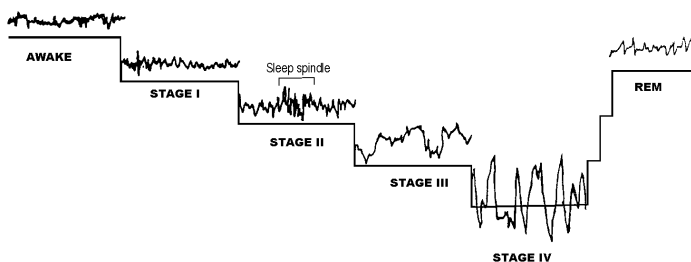


Figure 1.2: Schematic representation of one sleep cycle with samples of characteristic EEG signals.

Sleep spindles and slow waves are the hallmarks of the electroencephalogram during NREM sleep in humans and other mammals. The onset of sleep is connected with appearance of sleep spindles in stage 1, their number increases in stage 2. They are present during all stages except REM. When sleep becomes deeper the amplitude of EEG increases and the frequency of

oscillations decreases. Spindle activity is highest during stage 2 NREM sleep, increases over consecutive NREM – REM sleep cycles, and is reduced after sleep deprivation. Sleep spindle is one of the characteristic transient EEG phenomena. It is easy to recognize, useful for the classification of NREM sleep, particularly to identify stage NREM2 sleep, and to evaluate the degree of arousal. This phenomenon is used in many laboratories to evaluate some aspects of brain function, such as the degree of brain maturity and brain stability [17].

### **1.2.2 Sleep spindles changes with age**

Sleep spindles are present in the sleep EEG from infancy throughout life until old age. Their morphology changes with age reflecting changes in brain connectivity. Spindles develop in humans at 6 weeks after birth at first at low amplitude, gradually increasing in amplitude but especially in duration. Maximum duration is reached at 13 weeks (mean 6 sec.), and then decreases till the end of the first year (mean 1.5 sec.). Many changes observed in the spindle characteristics in the first weeks of life may be related to the development of the dendritic tree of reticular nucleus [44]. The most pronounced effect of age in respect to sleep spindle activity is the reduction of spindle activity in the elderly [64, 39, 86]. The rise of spindle frequency activity (SFA) across consecutive NREM sleep episodes, which is typical for young adults, is not present for the middle-aged men. The sleep-dependent changes of SFA are attenuated or abolished with increasing age. It is not established how the age-related changes in SFA relate to thalamocortical and cortical systems involved in the genesis of sleep spindles [50]. Some clue to the relationship between changes of SFA with age and the condition of brain structures generating them can be found in the fact that there is significant relation between sulcal atrophy and spindle amplitude [39].

### **1.2.3 Sleep spindles in pathologies**

Neurological disorders influence characteristics of sleep spindles. Spindle frequency is reported to be significantly less for patients with generalized epilepsy than for those with partial seizures. It was also found that patients with complex partial seizures significantly differed from those with partial seizures with secondary generalization in distribution of frequencies of spindles. The mechanisms of those changes are not clear. Differences in frequency of spindles may be due to residual medication effects, underlying encephalopathy or physiological differences between partial and generalized epilepsy [24].

Since sleep spindles reflect the activity of sleep-wake control system one could expect relation between parameters of sleep spindles and hypersomnia. Hypersomnia can be defined as excessive daytime sleepiness or prolonged sleep or both [4]. Indeed, it is reported that the average sleep spindle density (number of sleep spindles per unit time) is higher in the hypersomnolent patients, especially those with the idiopathic hypersomnia. At the beginning and at the end of the nocturnal sleep time, sleep spindles density is increased in the hypersomnolent patients compared to normal subjects [8]. In the special case of hypersomnia following paramedian thalamic stroke [4] it was found that this disorder is accompanied by deficient arousal during the day and insufficient spindling and slow wave sleep at night.

#### **1.2.4 Relation of sleep spindles to other rhythms of EEG**

Sleep spindles are just one of the rhythms present in sleep EEG. It is very interesting whether there is any relationship between different rhythms. Especially the relation between sleep spindles activity and slow wave activity SWA has been studied in a number of laboratories. The main conclusion is that an inverse relationship exists between SWA and spindle activity averaged over NREM sleep episode. However, when considered on the fine time scale this relation is more complex. In the initial and final part of NREM sleep episodes the correlation between sleep spindle and SWA is positive, and in the middle part is negative [22, 1, 2, 23]. After sleep deprivation, the transition from a positive to a negative association between SWA and spindle activity occurs at an earlier time after sleep onset [22, 2].

#### **1.2.5 Sleep spindles studies in pharmacology**

From a clinical point of view, the amount and distribution of sleep spindles and relation to other rhythms of EEG can be used to describe changes in the morphology of sleep EEG. The sleep spindles are of particular interest for the pharmacologists working on hypnotics as they may be connected with the mechanism of the transition from sleep to wakefulness. Therefore, the analysis of sleep spindles parameters constitutes an important part of research on the effects of different drugs and hypnotics on a brain [10, 45, 2]. SWA and SFA activity may be generated by common thalamocortical mechanisms. These processes at the neural level may account for the typical time course of SWA and SFA in the sleep EEG.

## 1.2.6 The hypothesis of two kinds of sleep spindles

Whereas in vitro and in vivo studies in animals, sleep spindles are treated as a homogenous group of oscillations within a rather broad frequency band, human studies have yielded evidence for variability and heterogeneity. It has been reported in early studies that "slow" and "fast" spindles show a different topographic distribution. Already Gibbs and Gibbs (1950) [36] observed that 12 Hz spindles showed a slightly more anterior localization than 14 Hz spindles. Further studies confirmed the frequency-specific topographic distribution of spindles [45, 66]. The hypothesis of the independence of two types of spindles was supported in the studies that followed.

Landolt (1996) [50] reported that the age related reduction of SFA did not include the SFA with frequency above 14 Hz. The largest variations of SFA during both the menstrual cycle [25] and pregnancy [11] were present for the faster SFA, above 14 Hz. Melatonin has been recently found to enhance SFA around 14 Hz and to reduce the activity in the frequency band 15-16.5 Hz [23]. Werth (1997) [87] reported the different time-evolution of the high- and low- frequency spindles during the overnight sleep. The sleep spindle power showed a declining trend over consecutive NREM sleep episodes in the low range of spindle frequency activity and a rising trend in the high range. The authors reported also large inter-subject variation in peak frequency compared to intra-subject variations between different electrodes and different recordings. The functional and topographic heterogeneity of sleep spindles in conjunction with the intra-subject stability of their frequency is important features for understanding of the sleep regulation.

## 1.3 Modeling methods

### 1.3.1 The problem of scale

The term "EEG signal" will be often used in this work, so it is worth to consider what the EEG signal is. At the first approximation, one could say EEG is a record of an electrical activity of the brain. Single cell electrical recordings can be either intracellular or extracellular. They reflect the actual output of single neurons. The origins and significance of aggregate recordings such as the EEG are more difficult to determine. The EEG is similar to extracellular single unit recording in the respect that it measures the field potential generated in the space around neurons. The main difference is that EEG recordings represent electrical activity over a wider area of the brain. Typically, EEG signals are recorded from an array of electrodes placed on the scalp. In this sense, one may think of EEG as the average electrical

activity of many neurons over a sizable area. Understanding in detail how extracellular potentials such as EEG are related to the activity of groups of single cells is not a straightforward matter. A neuron can be thought of as a very complex electric circuit obeying Kirchoff's current law. It means that if synaptic current enters the cell at one point (a current sink) it must leak from another (a current source), thereby generating an extracellular current in a volume conductor. Net current measured by an EEG electrode is a superposition of currents generated by all the sinks and sources in the brain. The weights of each source or sink in the total sum are inversely proportional to the distance between the source and the electrode and directly proportional to the total current flow from it [60]. This suggests that the action potentials of individual neurons often make little contribution to the EEG. Because the extracellular currents produced during spike generation are generally small, the greater magnitude of synaptic currents makes contributions that are more significant. Since the EEG represents the averaged electrical activity of many neurons, *the more synchronous is the activity the stronger the signal*. At this point, it could seem that the simplest way to model the EEG is through modeling of all the neurons involved in its generation with particular respect to the synaptic currents. Although it is a tempting idea, it is still impossible to make EEG model in 1:1 scale. To appreciate the size of the problem, let's consider a few numbers characterizing the complexity of the system in question. Human brain contains about  $10^{10}$  neurons, each of them making about  $10^4$  synaptic contacts with other neurons. The density of connections is extremely high — any cortical neuron lies within no more than two or three synapses of any other cortical neuron. Furthermore, the processing of information in the brain seems to run in parallel on a number of spatial scales. These scales are summarized in the Table 1.1.

### 1.3.2 The need of models of EEG

The EEG signal is very complex. The traditional clinical method of EEG analysis is visual inspection of measured voltage time series and spectra. The complexity of EEG signal makes difficult understanding of the processes that generate it. ECG (electrocardiogram) is a good example of signal generated by a system for which proper models of generation have been developed [3, 81, 79]. System that generates that signal is relatively simple. Models describing it increased our understanding of the system and made possible to find parameters that allow diagnosis and construction of better medical equipment e.g. peacemaker based on chaotic models. The need for a new, deeper look at brain activity initiated new areas of research. One area consists of different techniques of imaging of the electrical activity of

Structure	Typical diameter (mm)	Number of Neurons	Description
Minicolumn	$3 * 10^{-2}$	$10^2$	Spatial extend of inhibitory connections
Corticocortical column	$3 * 10^{-1}$	$10^3$ $10^4$	– Width of aborization column of corticocortical afferents, i.e., input scale for specific long-range connections.
Macrocolumn	0.5 – 3.0	$10^5$ $10^6$	– Extend of axon collateral system of single pyramidal cell, i.e., spatial scale for intracortical excitatory output.
Regional scale	50	$10^8$	Average length of corticocortical fibers, i.e., one spatial scale for long range excitatory output; typical scale of cytoarchitectonic (Brodmann) area; EEG must be correlated over area of this size to be measurable on scalp without averaging.
Lobeal scale	170	$10^9$	Ten lobes defined in relation to prominent sulci and gyri; scale of conventional EEG recording methods.
Hemisphere	400	$10^{10}$	Longest corticocortical fibers.

Table 1.1: Spatial scales of human neocortex [61]

the brain. That includes topographic mapping of different parameters like: electric potential, spectral power etc., spatial 3D reconstruction of electrical activity in the brain volume with conjunction in NMR or CT based realistic models of conducting tissues (e.g. [63]). These methods, although generate impressive images and increase our understanding of spatial organization of information processing in the brain do not answer the question of *how* the information is being processed. The functional questions are the scope of models of neural networks and neural masses. The aim is to formulate models based on neurophysiological facts that describe the EEG signal, its properties and generation. If that is achieved, it could indicate how data processing of EEG signals should be further developed. It may lead to definition of appropriate parameters carrying information useful for diagnosis. It could also increase our understanding of how the nervous system processes information and controls behavior. Nervous system is not simply a collection of isolated elementary units, the neurons. It is important to emphasize that neurons are organized in networks, which are, as such, responsible for more or less well defined functional properties. Our present knowledge of this organization depends mainly upon neurohistology, and electrophysiology but it can only advance, if this knowledge is integrated with functional concepts. This problem is complex and very difficult to treat exclusively by experimental methods. Indeed, it is not possible to record simultaneously from all single neurons that form a given structure. Similarly, it is not easy to interpret the field potentials generated by a large group of neurons. In order to make progress in this field it is necessary to develop conceptual models of interaction patterns of neural networks. Therefore, it is necessary to employ both analytical and synthetic methods. The experimental data obtained through histological and physiological analytical methods has to be put together. The aim is to put together the available data in such a way as to form the most likely pattern, which can be conceived. In this way, a model of neurophysiological system can be constructed. Such a model can contribute to advancement of knowledge about the system in two respects:

1. it provides a possibility of testing the influence of different types of inputs, or of changes of some of the properties of the constituting elements, on the output of the system — in this way the model helps in understanding of the systems behavior,
2. it implies the formulation of hypotheses concerning new elementary properties, relationships and overall behavior — it may thus predict new properties of the system, rise new questions and suggest new experiments to explore these hypotheses.

Constructing a model of EEG, we have to consider at which spatial scale we try to describe the system and to which scale our experimental data are relevant.

## 1.4 Aim of the work

Previous sections showed that sleep spindles are interesting phenomena from both practical (clinical, pharmacological, etc.) and purely scientific points of view. The main aim of this work is to analyze the sleep spindles in a comprehensive way. This will be achieved in three steps.

**First, sleep spindles will be analyzed as a phenomena occurring in EEG signal in humans.** In our research, we applied Matching Pursuit (MP) method for detection and parameterization of sleep spindles. High time-frequency resolution of the method allowed to describe spectral properties of sleep spindles with accuracy not available with other methods. We describe topographical distribution of spectral properties of sleep spindles with the highest available frequency resolution.

Precise identification of each sleep spindle makes possible analysis of short and long time range dependances between them and allows to study the reappearance patterns of sleep spindles.

We present the MP based paradigm for characterization of superimposed sleep spindles. The superimposed sleep spindles are phenomena arising when spindles differing in frequency are recorded almost simultaneously. Investigation of these phenomena provides insight into the relation between spindles of different frequencies.

High time-frequency resolution of MP allowed to find fine differences in characteristics of sleep spindles of normal and insomniac subjects.

**Second, a model of sleep spindles generation, on the level of neural populations, will be constructed.** There are two reasons why we construct a new model of sleep spindle generation. First, models reported so far (e.g.[82, 83, 84, 21, 37, 20, 38]) are aimed for explanation of the results of experiments on animals and neuronal tissue slices on the level of single neurons. They mainly deal with the problems of synchronization and propagation of the spindle activity in networks of single neurons. *Our aim is to relate the model output to the EEG signal in humans.* For that reason, we are interested in more global view of spindle activity. Second, distributed models of neural networks are computationally expensive. Since we are interested in study of short

(order of ms) and long range (order of minutes) time dependences in model output, we are looking for ways to simplify and to reduce the model.

The proposed model includes neurophysiological data about intrinsic properties of membranes of neurons building the modeled system. It allows also for direct comparison of parameters measured in EEG with those obtained from simulations.

**Third, the model will be used to explain properties of sleep spindles observed in the EEG signal.**

# Chapter 2

## Analysis of sleep spindles in overnight sleep EEG recordings by means of high resolution time-frequency method

### 2.1 Time-Frequency Parameterization of Time Series - the MP Method

#### 2.1.1 Adaptive approximations of time series

The Matching Pursuit algorithm was developed by Mallat and Zhang (1993) [54]. The method relies on adaptive fitting functions, belonging to the huge set of the waveforms (dictionary), to the signal. The signal is decomposed into time-frequency waveforms called also *time-frequency atoms* in the iterative procedure. Usually Gabor functions, i.e. Gaussian modulated sine waves, are used as basic waveforms due to their optimal time-frequency localization. To the set of Gabor functions, the standard Dirac's and Fourier bases are added. From this ensemble, functions best representing signal's structures are chosen and their weights are computed. The formulas describing basic functions and the Matching Pursuit algorithm, which decomposes the signal into atoms, are given in the next subsection.

The feature, which distinguishes MP from other methods, is the richness of its dictionary, that is — a variety of functions it uses to describe a signal. In Fourier Transform, the dictionary is limited to sine functions, in case of wavelet transform the basic function can be only dilated and translated. In the case of MP, the repertoire of basic functions is very large, which

gives high flexibility in signal structures identification and parameterization. Richer vocabulary allows more precise description of phenomena.

### 2.1.2 Outline of Matching Pursuit algorithm with time-frequency dictionaries of Gabor functions

A large and redundant dictionary of basic waveforms can be generated e.g. by scaling, translating and modulating a single window function  $g(t)$ :

$$g_\gamma(t) = K(\gamma, \phi)e^{-\pi\left(\frac{t-u}{s}\right)^2} \sin(\omega(t-u) + \phi) \quad (2.1)$$

where:  $s$  – scale,

$\omega$  – frequency modulation,

$u$  – translation,

$\phi$  – phase.

$K(\gamma, \phi)$  – is a normalizing constant. Index  $\gamma = (\omega, s, u)$  describes the set of parameters. The window function  $g(t)$  is usually even and its energy is mostly concentrated around  $u$  in time domain with spread proportional to  $s$ . In frequency domain, the energy is mostly concentrated around  $\omega$  with spread proportional to  $\frac{1}{s}$ . The minimum of time and frequency variance product is obtained when  $g(t)$  is Gaussian. The dictionaries of windowed Fourier transform and wavelet transform can be derived as subsets of this dictionary, defined by certain restrictions on the choice of parameters. In case of the windowed Fourier transform, the scale  $s$  is constant – equal to the window length – and the parameters  $\omega$  and  $u$  are uniformly sampled. In the case of wavelet transform the frequency modulation is limited by the restriction on the frequency parameter  $\omega = \frac{\omega_0}{s}$ ,  $\omega_0 = const$ . A comprehensive comparison of different time-frequency analyses methods with special regard to MP is given in Ph.D. Thesis by P.J. Durka [26].

In the first step of the iterative procedure, we choose the vector which gives the largest product with the signal  $f(t)$  :

$$f = \langle f, g_{\gamma_0} \rangle g_{\gamma_0} + R^1 f \quad (2.2)$$

Then the residual vector  $R^1 f$  obtained after approximating  $f$  in the direction  $g_{\gamma_0}$  is decomposed in a similar way. The iterative procedure is repeated on consecutive residues obtained in the following way:

$$R^n f = \langle R^n f, g_{\gamma_n} \rangle g_{\gamma_n} + R^{n+1} f \quad (2.3)$$

In this way the signal  $f$  is decomposed into a sum of time-frequency atoms, chosen to match optimally the signal's residues:

$$f = \sum_{n=0}^m \langle R^n f, g_{\gamma_n} \rangle g_{\gamma_n} + R^{m+1} f \quad (2.4)$$

It was proven by Davis (1994) [16] that the procedure converges to  $f$ , i.e.

$$f = \sum_{n=0}^{\infty} \langle R^n f, g_{\gamma_n} \rangle g_{\gamma_n} \quad (2.5)$$

and

$$\|f\|^2 = \sum_{n=0}^{\infty} |\langle R^n f, g_{\gamma_n} \rangle|^2 \quad (2.6)$$

For visualization of the energy density in time-frequency plane of signal's representation obtained by means of MP we define a magnitude  $Ef(t, \omega)$ :

$$Ef(t, \omega) = \sum_{n=0}^{\infty} |\langle R^n f, g_{\gamma_n} \rangle|^2 Wg_{\gamma_n}(t, \omega) \quad (2.7)$$

where

$$Wg_{\gamma_n}(t, \omega) = \frac{1}{2\pi} \int_{-\infty}^{+\infty} g_{\gamma_n}(t + \tau) \overline{g_{\gamma_n}(t - \tau)} e^{-i\omega\tau} d\tau \quad (2.8)$$

is the Wigner distribution of an atom  $g_{\gamma_n}$ . Wigner distribution of a single atom  $g_{\gamma}$  conserves its energy over the time-frequency space

$$\int_{-\infty}^{+\infty} \int_{-\infty}^{+\infty} Wg_{\gamma}(t, \omega) dt d\omega = \|g_{\gamma}\|^2 = 1 \quad (2.9)$$

Combining this with energy conservation of the MP expansion (2.6) and (2.7) yields

$$\int_{-\infty}^{+\infty} \int_{-\infty}^{+\infty} Ef(t, \omega) dt d\omega = \|f\|^2 \quad (2.10)$$

This justifies the interpretation of  $Ef(t, \omega)$  as the energy density of signal  $f(t)$  in the time-frequency plane. All the presentations in this work referred to as "Wigner maps" are based upon formula (2.7) — except for the fact that the sum is finite. The number of atoms in expansion (2.4), can be chosen individually for each signal based upon mathematical criteria [54] or can be set arbitrary.

## 2.2 Experimental Data

15 healthy controls (mean age:  $40 \text{ SD} \pm 11$ ) and 15 patients (mean age:  $40 \text{ SD} \pm 11$ ) with primary insomnia, meeting DSM-IV criteria were included into the study. Overnight EEG data were recorded<sup>1</sup> during the second night of each subject examination. Data were acquired from standard polysomnographic channels and from 21 EEG derivations, according to the 10–20 system (fig. 2.1). The signal was filtered with an analog bandpass filter (0.15–30 Hz) and then sampled with frequency 128 Hz. Analog-digital 12-bit converter was used. Silver electrodes were applied with collodion. Maximal resistance was 5 k $\Omega$ . Both the visual and numerical analyses were performed on signals referenced to the linked A1–A2 electrodes.

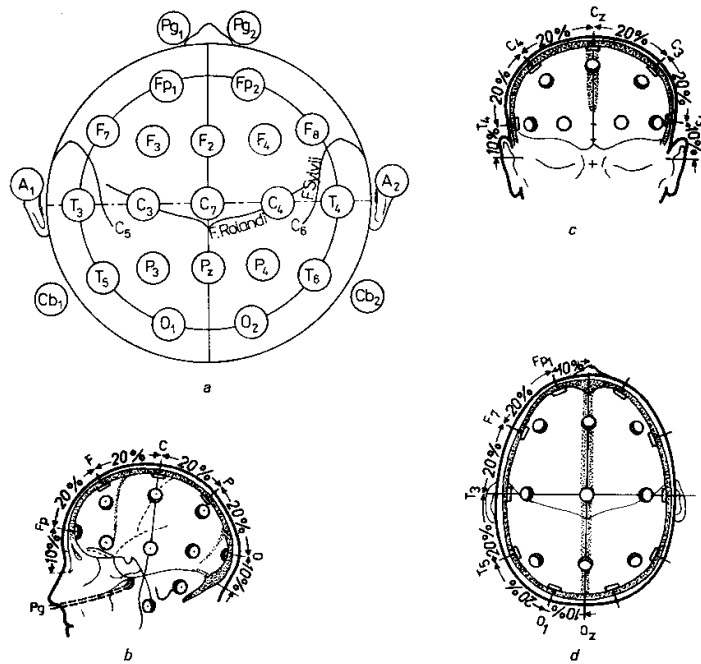


Figure 2.1: Positions of the EEG electrodes in 10 – 20 standard. (From [53])

## 2.3 MP-based sleep spindles detection method

P.J. Durka (1996)[26] proposed the MP paradigm as a general approach to analysis of EEG signals. Sleep spindles detection is a special case in the

<sup>1</sup>All the EEG recordings were done at the Sleep Research Laboratory, Medical University of Warsaw.

MP-based parameterization of signals and analysis method. In this work, we focus on analysis of sleep spindles by means of MP. We extended the application of MP to analysis of:

- time dependencies between sleep spindles of different frequencies occurring almost simultaneously,
- periodicity of spindles occurrences,
- differences between features of sleep spindles of normal and insomniac subjects.

It was shown in a series of papers that the MP-based methods are valid for description and analysis of different types of EEG signals like: transients (e.g. sleep spindles) [31, 96, 30, 92, 94, 77, 93]<sup>a</sup>, [5, 7, 6, 27, 28, 29, 78], epileptic seizures [33, 34, 35] and vibrotactile driving responses [32], [95]<sup>a</sup>.

### 2.3.1 Other sleep spindles detection methods

Visual scoring of sleep spindles in overnight recordings is a laborious and often unreliable task. Therefore several methods for automatic detection of sleep spindles were developed.

Campbell et. al. (1980) [12] reported 65 to 72 % of true positive detections for two phase-locked loop spindles detector systems, devised by Broughton et. al. (1978)[9] and Kumar (1975)[49], as compared to visual scoring and 86 % of concordance between two independent human experts.

Declerck et. al. (1986) [17] reported better performance of software over hardware methods - agreement of more than 90 % with the visual analysis. An important conclusion can be quoted from their paper: “*An exact specification of the criteria used to describe sleep spindles is extremely necessary to be able to compare the results of the different sleep spindles detection methods applied in many laboratories.*”

Jobert et. al. (1992) [45] applied matched filters with 1 Hz frequency resolution. The reported performance was 80% of true positive detections.

Schimicek et. al. (1994) [67] used filtering in 11.5 – 16 Hz frequency band and to the resulting signal applied amplitude ( $> 25 \mu\text{V}$ ) and time span ( $> 0.5$  s) criteria. They achieved average of 90% true positives.

These methods as well as others (Dijk et al., 1993 [22]; Werth et al., 1997 [87]) were specifically tailored to reproduce the human judgment and consent with experts was their only criterion.

### 2.3.2 Implementation of MP-based sleep spindles detection

A sleep spindle according to definition (sec.: 1.1) is a simple time-frequency structure. In this sense, it is perfectly suited for description in language offered by MP method.

The sleep spindles detection method consists of two major steps.

**First step** — the EEG signal must be decomposed into a set of time-frequency atoms (eq. 2.4). The decomposition is done for each EEG channel separately. Consequently, the original signal is represented as a database of simple time-frequency structures. Each structure is described by the following set of parameters:

1. time of occurrence  $\equiv u$ ,
2. frequency  $\equiv \omega$ ,
3. spread in time  $\equiv \frac{s}{f_s}$ ,
4. spread in frequency  $\equiv \frac{f_s}{s}$ ,
5. amplitude  $\equiv 2 \langle R^n f, g_{\gamma_n} \rangle K_{(\gamma, \phi)} / U_0$ ,
6. energy  $\equiv | \langle R^n f, g_{\gamma_n} \rangle |^2$ ,
7. phase  $\equiv \phi$ .

where  $u, \omega, s, \phi, g_{\gamma}, K_{(\gamma, \phi)}$  are defined by equation (2.1),  $R^n f$  is defined by equation (2.3),  $f_s$  is sampling frequency and  $U_0$  is the calibrating constant of an EEG machine. This structured and parameterized representation of EEG (*MP representation*) is well suited for further analysis. In particular this representation is convenient for applying ideas and definitions formed by the tradition of visual EEG analysis.

**Second step** — from the database, structures describing sleep spindles must be selected. The description of sleep spindles (sec. 1.1) can be almost directly applied to construct a filter for sleep spindles selection. *At this point we assumed that a single sleep spindle can be characterized by a single time-frequency structure in the MP representation.* The sleep spindle selection filter consists of the following constraints set upon the time-frequency structures:

1. 11 Hz < frequency of the structure < 15 Hz
2. 0.5 s  $\leq$  time span of the structure  $\leq$  2.5 s
3. amplitude of the structure  $> A_{tr}$ , where  $A_{tr}$  threshold for amplitude.

The first two constraints are obvious – they are given directly by the definition of a sleep spindle. The third constraint is to ensure that the selected structure is not a fluctuation of the background activity.

We used the discrete implementation of the Matching Pursuit algorithm described in section 2.1.2 implemented by Mallat and Zhang ([54]) available in the WWW (ftp://cs.nyu.edu/pub/wave/software/mpp.tar.Z). The discretization was done in a dyadic way by introducing a variable  $j$  – *octave* and *oversampling* –  $l$ . Sampling of each parameter is described in Table 2.1. It is worth to note that time and frequency position of time-frequency atoms can be made arbitrary dense while frequency span and time span of a given atom are bounded by the Heisenberg law (in case of Gabor functions – equality):  $\Delta t * \Delta f = 1$ .

Parameter	Sampling	Range
Frequency	$f_s 2^{-(j+l)}$	$0 - \frac{f_s}{2}$
Time position	$T f_s 2^{-(j+l)}$	$0-T$
Frequency span	$\frac{f_s}{2^j}$	
Time span	$\frac{2^j}{f_s}$	

where:  $f_s$ – EEG signal sampling frequency,  
 $T$ – duration of an epoch of decomposed EEG signal.

Table 2.1: Discretization of MP parameters

### 2.3.3 Validation of MP-based sleep spindles detection method

Here we shortly summarize the evidence that MP is a valid method for detection and analysis of sleep spindles.

In general, there are two types of criteria used for evaluation of new methods. One is concordance of the results obtained by means of a new method with the results obtained by a standard method. In case of EEG analysis, the only method widely accepted as standard is visual inspection of EEG traces by an expert. The other way to test a new method is to reproduce well-known facts.

## Validation against sleep spindles scoring by human expert

The preliminary results of comparison of MP-based spindles detection and human expert scoring based on one night recordings scored by one expert was presented in [91]<sup>a</sup> and [26]. In further studies, we increased the number of experts and the number of EEG recordings on which the comparison was performed. In order to reduce the influence of other types of EEG activity on human experts scoring we decided to perform the comparison only on EEG signal epochs of sleep stage 2. The visual evaluation was performed by three independent experts. Each expert inspected three recordings of stage two sleep. Each recording was obtained from a different subject.

In automatic analysis, the amplitude threshold applied to identify given structure as a sleep spindle was a free parameter and the agreement between automatic and visual analysis was evaluated as a function of that parameter. In fig. 2.2, the concordance between averaged assessment of experts and the automatic method is shown.

The concordance is defined by the following ratio:

$$\frac{\text{number of sleep spindles correctly detected by MP method}}{\text{number of all spindles detected by MP method}}$$

The agreement increases with the increase of amplitude threshold, since the MP method is able to detect spindle-like structures buried in noise (see fig. 2.3 ). For the amplitude threshold of 25  $\mu\text{V}$ , the agreement reaches 90%. For the threshold of 15  $\mu\text{V}$ , the average consent is around 70%, which corresponds to the degree of consent between experts ( $70\pm 8$ )%.

The proposed method gives good agreement with visual analysis for amplitudes of sleep spindles high enough. Moreover, it provides identification of

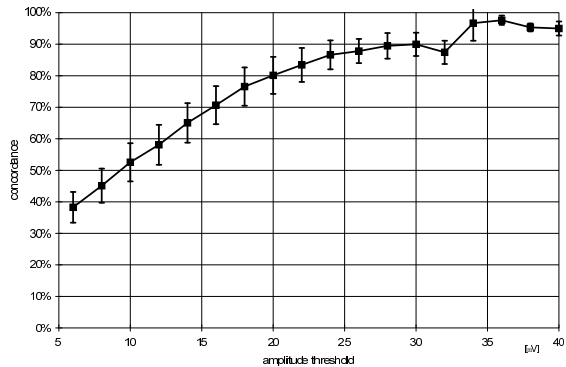


Figure 2.2: Comparison of automatic and visual detection of sleep spindles as a function of threshold amplitude. Presented curve is an average of nine curves describing agreement between automatic detection made by three experts for three episodes of EEG stage 2 sleep; bars indicate mean's error.

sleep spindles buried in noise or very closely spaced in time, surpassing the possibilities of the human judgment.

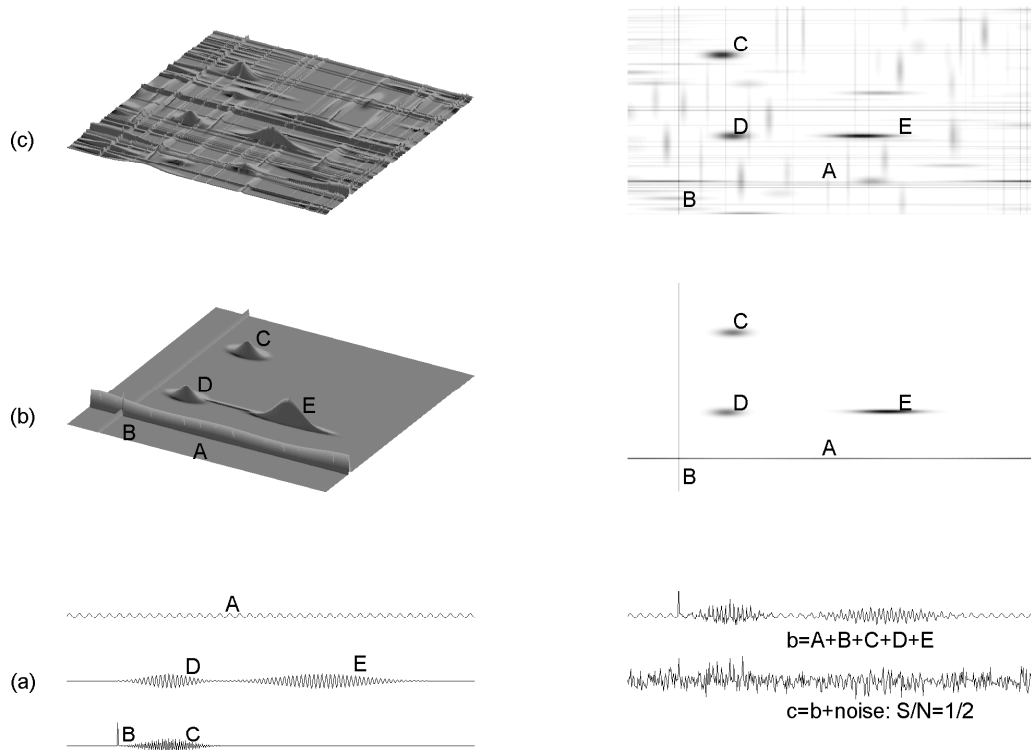


Figure 2.3: Energy density in time-frequency coordinates (Wigner maps) obtained from MP decomposition of simulated signals. Panels (a) components of simulated signals A - sinusoid, B - Dirac's delta, C, D, E - Gabor functions;  $b$  — is a signal composed of structures A, B, C, D, E;  $c$  — is a noisy version of  $b$ . Panels (b): 3D and 2D Wigner maps of signal  $b$ . Panels (c) - 3D and 2D Wigner maps of signal  $c$ .

### Concordance with known facts

**Sleep spindles in REM sleep.** Absence of sleep spindles in REM sleep is a generally recognized fact in visual sleep staging. In fig. 2.4, a typical example of time evolution of sleep spindles during overnight sleep is shown. In panel (B), each sleep spindle is shown as a bar of the height proportional to the amplitude. The number of sleep spindles occurrences per minute (sleep spindles density) is shown below (C). We can see that the spindles density and amplitude of spindles are much smaller in REM than in NREM periods.

The ratio of sleep spindles occurring in REM episodes compared to those occurring in NREM sleep ranges from 0 to 2.4 % with average 0.8% .

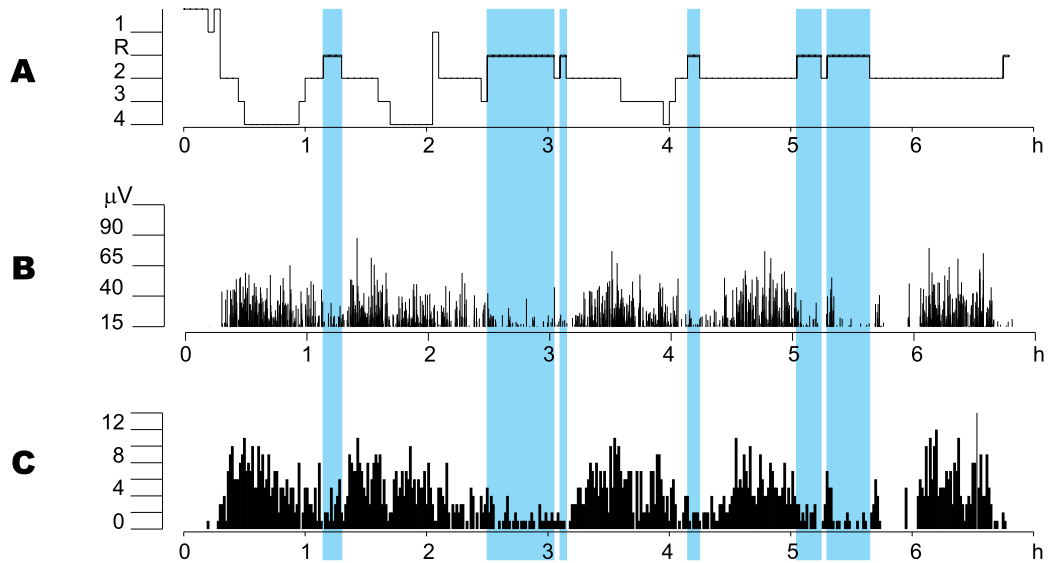


Figure 2.4: Time evolution of sleep spindles. A - hypnogram, B - spindles amplitudes, C - spindles/min. At plot B, each bar represents amplitude of one spindle. Blue markers show REM sleep episodes.

**Relation between sleep spindles and SWA** The SWA activity can be described in the MP-based framework, similarly to sleep spindles. The criteria for classifying time-frequency structures, found in MP decomposition, as slow waves were following: frequency in the range 0.5 – 4 Hz, time span  $> 2$  s., amplitude  $> 75 \mu\text{V}$ . This criteria follow definition of SWA by A. Rechtschaffen and A. Kales(1968)[65].

As was already mentioned in section 1.2.4 sleep spindles and Slow Wave Activity (SWA) form a characteristic pattern, described by Aeschbach et al [2] as: *“The pattern of their [spindles]occurrence during sleep corresponds to a large extend to the pattern of spectral SFA [spindles frequency activity, spectral power density in spindle frequency range](Dijk et al. 1993). Both SWA and SFA rise in the beginning of a NREMS episode and decline priori the transition to REMS (Aeschbach and Borbély 1993). This positive correlation between the two activities reverses to a negative correlation in the middle part of the NREMS episode where SWA exhibits a peak and SFA a trough. This gives rise to a U-shaped time course of SFA that is most prominent in early NREMS episodes. An inversely relationship between SWA and SFA had been recognized previously [...]”*

Figure 2.5 shows typical relation of slow wave power and sleep spindles power in an all-night sleep. The relation follows exactly the above quoted description.

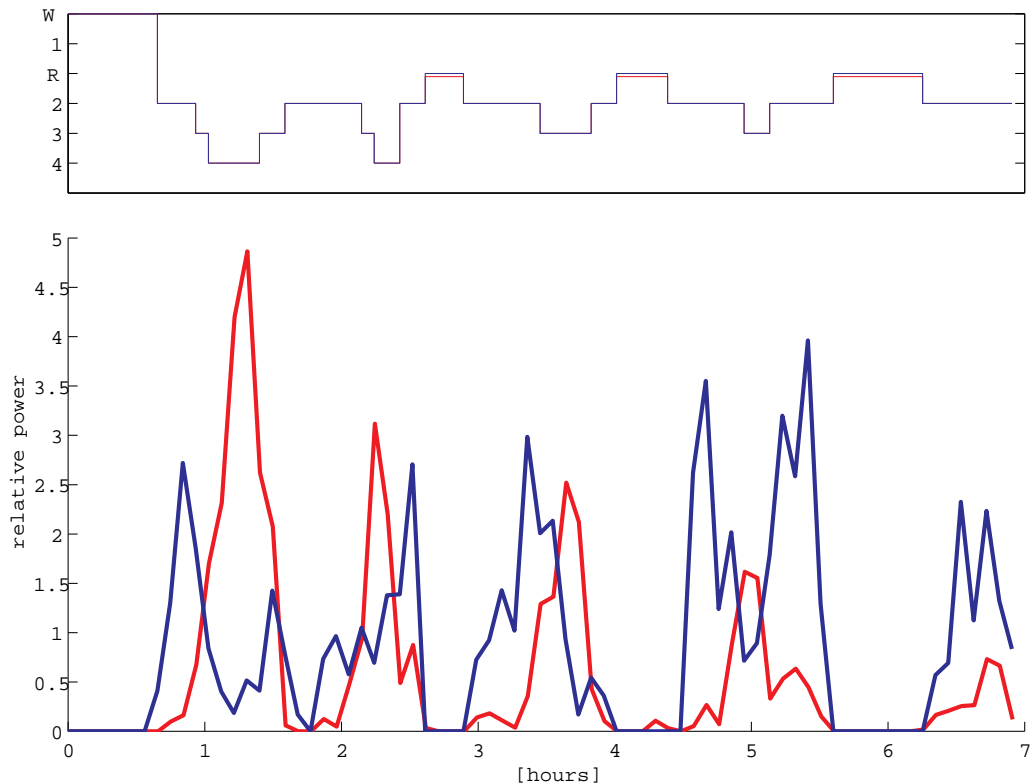


Figure 2.5: Relation between relative power of sleep spindles (blue) and slow waves (red). The power of each type of activity was averaged over episodes of 5 min. duration. To make the comparison of the curves easier, each of them was transformed by the normal transformation  $\tilde{P}(t) = \frac{P(t) - \bar{P}(t)}{\sigma_P}$  and  $\min \tilde{P}(t)$  was subtracted.

## 2.4 Properties of sleep spindles of normal subjects

### 2.4.1 Topographic distribution of sleep spindles properties

In fig. 2.6, the topographic distribution of relation between amplitudes and frequency of sleep spindles is shown. Each dot corresponds to a single sleep spindle. Each plot corresponds to one electrode from 10–20 system. The preponderance of lower frequency sleep spindles in frontal derivations, and preponderance of higher frequency sleep spindles in posterior derivations is clearly visible. We can also observe the decrease of the number and amplitude of sleep spindles toward the temporal electrodes. The same tendency can be observed in fig. 2.7, where the topographic distributions of power spectra of sleep spindles are shown. The power spectra were computed from waveforms representing sleep spindles, therefore the spectra show only power contributed by sleep spindles, not total power at "spindle frequency band". Figures 2.6 and 2.7 were obtained for one typical subject. All investigated subjects revealed similar patterns, only positions of peaks differed slightly.

Based upon these observations we distinguished two groups of sleep spindles: low-frequency spindles (LFS) with frequency around 11 Hz and high frequency spindles (HFS) with frequency around 13 Hz.

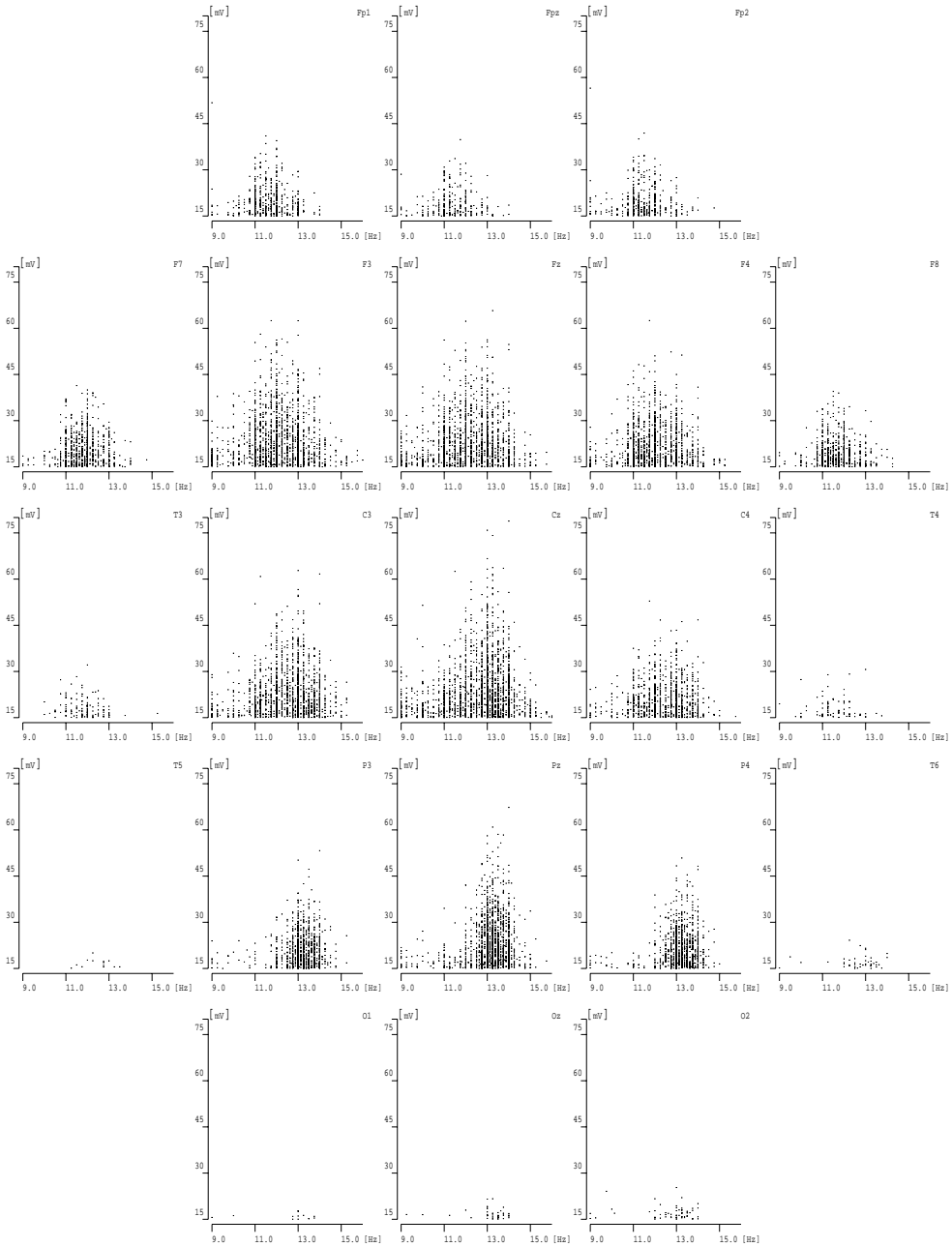


Figure 2.6: Topographic distribution of relation between sleep spindles amplitude and frequency. Each dot corresponds to one spindle. Positions of plots correspond to arrangement of electrodes in 10/20 system.

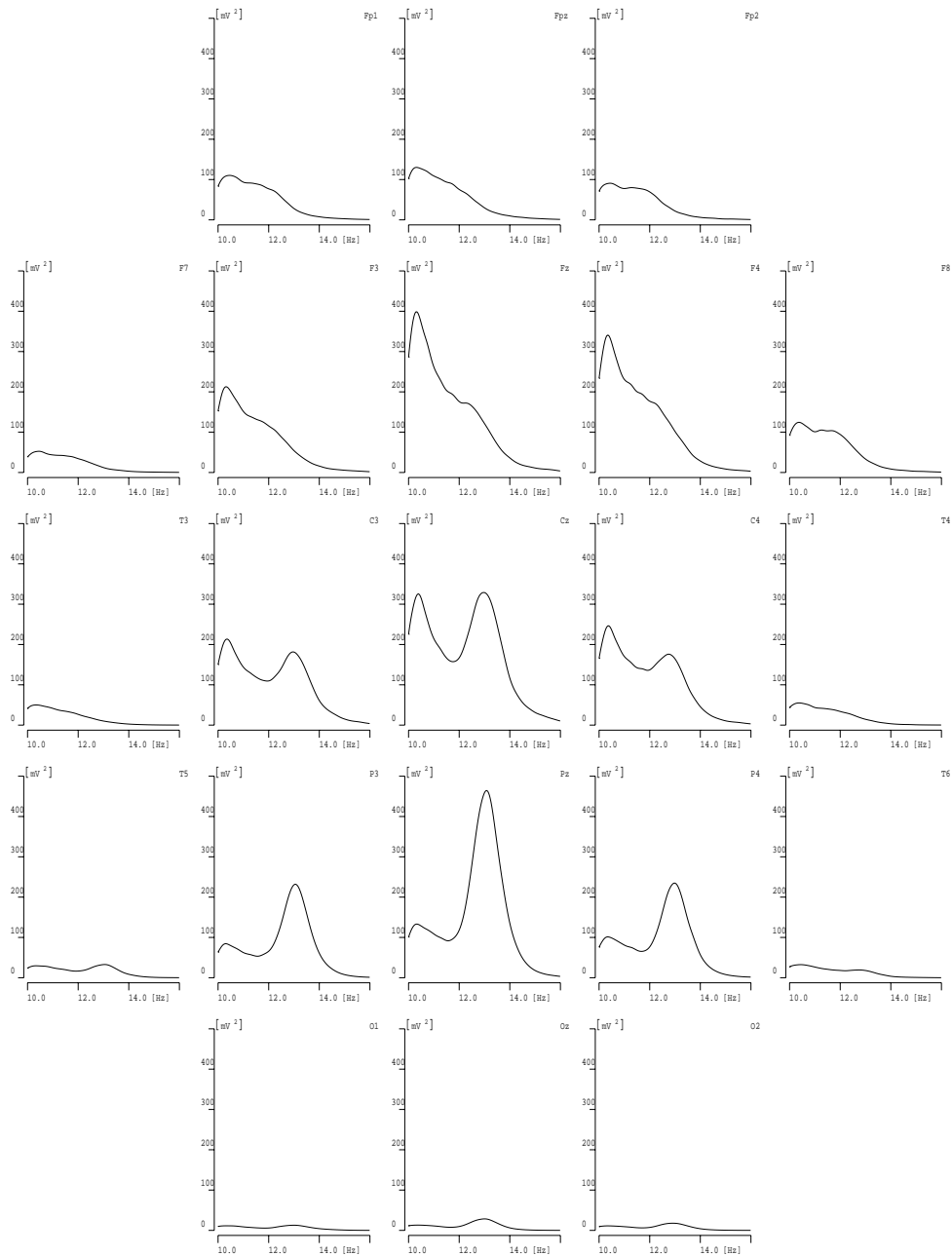


Figure 2.7: Topographical distribution of sleep spindles power spectra. Presented spectra were constructed from waveforms representing spindles, therefore they show sleep spindles power at given frequency, not the energy of whole EEG in the spindles frequency band.

Figure 2.8 shows the topographical distribution of proportion of LFS and HFS for the group of normal subjects. For each subject the classification of spindles as LFS or HFS was based on cluster K-means analysis performed on frequencies of spindles detected in channel Cz. We can observe that LFS are more pronounced in the frontal derivations and HFS in the posterior derivations. We tested the hypothesis that the relative number of HFS, averaged over frontal electrodes (Fp1, Fpz, Fp2, F3, Fz, F4), had the same mean over subjects, as the HFS relative number averaged over posterior electrodes (P3, Pz, P4, O1, Oz, O2). The relative numbers have almost normal distribution so we used one tailed T-test. The hypothesis can be rejected with probability  $p = 3 * 10^{-7}$ .

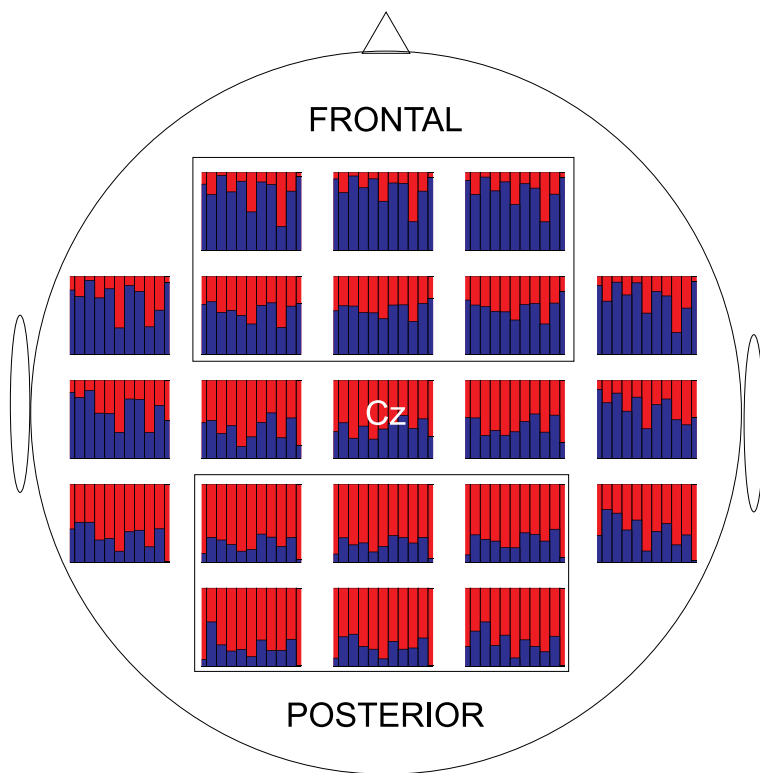


Figure 2.8: Topographic representation of relative number of low and high frequency sleep spindles for the group of normal subjects; each bar represents one subject, blue part — fraction of LFS, red part — fraction of HFS. For each subject the distinction between LFS and HFS was based on cluster K-means analysis performed on frequencies of spindles recorded in the Cz channel.

## 2.4.2 Periodicity of sleep spindles occurrence

We investigated long-term characteristics of generation of sleep spindles by means of autocorrelation function. First, we constructed a signal build of Gaussian envelopes of MP atoms representing sleep spindles detected in a given channel. For channel Fz we constructed a signal representing time series of LFS and for channel Pz a signal representing time series of HFS. In case of HFS, in the autocorrelation functions of all subjects the low frequency rhythmical component was observed (fig. 2.9 A). The average value of the period of sleep spindles reoccurrence was  $(3.9\pm 0.3)$  s. No low frequency rhythmicity was found in case of LFS (fig. 2.9 B).

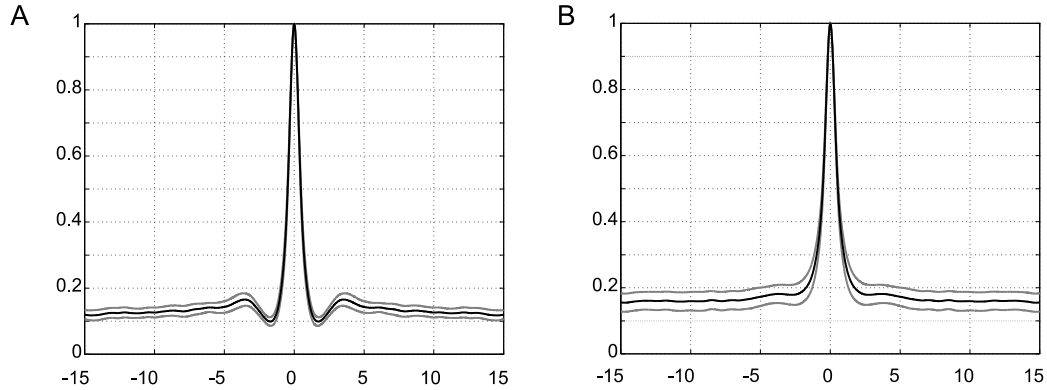


Figure 2.9: A — auto-correlation of HFS for electrode Pz; B — auto-correlation of LFS calculated for electrode Fz. Horizontal scale in seconds. Grey outlines represent mean's errors.

## 2.4.3 Superimposed sleep spindles

A very interesting problem is the existence of superimposed spindles and their relationship to the two types, LFS and HFS, of sleep spindles. MP-based algorithm automatically identifies superimposed spindles. The average ratio of superimposed spindles events to the total number of sleep spindles was found as  $(5\pm 1)\%$ . The time evolution of superimposed sleep spindles was quite similar to the one presented in fig. 2.4 (panels B and C). The MP-based method of signal analysis allows to identify and reconstruct signal components. In the left panel of fig. 2.10, we can see a fragment of EEG with a structure, which was identified as two sleep spindles differing in frequencies by 2.2 Hz and shifted in time by 0.4 s. The fragments of Wigner maps containing both sleep spindles are shown topographically in right panel of fig. 2.10. When

inspecting the illustration from the frontal toward posterior electrodes we can see that the amplitude of the low frequency spindle is decreasing and of the high frequency spindle — increasing. It means that we have one LFS and one HFS occurring almost simultaneously. This observation has encouraged us to investigate the time relationships between occurrences of both types of sleep spindles.

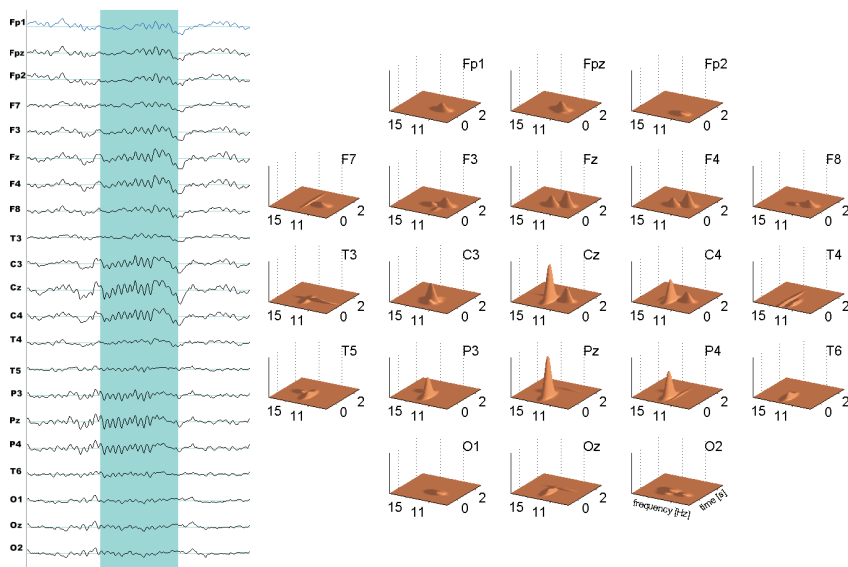


Figure 2.10: Left — fragment of sleep EEG, marked fragment corresponds to structure, identified by the algorithm as a superposition of two sleep spindles. Right — topographic representation of superimposed sleep spindles energy in time-frequency coordinates.

We have calculated auto- and cross-correlation functions for signals constructed from envelopes of each type of sleep spindles. The envelopes of sleep spindles were approximated with Gaussian functions and each signal contained only LFS or HFS for a given derivation. Auto- and cross-correlation functions of signals obtained in that way indicate relation between occurrences of spindles regardless of their frequency. In the cross-correlation between LFS recorded by different electrodes, no time delay was observed; it was also the case for HFS (fig.2.11 A). In both cases, no statistically significant shift of the maximum of the cross-correlation function from zero was present. Sleep spindles of the same type occurred practically simultaneously at different derivations.

The cross-correlation functions of the signal derived from low-frequency

spindles at the electrode Fz and the one derived from high-frequency spindles occurring at the electrode Pz showed a consistent time delay of  $(0.43 \pm 0.06)$  s - HFS preceding LFS (fig.2.11 B). The same tendency of high-frequency spindles occurring before low-frequency spindles was found for superimposed HFS and LFS calculated for the same electrode. In this case, the variance of delays was bigger in the group of subjects, which was related to the fact that for some subjects both kinds of sleep spindles were not always detectable at the same electrode. The above observations indicate that perhaps both hypothetical sleep spindles generators work independently most of the time, but from time to time HFS influences LFS.

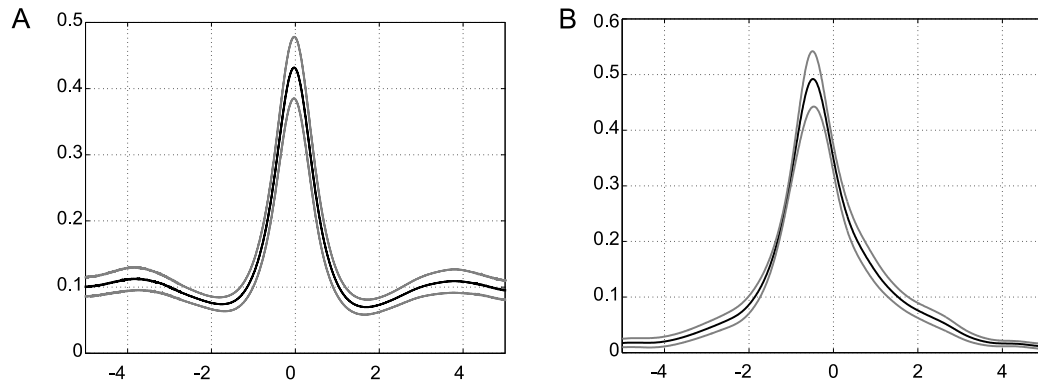


Figure 2.11: A — cross-correlation of HFS from electrodes Fz and Pz; B— cross-correlation of HFS from Pz and LFS from Fz. Horizontal scale in seconds. Grey outlines represent mean's errors.

## 2.5 Sleep spindles in insomnia

We investigated the properties of sleep spindles in a group of insomniac subjects. Especially, we tested the differences between normal and insomniac subjects in average frequency of LFS and HFS type of spindles. We focused the comparison on the three derivations: Fz, Cz and Pz.

In figure 2.12 histograms of frequencies of sleep spindles detected in these derivations are shown. The histograms are weighted by energy of spindles, normalized to 1 and averaged over subjects in each group. The whiskers extending from the bars show standard deviations. We can notice a tendency that HFS (in derivations Cz and Pz) in insomniac subjects are shifted towards higher frequencies.

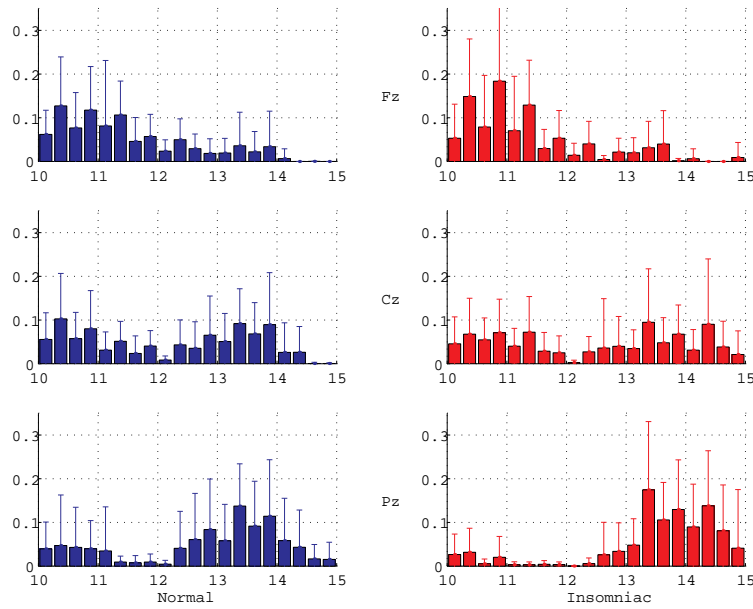


Figure 2.12: Normalized histograms of frequencies of sleep spindles weighted by their energy.

We tested the observation statistically. For each subject separately, mean frequency of spindles belonging to type LFS or HFS in derivations Fz, Cz and Pz was computed. The distribution of resulting variables is almost normal, which allowed to apply the parametric test T. During the first two sleep cycles the frequency of HFS in electrode Cz is, indeed, significantly higher ( $p=0.01$ ) for insomniac than for normal subjects (fig. 2.13).

A close examination of fig. 2.12 reveals, that the biggest difference between histograms for normal and for insomniac subjects relies on the fact that for insomniac subjects we can detect sleep spindles with frequencies above 14.5 Hz in electrode Cz, while for normal subjects we can not. In electrode Pz we can also see a tendency that sleep spindles with frequencies above 14 Hz are stronger in insomniac than in normal subjects, but this difference is not statistically significant.

In the previous section, we described periodic reoccurrence of HFS type of sleep spindles in normal subjects. The same type of periodicity can be noticed for insomniac subjects. We compared the distribution of intervals between successive HFS in these two groups of subjects. The periodicity estimated from the previous section was around 3 – 4 s, thus we focused our comparison in the range 1 – 6 s. The distribution of intervals for normal and insomniac groups are shown in the figure 2.14. We can notice that the

distribution for the normal group has a maximum for slightly longer intervals than for insomniacs.

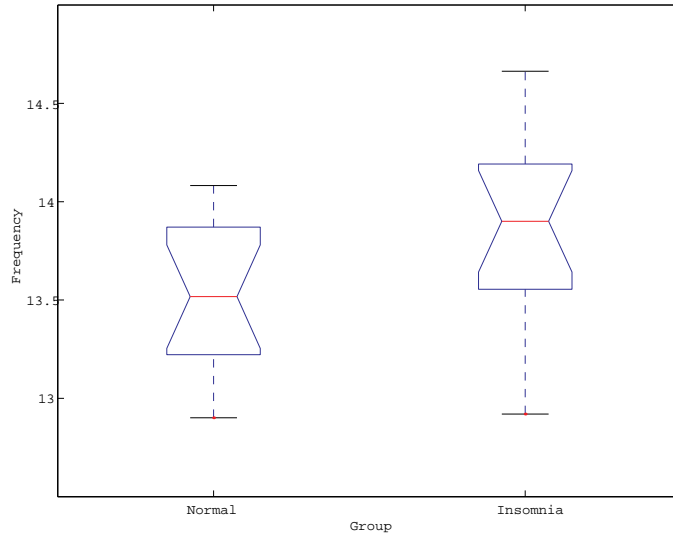


Figure 2.13: Boxplots of average frequency of HFS for normal and insomniac group of subjects. Each box has lines at the lower quartile, median, and upper quartile values. The whiskers are lines extending from each end of the box to show the extent of the rest of the data. Notches graph a robust estimate of the uncertainty about the means for box to box comparison.

In order to validate the observation that in insomniac subjects the period of sleep spindles reoccurrence is shorter we performed T-test. The null hypothesis was that the average interval for normal and insomniac subjects is equal. This hypothesis can be rejected with probability 0.006. Thus we can state that indeed the average interval in insomniac subjects  $(3.5 \pm 0.05)[s]$  is shorter than in normals  $(3.8 \pm 0.08)[s]$  (fig. 2.15).

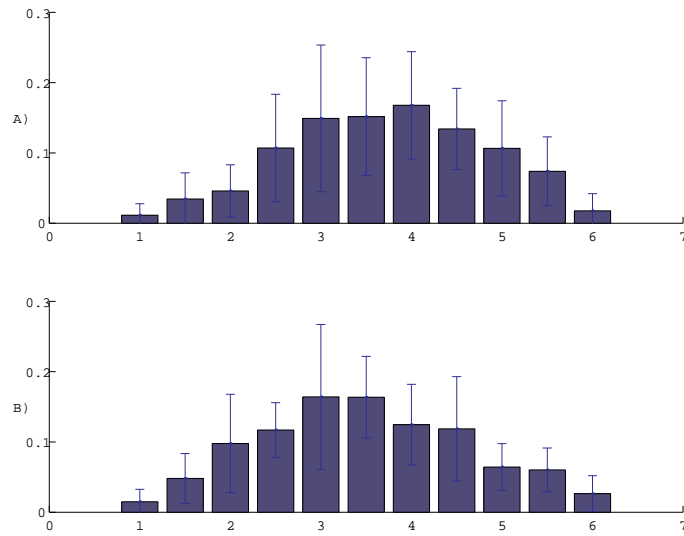


Figure 2.14: Histograms of intervals between occurrences of successive sleep spindles. Bars indicate mean relative number of given interval, error bars show standard deviation in a group of subjects. Horizontal scale — seconds. The histograms were normalized in the range 1 – 6 s for each subject. Panel A) — normal group, B) — insomniac.

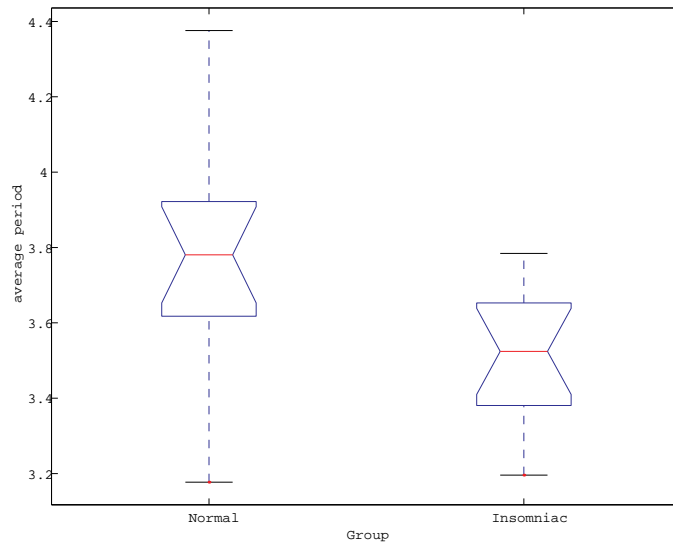


Figure 2.15: Boxplots of average intervals of HFS spindles for normal and insomniac group of subjects.

# Chapter 3

## Model of sleep spindles generation

### 3.1 Different approaches to modeling of neuronal activity

#### 3.1.1 Biophysical models of a single neuron

Biophysical models of electric activity of a single neuron are based on a concept of excitable membrane. A neuron is surrounded by a thin lipid membrane (500 – 700 nm) separating its interior from exterior. There is a difference of electrical potential and ion concentrations across the membrane. The difference of ion concentrations is maintained by active metabolic process — the sodium-potassium pump. The active properties of the neuronal membrane depend on the type of specific ion channels it possesses. The macroscopic membrane conductances arise from the combined effects of a large number of microscopic ion channels embedded in the membrane. Each individual ion channel contains a small number of physical simple units — *gates* that regulate the flow of ions through the channel. An individual gate can be in one of the two states, *permissive* or *non-permissive*. When all of the gates for a particular channel are in the permissive state, ions can pass through the channel and the channel is open. If any of the gates is in non-permissive state, ions do not flow through the channel and the gate is closed. An effective way of describing macroscopic current flow through ion channels in a neuron was introduced by Hodgkin and Huxley [41]. From their experiments followed that the ionic currents are governed by the Ohm law:

$$I_k = \bar{g}_k o_k (V - E_k) \tag{3.1}$$

where:  $o_k$  is the fraction of open channels,  $\bar{g}_k$  is the maximum conductance and  $E_k$  is the apparent equilibrium (*reversal*) potential.  $\bar{g}_k$  is the product of the single-channel conductance and the channel density. The fraction of open channels depends on the probability that the gates are in the permissive state. Gates are divided into two types, usually several gates for *activation* —  $m$  and a single gate for *inactivation* —  $h$ . All activation gates are assumed identical. The transition from one state to the other is governed by the first order kinetic scheme:



where  $\alpha(V)$  and  $\beta(V)$  are voltage dependent rates. The probability of a gate being in open state is thus governed by:

$$\dot{p} = \alpha(V)(1 - p) - \beta(V)p \quad (3.3)$$

Equation 3.3 is often presented in a more intuitive form that describes the rate of approaching the equilibrium:

$$\dot{p} = \frac{p_\infty(V) - p}{\tau(V)} \quad (3.4)$$

where

$$p_\infty(V) = \frac{\alpha(V)}{\alpha(V) + \beta(V)} \quad (3.5)$$

$$\tau(V) = \frac{1}{\alpha(V) + \beta(V)} \quad (3.6)$$

The relative concentration of channels being in open state is:

$$o_k = m^M h \quad (3.7)$$

where M — number of activating gates. The equation 3.1 and 3.7 gives

$$I_k = \bar{g}_k m^M h (V - E_k) \quad (3.8)$$

The simplest model of a neuron is an isopotential compartment with active membrane represented by equivalent electric circuit (fig. 3.1 ):

The electric charge conservation in the circuit gives:

$$C_m \dot{V} = - \sum_k \bar{g}_k m_k^M h_k (V - E_k) \quad (3.9)$$

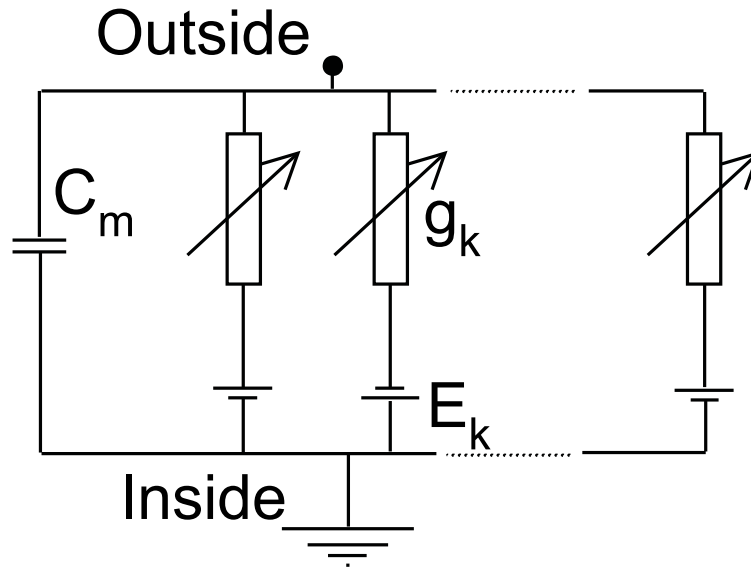


Figure 3.1: Equivalent electric circuit for active membrane

where  $C_m$  — membrane capacitance. The isopotential compartment is a starting point for constructing more accurate and complicated models of real neurons, taking into account very complex geometrical properties such as in the model of Purkinje cell by De Schutter and Bower [68]. That kind of models is beyond the scope of this work.

### 3.1.2 Distributed versus lumped models of neural network

The idea of a distributed model is to describe the dynamics of single neurons by equations of type 3.9, and to connect them in spatially expanded network with architecture possibly close to neurophysiological reality. In fact, even with the tremendous increases in available computing power, no existing computer can practically simulate all that is known about large neural networks, while at the same time no neural structure has yet been described in all its structural details. Thus, the major task in simulating large-scale realistic networks is determining the appropriate modeling approximations. The possible method to manage the problem is to use sparse samples of single cells over a broad area of a real network. However using cells as subsamples of larger tissue area introduces the problem of compensation for the activity of cells not included in the simulation. The problem can be solved in a

number of ways. For example, single-spike nature of single-cell output can be preserved. In this case, the properties of single modeled cells are designed to resemble actual single cells as closely as possible, but synaptic strengths are adjusted to compensate for missing neurons. We shall call this approach a distributed model. Another possibility is that a single cell can represent an average response of a group of cells. In fact, in this case we should rather refer to the object not "a cell" but a population of cells. The output of this population would consist of continuous estimate of spatially averaged activity over a region occupied by that population. We shall call this approach a lumped model.

### 3.1.3 Lumped models

One of the simplest system modeled in a lumped formalism consists of two neuronal populations one excitatory and one inhibitory. We assume that each population behaves homogeneously and the spatial extend of the populations is not important. Following Wilson and Cowan (1972) [88] and Zetterberg at al (1978)[89] we define the variables:

$E(t)$  — which measures the proportion of excitatory cells firing per unit of time at time  $t$ .

$I(t)$  — which measures the proportion of inhibitory cells firing per unit of time at time  $t$ .

The action potentials propagate through axons and reach synaptic contacts where they are transformed into synaptic potentials. The synaptic potentials sum up linearly to form a cell membrane potential, which may cause the cell to fire. The average membrane potentials  $V_e(t)$  of the excitatory population and the average membrane potential of the inhibitory population  $V_i(t)$  may be expressed as follows:

$$V_e(t) = \int_0^\infty [c_1 E(t - \tau) + P(t - \tau)] h_e(\tau) d\tau - \int_0^\infty c_2 I(t - \tau) h_i(\tau) d\tau \quad (3.10)$$

$$V_i(t) = \int_0^\infty [c_3 E(t - \tau) + Q(t - \tau)] h_e(\tau) d\tau - \int_0^\infty c_4 I(t - \tau) h_i(\tau) d\tau \quad (3.11)$$

The constants  $c_1$  and  $c_2$  may be interpreted as the average number of excitatory and inhibitory synapses per excitatory cell and correspondingly  $c_3$  and  $c_4$  are defined for the inhibitory population. We can interpret

$c_1E(t)$  — as the average number of synapses of an excitatory cell that receive an action potential during one time unit from the population itself,

$c_2I(t)$  — from the inhibitory population and

$P(t)$  — is an average number of excitatory pulses from outside per cell and time unit.

Correspondingly are defined  $c_3E(t)$ ,  $c_4I(t)$  and  $Q(t)$ . The functions  $h_e(\tau)$  and  $h_i(\tau)$  are the excitatory and inhibitory postsynaptic potentials, but they may also include attenuation and delay due to pulse transmission and passive spread of postsynaptic potentials. Further, we assume that the fraction  $E(t)$  of excitatory cells that fire during a time unit at time  $t$  is proportional to the probability that the membrane potential of a cell is above a threshold and at the same time it is in an excitatory state, i.e. it should not be in its refractory period. The probability that an excitatory cell is excitable may be written as:

$$1 - \int_{t-r_e}^t E(t')dt' \quad (3.12)$$

where  $r_e$  is the absolute refractory period. It was shown by Wilson and Cowan(1972) [88] that the conditional probability that a cell will fire given that it is in an excitatory state only depends on the average potential in the population that is, for excitatory population on  $V_e(t)$ . As a result

$$E(t) = \lambda_e \left[ 1 - \int_{t-r_e}^t E(t')dt' \right] f(V_e(t)) \quad (3.13)$$

and analogously

$$I(t) = \lambda_i \left[ 1 - \int_{t-r_i}^t I(t')dt' \right] f(V_i(t)) \quad (3.14)$$

The constants  $\lambda_e$  and  $\lambda_i$  measure the maximum average firing rate of a cell in each of the two populations. The function  $f(x)$  must be monotonically increasing from 0 to 1 — usually  $f$  is a sigmoid curve. If we investigate network behavior at frequencies present in the EEG then the refractory periods are much shorter than the characteristic time constant of the entire network.

Thus we can substitute the integrals in equations 3.13 and 3.14 by  $r_e E(t)$  and  $r_i I(t)$  respectively. We obtain that :

$$E(t) = \frac{\lambda_e f(V_e(t))}{1 + \lambda_e r_e f(V_e(t))} \equiv \lambda_e g_e(V_e(t)) \quad (3.15)$$

$$I(t) = \frac{\lambda_i f(V_i(t))}{1 + \lambda_i r_i f(V_i(t))} \equiv \lambda_i g_i(V_i(t)) \quad (3.16)$$

The new functions  $g_e(x)$  and  $g_i(x)$  also have a sigmoid shape but with less slope than  $f(x)$ . It is worth to notice that the presence of the refractory period can be taken into account through a transformation of the nonlinear function from  $f(x)$  into either  $g_e(x)$  or  $g_i(x)$ . The resulting model of two interacting populations one excitatory and one inhibitory is depicted as a block diagram in fig. 3.2.

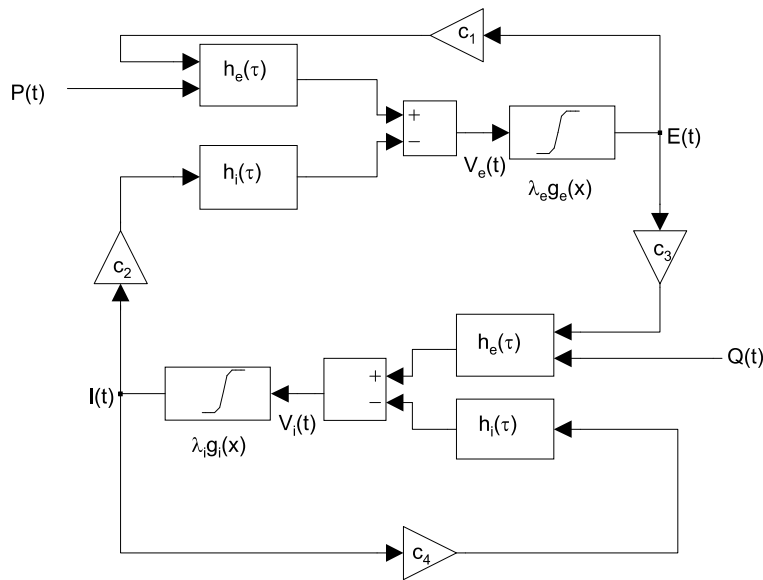


Figure 3.2: Block diagram of a lumped model of interacting excitatory and inhibitory populations. Based on [89].

## 3.2 Physiological bases of models of sleep spindles and mechanisms of their generation

Sleep spindles, as well as many other rhythms present in EEG signal are the effect of synchronous oscillations of large number of neurons. With sufficient level of synchronization their summed field potentials become large enough to be recorded with electrodes over the scalp. The phenomena of sleep spindles were observed for a long time but only since 1980 some understanding of how they are produced and what kind of activity they reflect has been gained. Many details of the intrinsic neuronal properties and network synchronization underlying spindle oscillation are already known. Most of this knowledge derives from experimental studies in cats and ferrets. These species were chosen for electrophysiological investigations of spindles because organization of sleep cycles is similar, EEG spindles are similarly shaped, and the anatomical features of structures generating them are similar in cats, ferrets and humans.

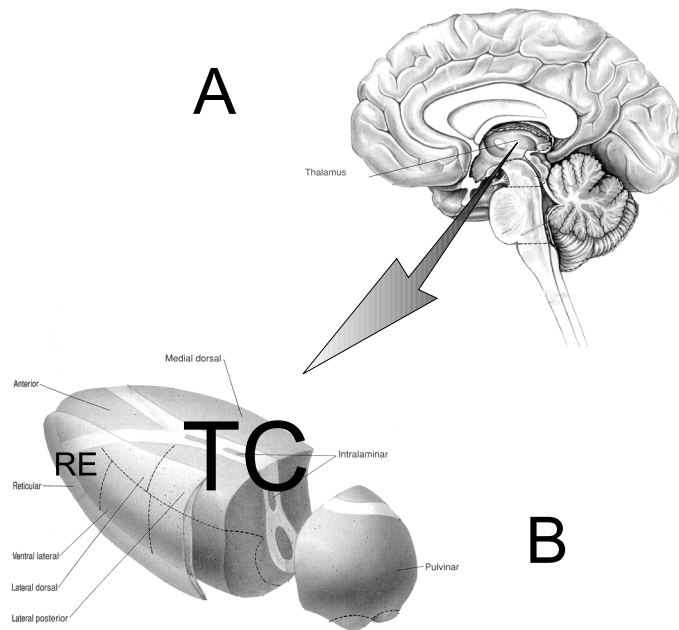


Figure 3.3: Location of thalamus in a human brain (A) and its anatomical structure (B). Adapted from [47] .

Spindles are produced within the thalamus (fig.3.3). This was first demon-

strated by Morison and Bassett (1945) [58] who showed that such waves are still recordable in the thalamus even after total decortication and high brainstem transection. Thalamic spindles survive even more radical procedures involving the removal of the striatum and rhinencephalon [80]. The most important role in spindle generation is played by two kinds of neurons: thalamocortical (TC) and neurons of reticular (RE) nucleus. The RE nucleus is a thin sheet of GABAergic neurons that covers the rostral, lateral, and ventral surfaces of the thalamus [46] (fig. 3.3 B). Its major inputs arise in the thalamus, cerebral cortex, rostral part of the brainstem, and basal forebrain. The output of RE neurons is mostly directed to the dorsal thalamus and, subsidiarily, to the rostral brainstem, but not to the cerebral cortex. Spindling is absent in the parts of the thalamus devoid of RE afferences [62]. The cells belonging to the RE nucleus are interconnected not only by their axons but also through their dendrites, which contain synaptic vesicles releasing GABA. The significance of dendrodendritic linkages is related to the possibility of synchronization of spindle oscillation through the peacemaking RE nucleus, with the consequence of synchronization of the whole thalamus. The axons of the RE cells have as their main target the TC neurons. Their dendrites make synaptic contacts with the axons of the TC cells. Thus, the TC and RE cells form a feedback loop as is schematically shown in fig. 3.4. RE neurons contain GABA as a transmitter. This implies that the feedback of the RE on the TC neurons is GABAergic and thus inhibitory.

Many experiments both in vitro and in vivo elucidated the specific properties of the thalamic circuit connectivity and intrinsic properties of neurons that make spindle generation possible.

The TC cells display two different types of response depending mainly on the polarization of their membrane.

1. If the membrane is hyperpolarized for time long enough, the TC cells at the removal of hyperpolarization generate a low threshold calcium spike. Too short period of hyperpolarization does not allow for unblocking  $Ca^{2+}$  channels, so there would be no response of TC cells. The bursts represent an intrinsic property of thalamic cells, due to a special conductance that is inactive at the resting membrane potential (around -60mV) or at more depolarized levels, but becomes ready to be activated when the membrane potential is hyperpolarized by about 7-15 mV, which is the case of thalamocortical neurons during sleep with EEG synchronization. High-frequency spike bursts, consisting of fast sodium action potentials, are triggered by a slow spike that occurs much below the usual firing threshold - so called LTS (low-threshold spike).
2. If the membrane is depolarized — the response is tonic firing.

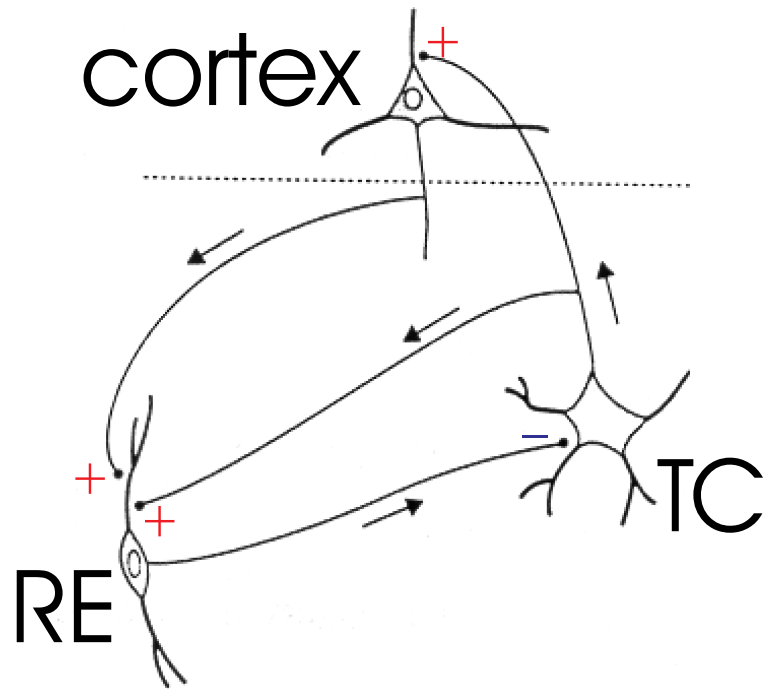


Figure 3.4: The scheme of thalamic network in which spindles are generated. Sign "+" indicates excitatory synaptic connection, "-" — inhibitory. Adapted from [70]

RE neurons also display a similar two modal behavior but in somewhat different range of membrane voltages.

Activation of a single RE cell results in a rebound burst of action potentials in TC neurons and a return barrage of EPSPs. A burst of action potentials in a single TC neuron results in a burst of action potentials in a RE cell and the generation of feedback IPSPs in TC cell.

The propagation of activity in monosynaptic loop consisting of TC and RE follows the scenario: excitation of single RE cell leads to generation of a  $Ca^{2+}$  spike. After delay of order of 100 ms, there is a clear response in TC population. Evoked  $Ca^{2+}$  spike in TC cell causes, with delay of order of 20ms, excitation of RE population. Those delays are of the correct order for the system to resonate at frequency close to 10 Hz.

It is known [70, 56] that :

1. Spindle oscillations are generated in the RE—TC network;
2. RE neurons impose synchronous inhibitory postsynaptic potentials

(IPSPs) onto thalamocortical cells.

3. TC cells transfer postinhibitory rebound bursts to RE neurons where they produce excitatory postsynaptic potentials (EPSPs), closing the negative feedback loop.
4. TC cells also transfer postinhibitory rebound bursts to the cerebral cortex, where they elicit EPSPs and spike discharges. *If the EPSPs are synchronized enough, they can sum up to the potential level high enough to be picked up by the EEG electrodes on the scalp as a sleep spindle.*
5. The cortical neurons give excitatory feedback to both RE and TC populations.

We shall discuss issue pointed out in (4). The cortex is build of 5 – 6 layers of neurons. The biggest contribution to EEG comes from pyramidal neurons. The pyramidal neurons are mostly parallel to each other and perpendicular to the surfaces of the layers. Their cell bodies are elongated with excitatory synaptic tree at one of the ends (fig 3.5).

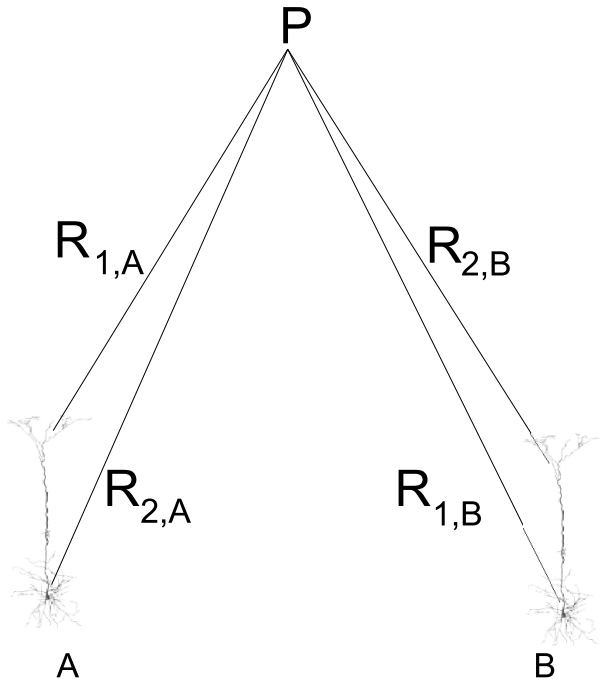


Figure 3.5: Two pyramidal cells A and B and a distant point P in which we measure the potential.

Due to charge conservation law, current flowing into a neuron through synapses must leak from the neuron at some distant locations. Thus at first approximation a pyramidal neuron can be thought of as a current dipole. Suppose, we measure an electric potential at a distant point  $P$  generated by  $M$  pyramidal neurons oscillating with frequencies  $\omega_i$ . The potential  $\Phi_P(t)$  is [60]:

$$\Phi_P(t) = \frac{1}{4\pi\sigma} \sum_{i=1}^M \left[ \frac{I_i}{R_{1,i}} \cos(\omega_i t + \alpha_i) - \frac{I_i}{R_{2,i}} \cos(\omega_i t + \alpha_i) \right] \quad (3.17)$$

where  $I_i$  are the amplitudes of current for each dipole, and we have assumed that all current flowing from a source returns to the same dipole;  $\alpha_i$  are phases;  $\sigma$  is the electric conductivity of a mass of tissue.

Let's assume that the distance between  $P$  and the dipoles —  $R$  is much larger than the effective pole separation  $d \ll R$  and  $R_i \approx R$ . Then the effect, of large number —  $M$  — of dipoles with roughly equal amplitudes and equal frequencies, on the potential at point  $P$  —  $\Phi_P$  — can be estimated in two extreme cases:

1) when the neurons are synchronous the terms in the sum 3.17 add up directly so

$$\Phi_P(t) \approx \frac{M}{4\pi\sigma} \frac{Id}{R^2} \cos(\omega t + \alpha) \quad (3.18)$$

so amplitude of  $\Phi_P$ :

$$|\Phi_P| \sim M \quad (3.19)$$

2) when the neurons are asynchronous — the phases are random

$$\Phi_P(t) \approx \frac{1}{4\pi\sigma} \frac{Id}{R^2} \sum_{i=1}^M \cos(\omega t + \alpha_i) \quad (3.20)$$

Let  $x_i$  be random variable with uniform distribution over  $\langle -\pi, \pi \rangle$  then  $y_i = \cos(x_i)$  is a random variable with mean  $\mu_y = 0$  and a nonzero variance  $\sigma_y^2 \neq 0$

then from central limit theorem for

$$S = \sum_{i=1}^M \cos(x_i)$$

we have the expected value  $E(S) = 0$  and variance  $\sigma_S^2 = M\sigma_y^2$ .

Thus amplitude of  $\Phi_P$  in eq. 3.20 due to fluctuations can be estimated as proportional to standard deviation of  $\sum_{i=1}^M \cos(\omega t + \alpha_i)$ :

$$|\Phi_P| \sim \sqrt{M} \quad (3.21)$$

To illustrate the role of synchronous neurons in EEG generation let us consider the following example given by Nunez(1985) [60]. If there are  $s$  synchronous and  $a$  asynchronous generators oscillating with similar amplitudes and located at similar distances from the recording electrode then relative contribution of the synchronous to asynchronous generators is of order  $s/\sqrt{a}$ . The typical EEG electrode measures activity of a mass of neurons of order  $10^8$ . Suppose, that 1% of that mass oscillates synchronously. Then the contribution to the scalp potential of the synchronous pool of neurons is  $(10^6/\sqrt{10^8 - 10^6})$  100 times bigger than that of the 99% of asynchronous neurons. *In practice, it means that in scalp EEG we can measure only the activity of synchronously oscillating neuronal pools.*

### 3.3 Existing models of spindles and similar type of oscillations

As was already mentioned, electrical activity in a brain can be characterized on multiple spatial scales. For some scales and some aspects of sleep spindles generation and dynamics appropriate models already exist.

#### 3.3.1 Single neuron models

At present, most neuroscientists agree that sleep spindles are generated in networks of TC (thalamocortical) and RE (reticular thalamic nucleus) neurons. Over the past few years a number of mathematical models of thalamic neurons have been published that successfully mimicked one or more features of thalamic relay cells, including the generation of low-threshold  $Ca^{2+}$  spikes, the generation of tonic single spike firing on depolarization and slow-frequency rhythm behavior in hyperpolarization. McCormick and Huguenard (1992) [57] analyzed a complex model of a thalamic relay neuron. They included and determined the role of many different ionic currents present in a TC neuron. The results of their simulations show that the various  $K^+$  currents in these neurons contribute to the repolarization of  $Na^+$  and

low-threshold  $Ca^{2+}$  spikes, control the temporal characteristics of repetitive firing, and generate an apparent rectification of the neuron at resting membrane potentials. The intrinsic ionic currents  $I_T$  —  $Ca^{2+}$  current which can be activated at resting membrane potential only after a period of hyperpolarization, during which it becomes "ready to be activated" — and  $I_h$  — mixed  $Na^+$  and  $K^+$  current which is activated in hyperpolarization — are critically involved in rhythmic low-threshold  $Ca^{2+}$  spike generation, which also depends critically on the status of the *leak* conductance that determine the membrane potential and apparent input resistance of the cell.

Wang and Rinzel (1994) [84] showed that the minimal model capable of intrinsic oscillation in the spindle frequency (7–14 Hz) and delta frequency (0.5–4 Hz) ranges involves only interplay between  $I_T$  and  $I_h$ .

Destexhe et al. (1994) [21] proposed a model of RE cell including low-threshold  $Ca^{2+}$  current and two other currents depending on intracellular concentration of  $Ca^{2+}$  ions. The modeled cells exhibited intrinsic bursting properties similar to those observed in vivo.

Wang and Rinzel (1993) [83] and Golomb et al. (1994) [37] proposed a simplified version of RE cell model. The minimal set of currents consisted of  $I_T$  and a simple passive *leak* current, which accounted for non-simulated specific currents.

### 3.3.2 Distributed models

Most of recently published models related to sleep spindles could be classified as distributed ones. New experimental results were the inspiration for modelers. In 1987, Steriade et al.[73] described rhythmic bursts in isolated RE nucleus in vivo, similar to those recorded during spindling, and suggested RE nucleus as a peacemaker of spindle activity. A series of papers ([82, 83, 84, 21, 37]) showed that the oscillations depend on the rebound excitability of RE cells due to the  $I_T$  current and mutual inhibition of RE nucleus cells. The important factors for synchronizing the network oscillation were the duration of synaptic currents time constants and the range and density of synaptic coupling. This kind of oscillations seems to be important only in the isolated RE nucleus. Golomb et al. (1994)[37] showed that when connected to TC population the RE network could oscillate synchronously even without the coupling between RE neurons. Another question that was investigated by means of models, was the mechanisms of synchronization and propagation of spindle like oscillations in TC-RE networks ([20, 38]). The mechanism of recruiting new cells into the oscillation at each oscillation cycle is proposed as the explanation of observed in extracellular and EEG recordings "waxing" of sleep spindles. So far, there is no agreement on the mechanisms of "waning".

### 3.3.3 The lumped model

The lumped formalism description of thalamocortical system and oscillations generated in it was developed and analyzed by Lopes da Silva's group ([90], [15], [14]). It is a model of interacting excitatory and inhibitory populations, similar to the one described in section 3.1.3. The development of the lumped model in analytical terms includes translating the properties of the discrete network of neurons into a system such as depicted in Figure 3.6.

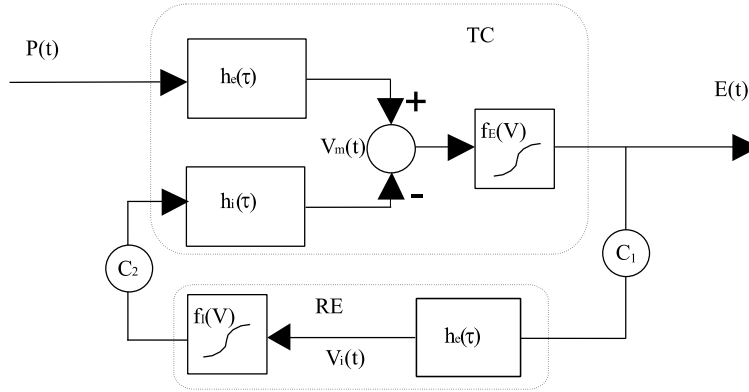


Figure 3.6: Block diagram of the lumped model (based on Lopes da Silva et al. 1974 [15]) for rhythmic activity. The system consists of two populations. TC, main cells with input and output pulse density, respectively  $P(t)$  and  $E(t)$ , and membrane potential  $V_m(t)$ . RE, inhibitory population with membrane potential  $V_i(t)$ , and output pulse density  $I(t)$ .

In this model, the excitatory population is identified as the thalamocortical relay nucleus — TC and an inhibitory population as the reticular thalamic nucleus — RE. The two sigmoid functions  $f_E(V)$  and  $f_I(V)$  play a crucial role. They represent the distribution of thresholds within the population. The value of  $V_m(t)$  is assumed to be proportional to the EEG. Thus, the model was constructed in the scale that is relevant for comparison with the EEG measurement. The system analysis of the model allowed for conclusion that the peak frequency of  $V_m(t)$  oscillations will increase and the bandwidth decrease with an increase of the coupling constants,  $C_1$  and  $C_2$ .

Recently the model was successfully extended to explain event related dynamics of alpha rhythm [76].

## 3.4 The model of sleep spindles generation

### 3.4.1 Assumptions

The model consists of two main neuronal populations in the thalamus: thalamocortical relay nucleus (TC) and thalamic reticular nucleus (RE). The objective of this model is to reproduce the characteristics of the oscillations of mean value of membrane potential in the TC population during sleep and to investigate the relation between those characteristics and a set of model parameters. In particular, it is aimed to show possible explanation for different frequencies of sleep spindles recorded at topographically different EEG derivations (the LFS and HFS type of spindles described in previous chapter), and to investigate the mechanisms of waxing and waning of a sleep spindle and of periodical reappearance of sleep spindles (Why HFS are periodical and LFS not?).

The model is based on the following assumptions:

1. We observe the oscillations of thalamic populations indirectly in the scalp EEG signal. The signal in which we are interested is a result of oscillation of currents in cortical pyramidal neurons driven via thalamocortical projections by oscillating TC populations. That allows to assume that average membrane potential in TC population is proportional to specific components of EEG signal.
2. The substantial contribution to EEG signal comes only from those cortical neurons, which are synchronized over a sizable area. It was shown in section 3.2 that a signal measurable on the EEG level is generated only by the synchronized pools of neurons.
3. From (1) and (2) it follows that, if we want to compare the model results with data derived from scalp EEG we can limit the model only to the synchronously oscillating thalamic neurons.
4. The electric activity of a neuron can be divided into two classes: *slow* potentials and *fast* potentials. *Slow* are these that synchronize easily due to the fact that their duration is relatively long compared to the possible delays between their occurrence in different neurons. For example membrane potential due to postsynaptic currents and intrinsic slow dynamic currents are slow potentials. *Fast* are those that have very little chance to occur simultaneously due to their short duration - these are e.g. action potentials.

5. The population is homogenous in respect to the intrinsic membrane properties.
6. The slow activity of the synchronized part of a homogeneous neural population can be approximated by the dynamics of the slow activity of a single representative neuron. Physiological evidence for that is provided by the work of Mountcastle [59] and Hubel and Wiesel [42, 43]. Their findings indicate that within relatively small volumes of cortical tissue there exist many cells with very nearly identical responses to identical stimuli. If we assume that membrane potential of a certain representative neuron is  $V(t)$  than the membrane potential of an  $i$ -th neuron can be expressed as

$$V_i(t) = V(t + \delta_i) + \varepsilon_i(t) \quad (3.22)$$

Where  $\delta_i$  is a small delay of the stimuli in  $i$ -th neuron in respect to the representative neuron, and  $\varepsilon_i(t)$  is a difference between the responses of the  $i$ -th neuron and the representative one. We shall assume that  $\varepsilon_i(t)$  at a given time  $t$  is normally random distributed with mean 0. The expansion of  $V(t + \delta_i)$  is

$$V(t + \delta_i) = V(t) + \delta_i \dot{V}(t) + \dots \quad (3.23)$$

And

$$\langle \varepsilon_i(t) \rangle_i = 0 \quad (3.24)$$

That gives the first order approximation of an average membrane potential

$$\langle V_i(t) \rangle_i \approx V(t) + \langle \delta_i \rangle_i \dot{V}(t) \quad (3.25)$$

For slow activity  $\dot{V}(t) \approx 0$  so the second part of equation (3.25) can be neglected. Thus in linear approximation we have:

$$\langle V_i(t) \rangle_i \approx V(t) \quad (3.26)$$

7. It was shown in section 3.1.3 that the fast activity (action potentials) can be modeled as a sigmoid function that relates the average membrane potential to the average firing rate. The shape of the function describes the distribution of individual neurons thresholds for firing action potentials. The sigmoid shape of the voltage-to-pulse conversion function also accounts for the refractory periods of action potential generation (eq. 3.15 and 3.16).

### 3.4.2 Structure

The structure of the model is depicted in Figure 3.7. The structure is based on the works of Lopes da Silva et al. [90], [15], [14] with one major difference. It accounts for the various intrinsic currents present in the neurons of TC and RE populations that play the crucial role in the system behavior. Another difference, but of lesser importance, is that the synaptic transfer functions convert the presynaptic pulse rate into postsynaptic currents instead of postsynaptic potential.

The populations interact with each other by means of pulse densities. The TC population generates excitatory pulse density  $E(t)$ . As was shown in section 3.1.3 pulse density of a population can be related to the average potential in a population. Analogously to eq. 3.15 we write:

$$E(t) = \lambda_{TC} g_{TC}(V_{TC}(t)) \quad (3.27)$$

Similarly pulse density generated by RE population —  $I(t)$  is:

$$I(t) = \lambda_{RE} g_{RE}(V_{RE}(t)) \quad (3.28)$$

In the above equations  $g_{TC}$  and  $g_{RE}$  are sigmoidal functions and  $\lambda_{TC}$  and  $\lambda_{RE}$  are maximal pulse densities. The formulas for functions and values of parameters are given in Appendix A.

The pulses generated in one population are transformed by the synapses of neurons in the other population into synaptic currents.

$$I_{GABA_{TC}}(t) = \int_0^\infty C_1 I(t - \tau) h_{GABA}(\tau) d\tau \quad (3.29)$$

$$I_{AMPA_{TC}}(t) = \int_0^\infty N(t - \tau) h_{AMPA}(\tau) d\tau \quad (3.30)$$

$$I_{AMPA_{RE}}(t) = \int_0^\infty C_2 E(t - \tau) h_{AMPA}(\tau) d\tau \quad (3.31)$$

where

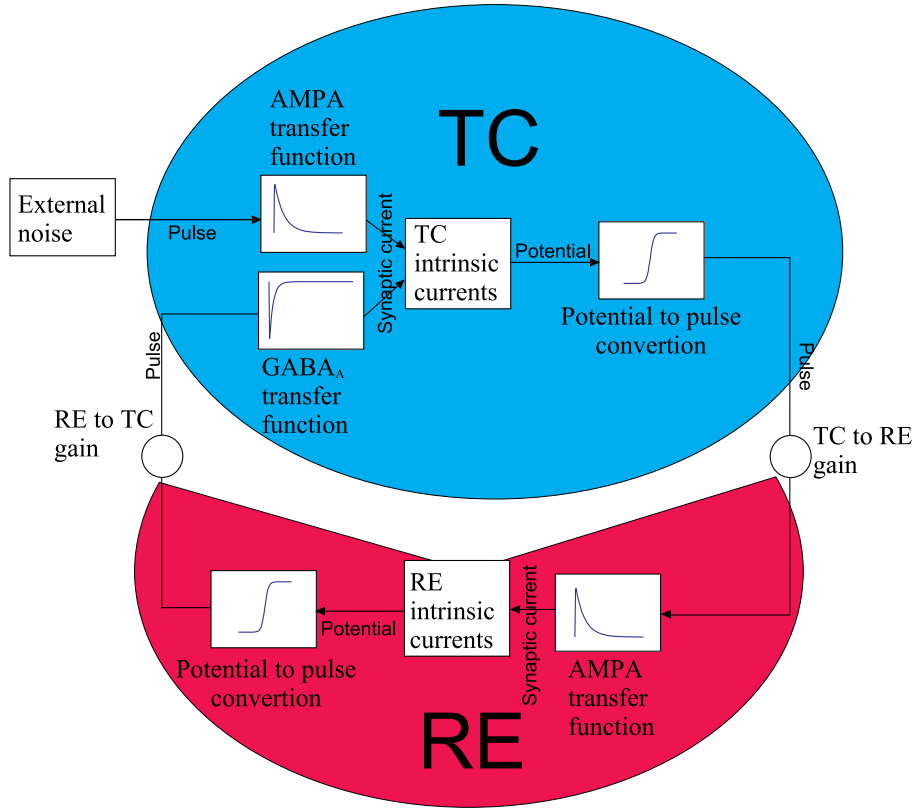


Figure 3.7: Structure of the model

$I_{GABA_{TC}}(t)$ ,  $I_{AMPA_{TC}}(t)$  are average synaptic currents from GABA and AMPA synapses in a TC neuron respectively,  $I_{AMPA_{RE}}(t)$  is an average current from AMPA synapses in a RE neuron;

$C_1$  is an average number of GABAergic synapses in a TC neuron receiving pulses from RE population;

$C_2$  is an average number of AMPA synapses in a RE neuron receiving pulses from TC population;

$N(t)$  is pulse density of input from other structures, that are not included in the model.

$h_{GABA}$  and  $h_{AMPA}$  are the synaptic transfer functions.

The synaptic currents contribute to the slow changes of membrane potential. The other contribution to the slow changes of membrane potential comes

form those intrinsic membrane currents, which are characterized by relatively slow dynamics. Considering these currents is the main difference between the model proposed here and that developed by Lopes da Silva et. al. [90, 15, 14]. According to assumption (6) the average membrane potential of each population is given by equation of the same form as in single cell models with slowly changing currents included only. Some parameters of the single cell models are adjusted to account for the fact that effects present in a single cell may be enhanced or diminished when viewed from the level of population.

Average membrane potentials in TC and RE population respectively are:

$$C_m \dot{V}_{TC} = -I_{LTC} - I_{TTC} - I_h - I_{GABA_{TC}} - I_{AMPA_{TC}} \quad (3.32)$$

$$C_m \dot{V}_{RE} = -I_{LRE} - I_{TRE} - I_{K(Ca)} - I_{CAN} - I_{AMPA_{RE}} \quad (3.33)$$

where:

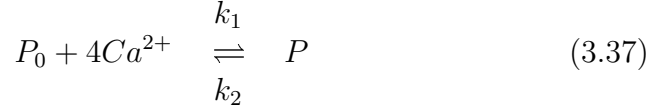
$I_{LTC}$  — **Leak current** is divided into two parts. The first one is nonspecific leakage with reversal potential  $E_{LTC}$  and fixed conductance  $g_{LTC}$ . The second one is potassium leakage with the reversal potential  $E_{LKTC}$  and the conductance  $g_{LKTC}$  which can be influenced by neuromodulators and thus is a model parameter.

$$I_{LTC} = g_{LTC}(V - E_{LTC}) + g_{LKTC}(V - E_{LKTC}) \quad (3.34)$$

$I_{TTC}$  — **Low threshold calcium current** We modeled low threshold calcium current as proposed by Wang et al. (1991) [85] and used by Destexhe et al. (1993) [19]

$$I_{TTC} = g_{TTC} m^3 h (V - E_T) \quad (3.35)$$

$I_h$  — **Hyperpolarization activated current** Destexhe and Babloyantz (1993) [18] proposed a model of hyperpolarization activated current that had two activating variables *slow*  $S$  and *fast*  $F$ . This model successfully accounted for voltage clamp data that indicated simple kinetics with considerably different time of activation and deactivation. The analogous current described in sino-atrial cells by Hagiwara and Irisawa (1989) [40] exhibited strong dependence on  $[Ca^{2+}]$ . Destexhe et al. (1996) [20] proposed kinetic scheme of indirect regulation of  $I_h$  by calcium. It was assumed that  $Ca^{2+}$  binds to a regulating factor ( $P$ ) which itself binds to the open ( $O$ ) form of the channel and blocks its transition to the closed form ( $C$ ).



where:

$P_0, P$  — unbound and calcium-bound forms of regulating factor,  
 $C, O, O_L$  — closed, open, open-locked states of a channel,

The current is proportional to the relative concentration of the open channels with the conductance of the locked state being twice of the unbound open state.

$$I_h = g_h(S_1 + 2S_2)(F_1 + 2F_2)(V - E_h) \quad (3.39)$$

where:

$S_1, S_2$  — open unbound and locked slow gates,  
 $F_1, F_2$  — open unbound and locked fast gates,  
 $g_h$  —  $I_h$  conductance,

$I_{LRE}$  — **passive leakage current.** Leakage is divided into two parts. The first one is nonspecific leakage with reversal potential  $E_{LRE}$  and fixed conductance  $g_{LRE}$ . The second one is potassium leakage with the reversal potential  $E_{LKRE}$  and the conductance  $g_{LKRE}$  which can be influenced by neuromodulators and thus is a model parameter.

$$I_{LRE} = g_{LRE}(V - E_{LRE}) + g_{LKRE}(V - E_{LKRE}) \quad (3.40)$$

$I_{TRE}$  — **Low threshold calcium current.**

$$I_{TRE} = g_{TRE}m^2h(V - E_T) \quad (3.41)$$

$I_{K(Ca)}$  — **Calcium dependent potassium current.**

$$I_{K(Ca)} = g_{K(Ca)}m^2(V - E_{K(Ca)}) \quad (3.42)$$

$I_{CAN}$  — **Calcium dependent nonspecific cation current**

$$I_{CAN} = g_{CAN}m^2(V - E_{CAN}) \quad (3.43)$$

Currents  $I_{TRE}$ ,  $I_{K(Ca)}$ ,  $I_{CAN}$  in equation 3.33 are based on a model developed by Destexhe et al. 1994 [21].

Values of all parameters are given in appendices.

## 3.5 Results of the model studies

### 3.5.1 Mechanisms of spindles generation

The model described in previous section was implemented in Matlab Simulink and subjected to a number of simulations that allow to determine the mechanisms of initiation, generation and termination of a sleep spindle.

There are two possible mechanisms for initiation of a sleep spindle. Depending on the input noise level a spindle can begin as an oscillation of membrane potential in RE or TC population (fig. 3.8).

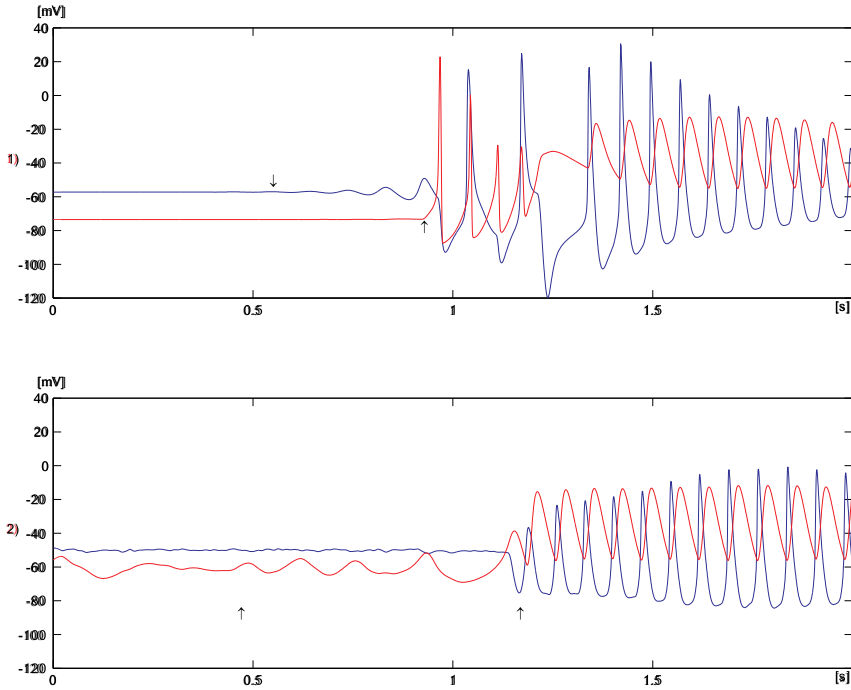


Figure 3.8: Two mechanisms of spindle initiation. Upper traces: without external noise, lower traces: in the presence of external noise. Blue — membrane potential in TC population, red — in RE population. First marker shows the beginning of a spindle, second marker shows when the other population joins the spindle oscillations.

### Mechanisms of spindle initiation in the absence of noise

In the absence of the external noise, the resting potential in TC population monotonically decreases in the intraspindle period. At certain value (around  $-57$  mV) the  $I_{TTC}$  current becomes oscillatory and causes membrane potential to oscillate (fig. 3.9 and 3.10 ).

In the hyperpolarizing phase of the oscillations  $I_h$  current activates and adds up to the depolarizing phase. After a few subthreshold oscillations the interplay between  $I_{TTC}$  and  $I_h$  current (fig. 3.10) increases the amplitude to the threshold for generation of action potentials.

Burst of action potentials — in the model represented by increase in the pulse density — in the TC population, causes a rebound burst in the RE

population. That burst, in turn, induces inhibitory postsynaptic potentials in TC population. The depth and length of hyperpolarization of TC cells by IPSP is enough to remove inactivation of the  $I_{TC}$  current and activate the  $I_h$  current. Now,  $I_h$  rises the membrane potential to the level at which low threshold calcium spike is generated. On top of the LTS, a burst of action potentials is generated and the cycle repeats — a spindle is initiated.

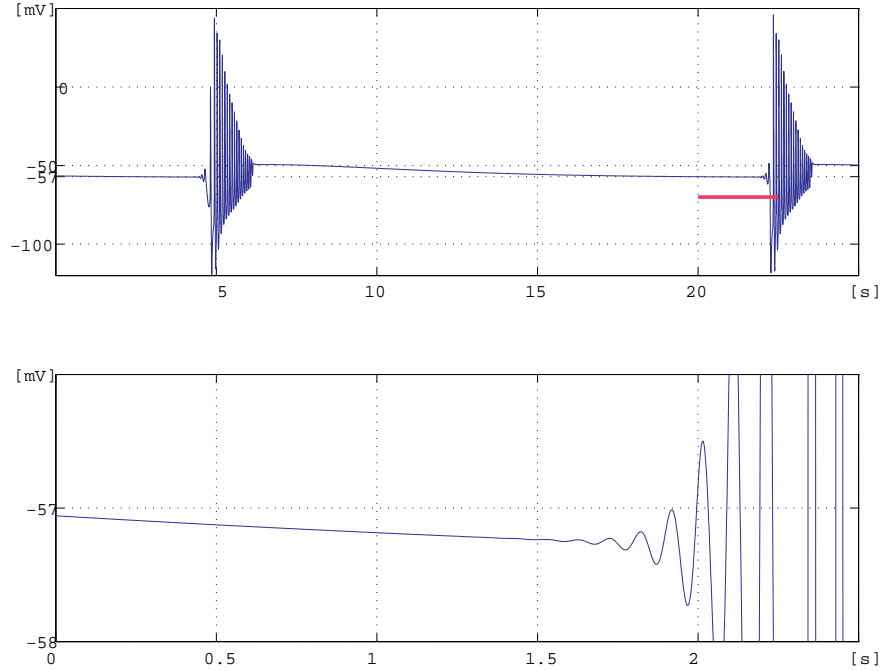


Figure 3.9: Membrane potential in TC population. Top: sequence of two spontaneously generated spindles in case of absence of external noise. Bottom: expanded fragment from the upper trace, initiation of the spindle.

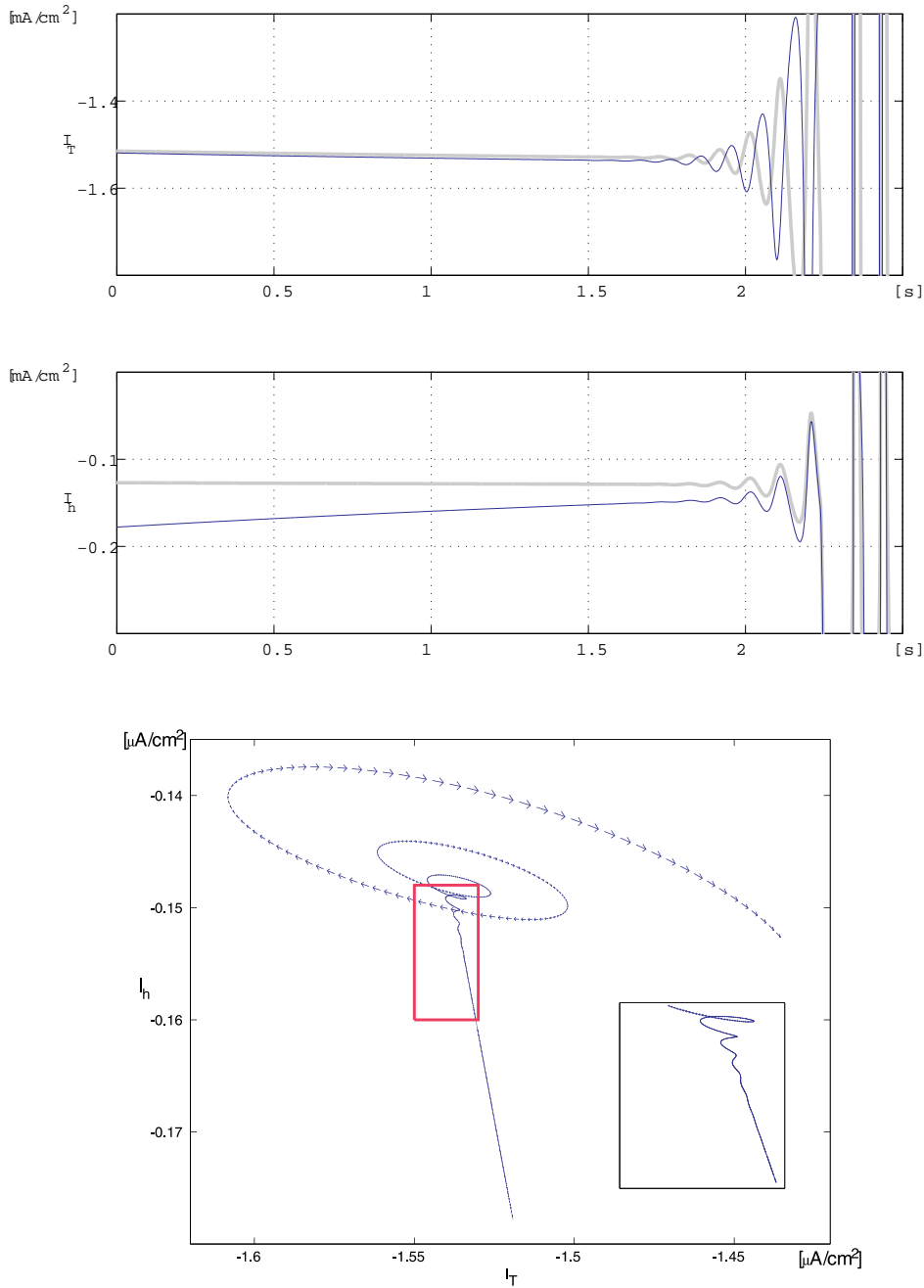


Figure 3.10: Upper two traces:  $I_{TTC}$  and  $I_h$  currents during initiation of a spindle (the same as in fig. 3.9) overlaid on the trace of membrane potential (gray). The lower panel:  $I_{TTC} - I_h$  plane shows the phase relation between  $I_{TTC}$  and  $I_h$ . In the zoom window the oscillatory behavior of the  $I_{TTC}$  current in the very beginning of a spindle generation is clearly seen.

## Mechanisms of spindle initiation in the presence of noise

In the presence of the external noise, the fact that in the range of membrane potential around -65 mV the RE membrane is highly excitable becomes crucial. As in the previous case, during the intra spindle period membrane potential in both — RE and TC — populations decreases. When membrane potential in RE population drops to about -65 mV, channels of  $I_{T_{RE}}$  current, present in RE cells' membrane, are ready to be activated and a small excitatory input from TC population is enough to activate  $I_{T_{RE}}$  and induce an LTS in RE neurons. The burst of action potentials generated on top of the LTS is enough to hyperpolarize TC neurons through GABAergic inhibitory synapses. This hyperpolarization leads to removal of inactivation of  $I_{T_{TC}}$  and activation of the  $I_h$  which results in the rebound burst in TC population (fig. 3.11). In this way, a spindle is initiated.

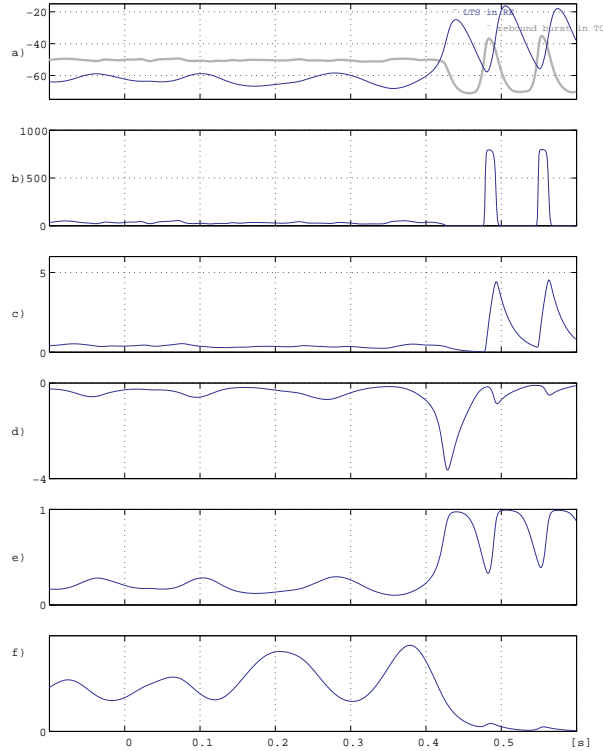


Figure 3.11: Initiation of a spindle in the presence of external noise. a) blue — membrane potential in RE, gray — in TC population (in [mV]); b) input pulse rate for RE population (in [Hz]); c) AMPA synaptic current in RE (in [ $\mu A/cm^2$ ]); d)  $I_{T_{RE}}$  current in RE (in [ $\mu A/cm^2$ ]); e) activation variable  $m$  of  $I_{T_{RE}}$ ; f) inactivation variable  $h$  of  $I_{T_{RE}}$ ;

## Maintenance of spindle oscillations

The mechanisms of maintenance of the spindle oscillation depend on the cooperation of the TC and RE population. One typical cycle of spindle oscillation is shown in fig. 3.12 with characteristic time points marked. In the following description of a cycle time points given in parentheses refer to the cycle presented in fig. 3.12.

Bursts of action potentials generated in TC population ( $0-16\text{ ms}$ ) induce strong excitatory postsynaptic potentials in RE neurons. The EPSPs are strong enough to excite RE neurons to generate a rebound burst of action potentials (*maximum at 27 ms*). Those rebound bursts induce inhibitory postsynaptic potentials in TC ( $12 - 59\text{ ms}$ ) neurons and hyperpolarize them enough to activate the described above mechanism of LTS generation in TC neurons (*maximum of LTS at 76 ms*). During one cycle average membrane potential in RE population does not return to its resting level but is still close to the threshold for generating action potentials when next barrage of EPSPs arrives. This cycle repeats several times.

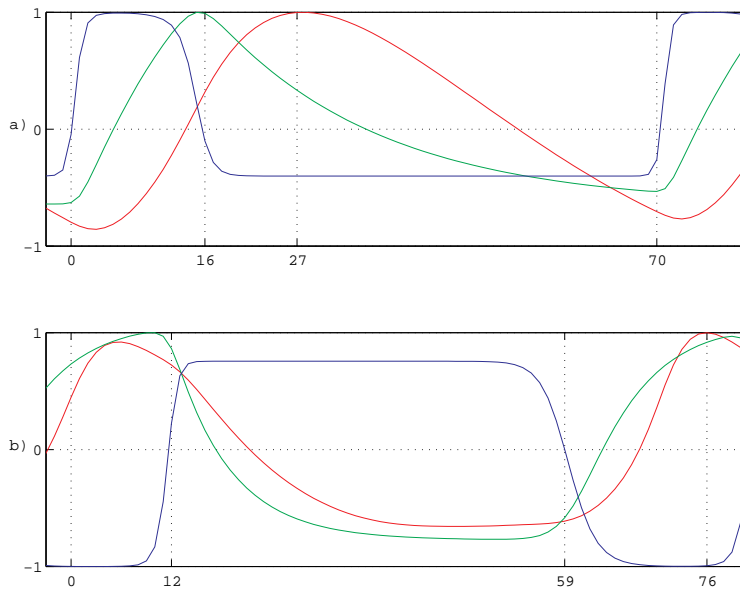


Figure 3.12: One cycle of a spindle. Vertical axis in arbitrary units, horizontal axis in [ms]. Panel a) shows traces of membrane potential (red), synaptic current (green), and input pulse rate (blue) in RE neurons; panel b) — the same for TC population.

## Termination of a spindle

As seen in fig. 3.13 a spindle after a few cycles terminates spontaneously. We can notice that:

1. The depth of successive hyperpolarizations of membrane potential is changing in time. At the beginning the hyperpolarization in consecutive cycles increases and then it decreases — fig 3.13 a);
2. The membrane potential averaged over a cycle increases by a few mV during a spindle — in fig 3.13 b).

The small increase in membrane potential in TC neurons and the decrease of depth of the hyperpolarizations can be attributed to the properties of the  $I_h$  current. In fig. 3.13 c) and d) we can see that during the first half of the spindle duration the absolute value of  $I_h$  current decreases and then in the second half it increases. The increase of absolute value of  $I_h$  is due to locking of its activating gates (fig 3.13 e) and f)). The increase of  $I_h$  results in slight depolarization of the resting potential and inactivation of  $I_{TTC}$ .

## Intra spindle period

In the intra spindle period in both cases — with or without noise — membrane potential decreases by a few mV (fig. 3.14a) and b)). It is due to slowly inactivating  $I_h$  current (fig. 3.14 c)). We can see in the fig. 3.14 c) that in order to start a new spindle the activity of  $I_h$  must drop to about half of its maximum. At this level of  $I_h$  activity, membrane potential is hyperpolarized enough to allow for activation of  $I_{TTC}$  current. It is necessary to establish rebound bursts interplay between TC and RE. The minimal length of the intra spindle period is thus determined by the time constants of  $I_h$  deactivation.

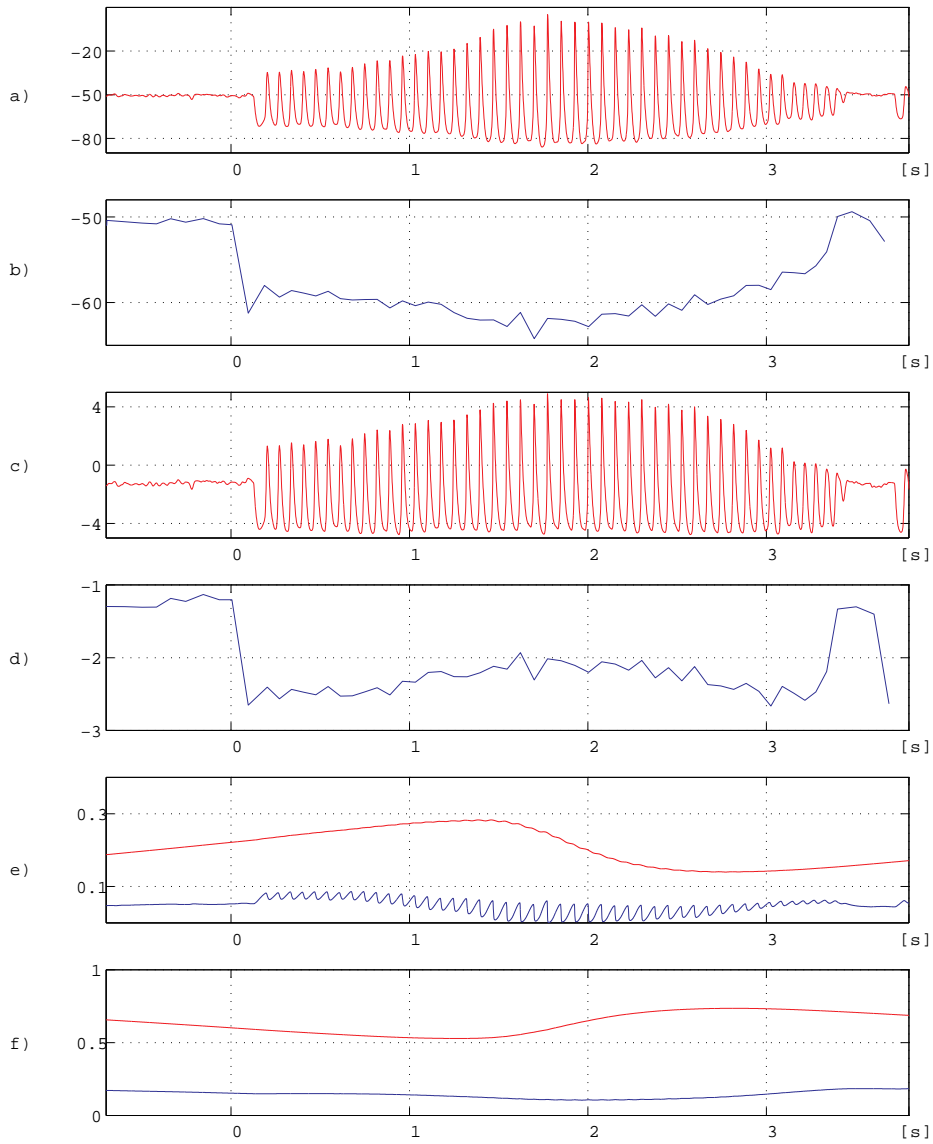


Figure 3.13: Termination of a spindle. a) membrane potential  $V_m$  in TC population ([mV]); b)  $V_m$  averaged over cycles; c)  $I_h$  during spindle ( $[\mu A/cm^2]$ ); d)  $I_h$  averaged over cycles; e) slow (red) and fast (blue) activation variables of the  $I_h$  current; f) slow (red) and fast (blue) activation variables of the  $I_h$  current in the locked form.

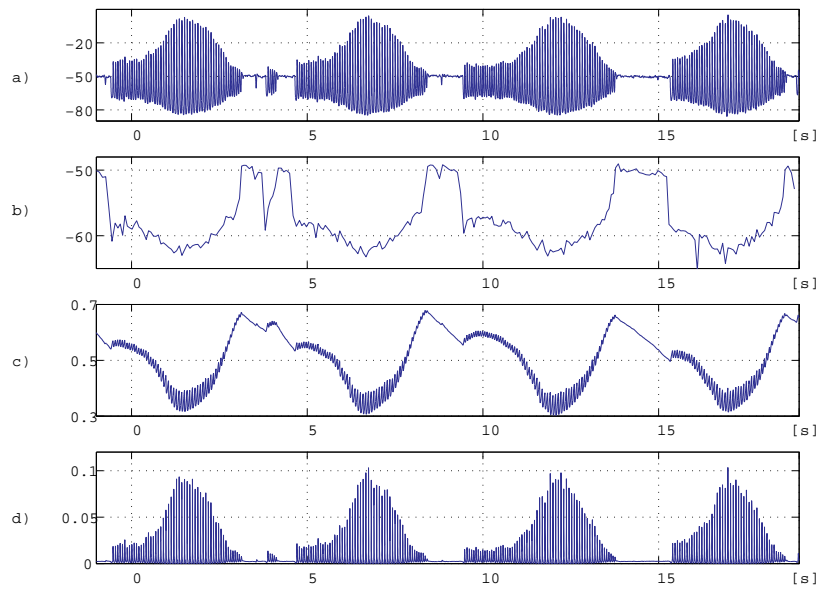
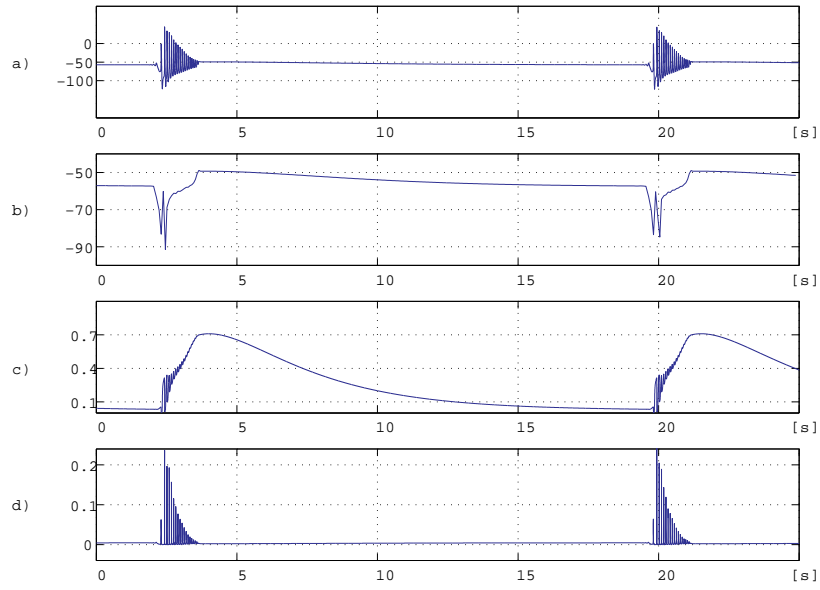


Figure 3.14: Intra spindle period. Upper set of traces corresponds to conditions without external noise, the lower — in the presence of noise. Trace a) membrane potential in TC; trace b) membrane potential averaged over time of one spindle cycle; c) activation of  $I_h$ ; d) activation of  $I_{TTC}$ .

### 3.5.2 How properties of generated spindles depend on model parameters

#### Methods of analysis of model behavior

The most important observables in the model, those that are suitable for direct comparison with experimental data described in chapter 2, are frequency of spindles and period of their reappearance. To obtain a robust estimate of those observables five minutes of output signal for each tested point in the parameter space was computed. In order to run the computations faster we used a variable step solver. It is suitable for stiff problems like solving the model equations during the spindle generation and in the intraspindle periods. On the other hand, variable step solver introduces problems of its own. The output signal samples are generated at uneven time grid, which is inconvenient for further analysis. To overcome this problem we interpolated the signal on even time grid. The proper size of the grid was estimated on the basis of spectral analysis of the output signal computed with a constant — very small time step (0.01 ms ). From the fig. 3.15, we can see that frequencies above 1kHz are attenuated by more than 9 orders of magnitude. That justifies 1 ms grid size for output signal sampling.

The sampled signal was then lowpass filtered and downsampled to 100Hz. In this form the signal was stored and used for further analysis.

Two main characteristics of the generated signal were computed for each set of parameters, namely: spindle frequency and intervals between spindles. We characterize frequency of a spindle by peak in its frequency power spectra. The spectra were estimated using Welch's averaged periodogram method. In order to estimate the spindle reappearance period, the signal was first lowpass filtered with the cut-off frequency 0.5 Hz. Next, autocorrelation function of the filtered signal was computed. Lag of the first order peak in the autocorrelation function was used to evaluate the reappearance period and value of this peak was used as a measure of degree of periodicity.

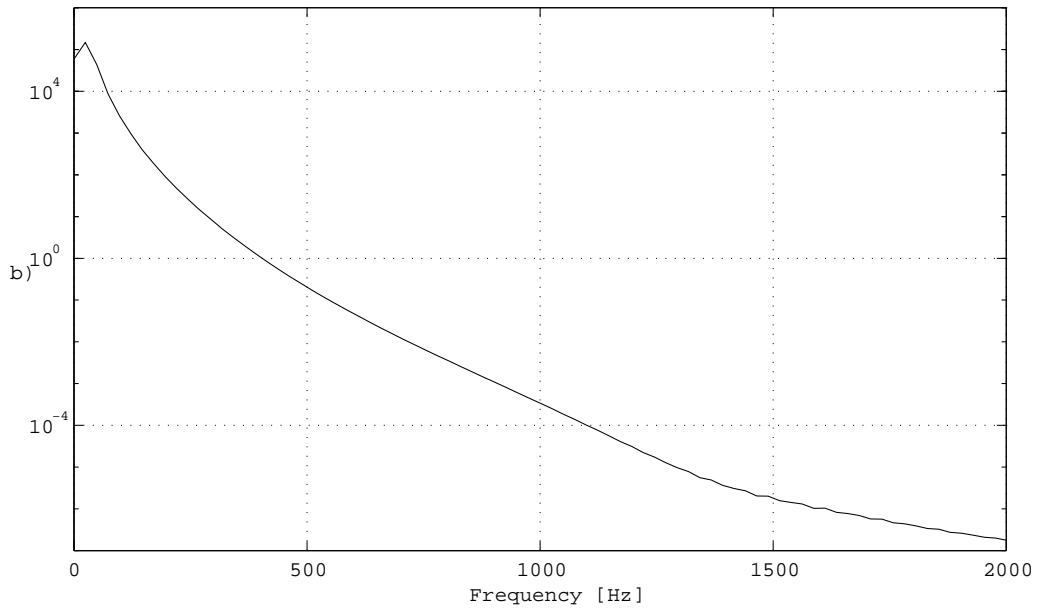
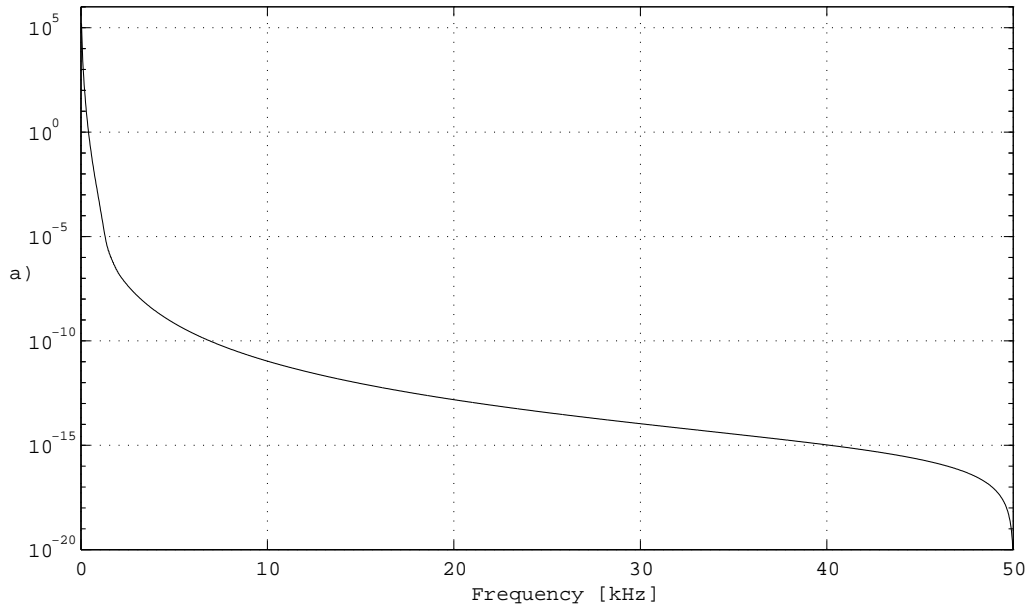


Figure 3.15: Spectral power estimate of representative signal (30 s.) generated by the model with constant time step solver: a) whole frequency range 0 – 50 kHz; b) zoomed to 0 – 2000 Hz.

## Model parameters space

The presented model has following parameters:

**RE to TC and TC to RE gain factors.** The two populations TC and RE interact with each other via synaptic connections. In the real TC-RE system strength of those couplings depends mainly on the density of corresponding synaptic contacts. In the model the density of connections is represented by the gain factors  $TC \rightarrow RE$  and  $RE \rightarrow TC$ .

**$K^+$  leakage conductivity in TC and RE population.** Values of these conductivities in a real system are influenced by neuromodulators. In a living organism the changes in concentration of neuromodulators cause switching between different states of behavior — like between sleep and wake.

**$I_h$  conductivity and half activation potential.** The properties of  $I_h$  current are crucial for mechanisms of waxing and waning of spindles and for switching between sleep and wake.

**Variance of input noise.** Input noise in the present model represents the input to TC population from other structures that are not included in the model. It has a form of white noise with zero mean. The variance of this noise is interpreted as level of activity in the other structures. A special case with zero variance can be considered a model of experiments in vitro.

The model has seven parameters. It is impossible to analyze model behavior in whole parameter space even though the range of each of the parameters is physiologically limited. Thus, we need to sample the parameters. Exact sets of parameters are given in following subsections.

## Frequency of sleep spindles

Spindle frequency strongly depends on the coupling strength between populations. Effects of each of the gain factors on the properties of the model was established in a series of simulations.

In a number of test-runs, the reasonable ranges of gain factors were found. These ranges were uniformly sampled. The resulting set of tested gain factor values is presented in table 3.1

$TC \rightarrow RE$	$RE \rightarrow TC$
1	1, 2, 3 ... 10
2	1, 2, 3 ... 8
3	1, 2, 3 ... 6

Table 3.1: Sampling of the gain factor parameters.

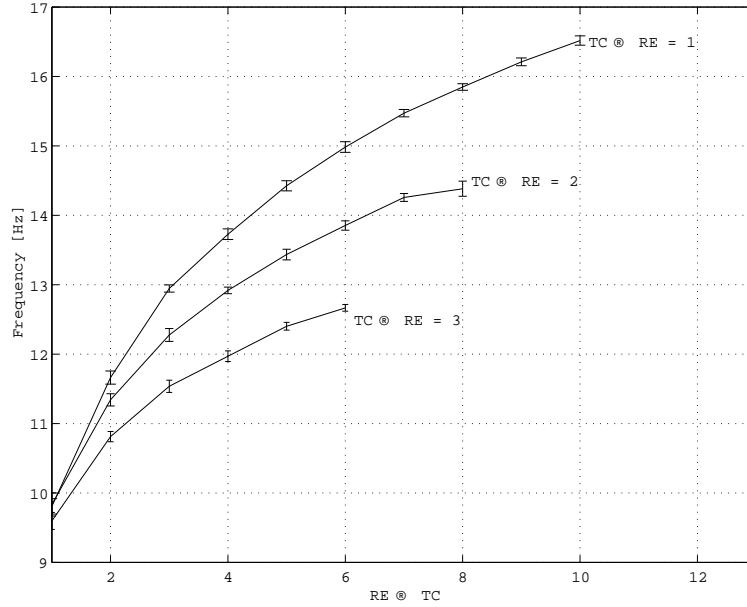


Figure 3.16: Spindle frequency as a function of coupling strength.

Increase in  $RE \rightarrow TC$  coupling causes increase of spindle frequency in the range 9.5 – 16 Hz, and increase of  $TC \rightarrow RE$  causes decrease of frequency by 0.5 – 2 Hz (fig. 3.16). Both changes in frequency have common mechanism. Changes in coupling strength result in different amplitude of oscillations in RE and that causes differences in duration of periods of IPSPs in TC (fig. 3.17).

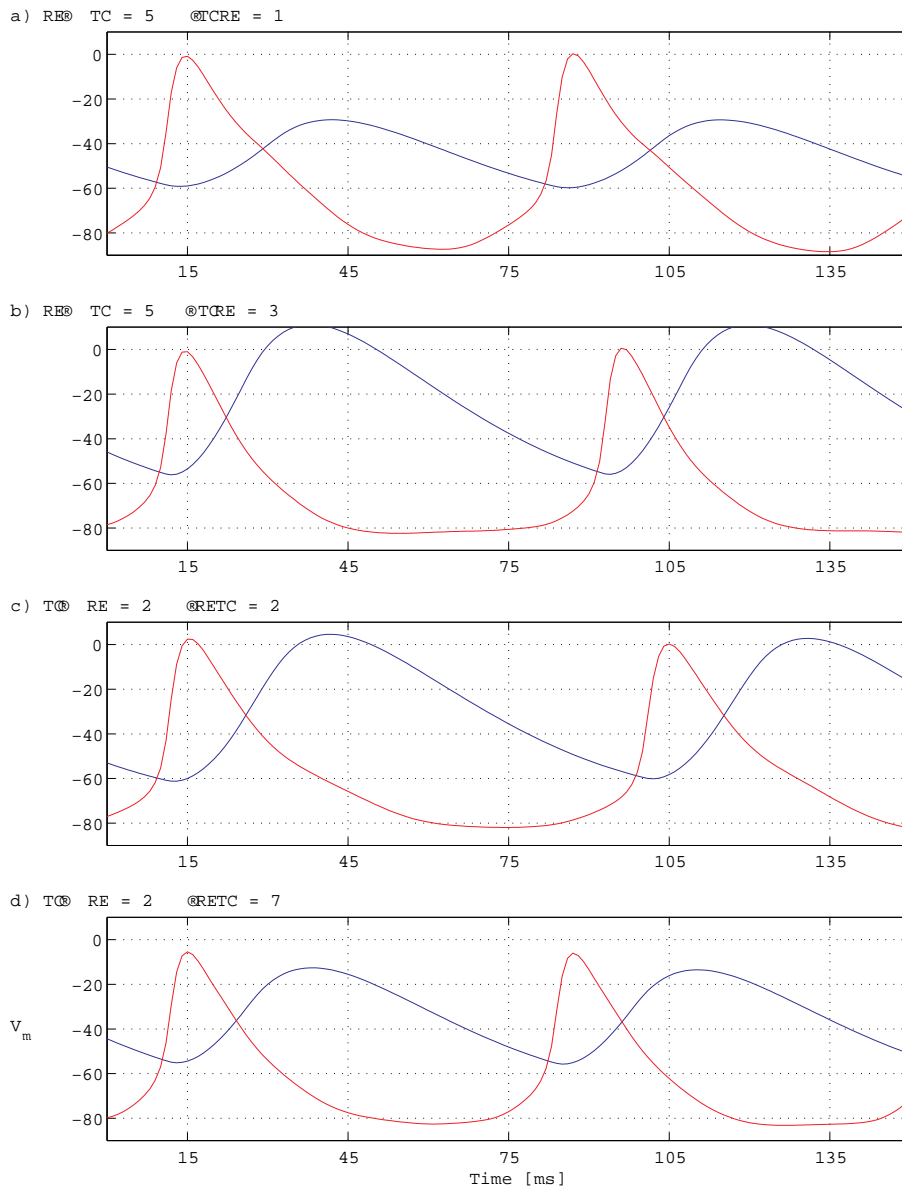


Figure 3.17: Mechanism of frequency changes with coupling strength. Red — membrane potential in TC, blue — in RE. Panels a) and b) the same  $RE \rightarrow TC$  strength, different  $TC \rightarrow RE$ ; Panels c) and d) the same  $TC \rightarrow RE$  strength, different  $RE \rightarrow TC$ . The main difference is in the amplitude of membrane potential in RE and consequently different periods of hyperpolarization of TC.

Another parameter that changes spindle frequency in a broad range is the potassium leakage in RE. Increase, in physiological range, of  $I_{LK_{RE}}$  conductance in RE increases spindle frequency in the range 10.5 – 15 Hz (fig. 3.18). Changes of  $I_{LK_{TC}}$  conductance in TC do not influence spindle frequency significantly. The increase in spindles frequency related to increase in potassium leakage conductance is due to reduction of IPSPs duration in TC population. This shorter duration results from both lower resting membrane potential and smaller membrane time constant in RE with larger  $I_{LK_{RE}}$  conductance (fig. 3.19).

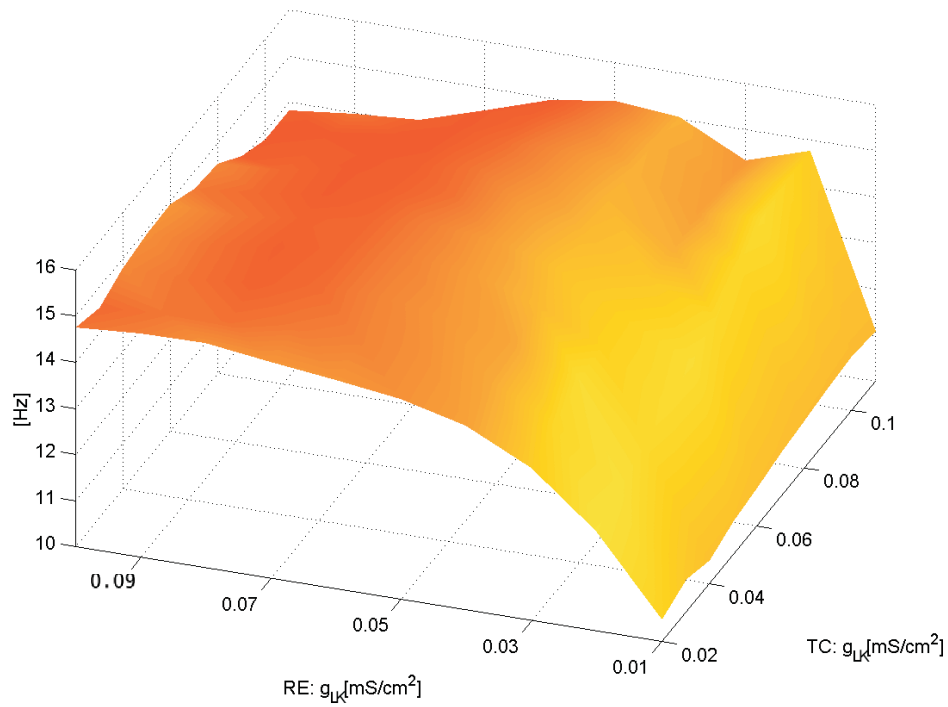


Figure 3.18: Spindle frequency as a function of  $I_{LK}$  in TC and RE.

Smaller increase in spindle frequency (in the range 0 – 1 Hz), but still significant, is induced by increase in  $I_h$  conductance  $\bar{g}_h$  in physiological range (0.2 – 0.6  $mS/cm^2$ ) (fig. 3.20).

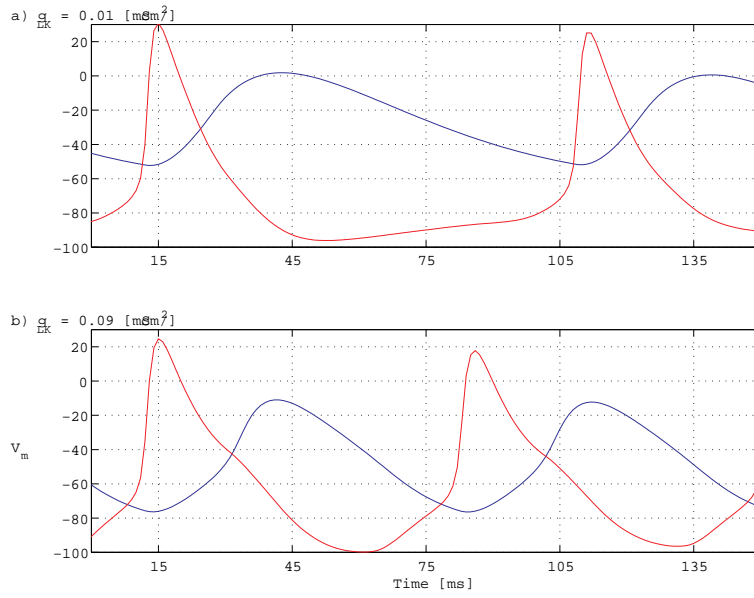


Figure 3.19: Mechanism of frequency changes with potassium leakage. Red — membrane potential in TC, blue — in RE.

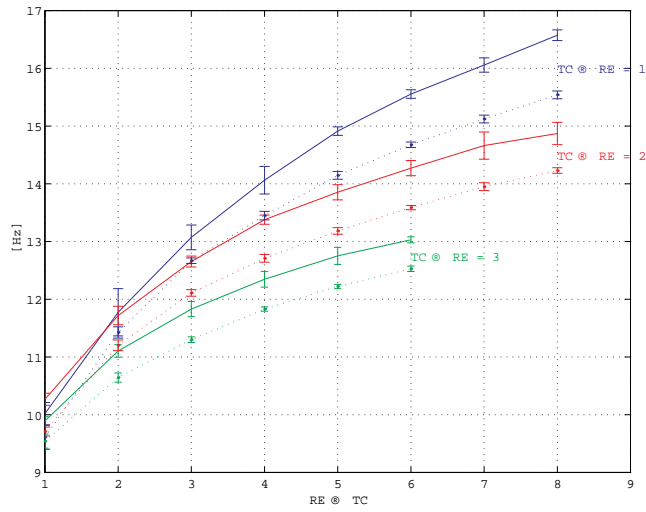


Figure 3.20: Shift in spindle frequency caused by increase in  $I_h$  conductance. Dotted lines  $\bar{g}_h = 0.2 \text{ mS/cm}^2$ , solid lines  $\bar{g}_h = 0.6 \text{ mS/cm}^2$ .

## Length of intraspindle period

The variance of input noise controls, which of the two possible methods of spindle initiation is realized (see sect. 3.5.1). In the presence of external noise the period between successive spindles is in the range 5 - 8 s. and decreases with the coupling strength. In case without noise, that period ranges from 14 to 19 s and increases with coupling strength (fig. 3.21).

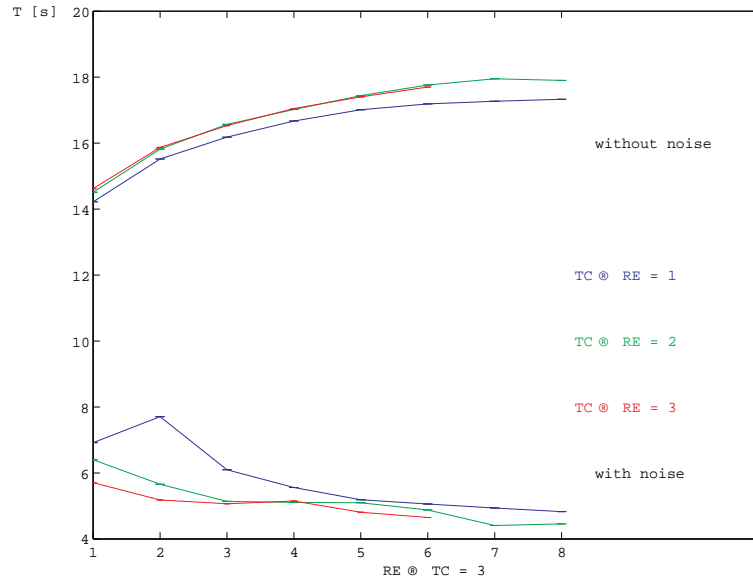


Figure 3.21: Dependence of intraspindle period duration on coupling strength.

The transition between these two types of behavior occurs rapidly, but continuously with the increasing variance of noise (fig. 3.22 a)). For the intermediate values of noise the two types of spindle initiation takes place. It results in more chaotic values of intraspindle duration. It can be observed in panel b) of fig. 3.22. as a decrease of degree of periodicity.

## Degree of periodicity

The degree of periodicity evaluated by means of autocorrelation function depends on the coupling strength (fig. 3.23). One can observe, comparing figures 3.16 and 3.23, that the degree of periodicity is small for coupling strengths corresponding to spindle frequency about 13 Hz and high for those corresponding to spindle frequency about 15 Hz.

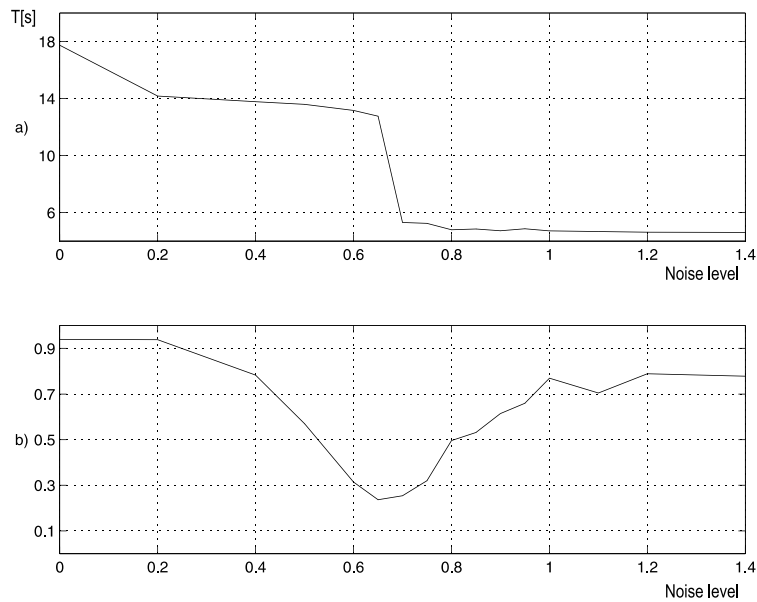


Figure 3.22: Transition from long to short intraspindle periods with increasing input noise. Panel a) — duration of the period; panel b) — autocorrelation based measure of degree of periodicity.

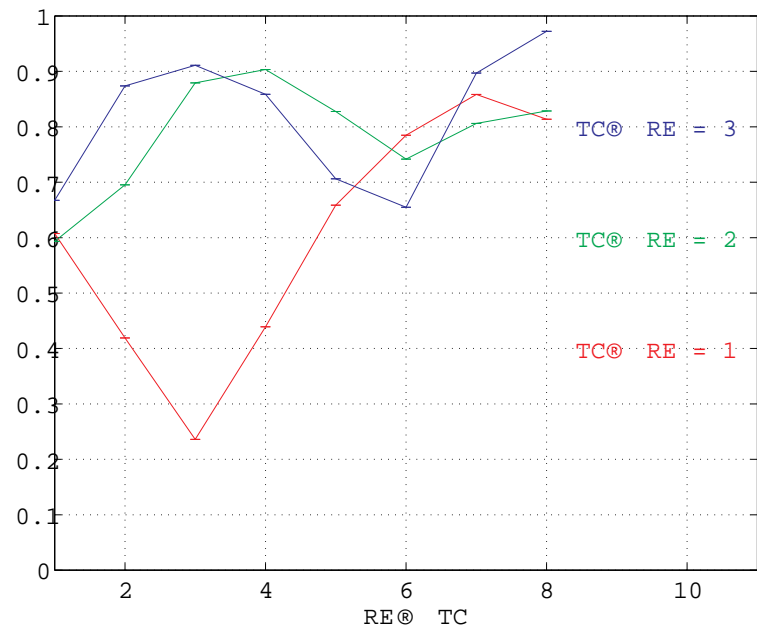


Figure 3.23: Degree of periodicity as a function of coupling strength.

### 3.5.3 Representation of other behavioral states in the model

The model was constructed mainly for analysis of mechanisms of sleep spindles oscillations. As an additional property the model is capable of generating other oscillations observed in the thalamus.

Especially, for increased conductivities of potassium leakage in both populations and activation of  $I_h$  shifted towards hyperpolarization the model generates 2 – 4 Hz  $\delta$  activity. In fact, this activity is generated by the TC population due to the interplay between  $I_{TTC}$  and  $I_h$  currents.

For decreased conductivities of potassium leakage in both populations and activation of  $I_h$  shifted towards depolarization the model is either at rest (membrane potential is at its resting value) in case without noise, or generates permanent  $\alpha$ -like activity in case with external noise.

The simultaneous increase of leakage  $K^+$  conductance in both populations and shift of  $I_h$  activation function towards hyperpolarization, in real thalamic system caused by neuromodulators, switches the oscillation modes from those characteristic for awake to light and then to deep sleep. (fig. 3.24).

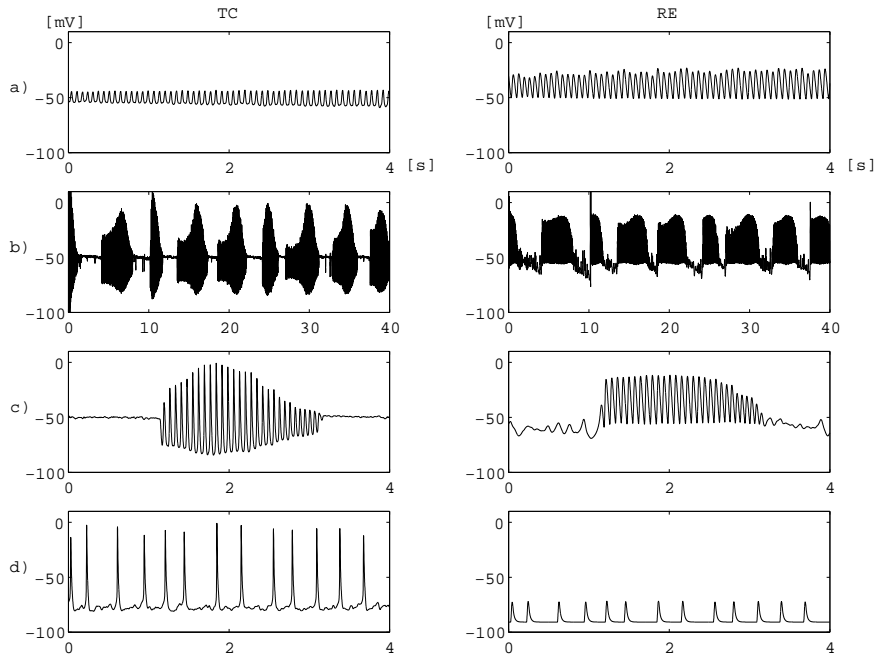


Figure 3.24: Modes of the membrane potential oscillations in the model. a)  $\alpha$ -like, b) and c) sleep spindles, d)  $\delta$  rhythm

# Chapter 4

## Discussion

**Motivations for construction of the presented model** The recent models of sleep spindle generation built as networks of individual neurons (e.g. [82, 83, 84, 21, 37, 20, 38]) generally were aimed to describe and explain results of neurophysiological in vitro experiments performed on thalamic slices by means of intracellular and extracellular microelectrode measurements. Analyzing EEG recorded from different locations on the scalp new features of sleep spindles become apparent. This especially includes the topographical distribution of properties such as frequency of sleep spindles and intervals between occurrences of successive spindles. These observations were the motivation for construction of a new model appropriate for the analysis on the level of neural masses and generating output that can be related to data derived from EEG. Attempts to build model relevant for comparison with EEG data were partially successfully accomplished in 70's by group of Lopes da Silva [90, 15, 14]. At that time, much less physiological data on thalamic neurons were available and consequently more abstract systems interpreted as populations of neurons were analyzed.

In this work, we presented a new model of sleep spindle generation. The most important methodological advantage of the model is that it makes possible to study neuronal populations with individual neurons properties included. The scale, at which the current model is constructed, allows for comparison of its output with data derived from EEG. In the following sections, we discuss in what extent the model explains features of sleep spindles observed on the level of EEG.

**Absence of sleep spindles in REM and the relation between sleep spindles and SWA** The transition from synchronized sleep NREM to desynchronized REM sleep is associated with abolition of sleep spindles. This effect is clearly seen in fig.2.4. The blockage of synchronized activ-

ity in thalamocortical network results from depolarization of thalamocortical and reticular thalamic neurons. The depolarized state of TC cells is presumably the result of the influence of ascending cholinergic and descending corticothalamic activity. The depolarization of RE cells may result from the combined influence of increased tonic firing in both thalamocortical and corticothalamic systems [56]. The investigations of neurotransmitter action in thalamus reveals that activation of muscarinic receptors by acetylcholine (ACh),  $\alpha_1$ -adrenoceptors by norepinephrine (NE), and  $H_1$  receptors by histamine (HA) results in prolonged depolarization of thalamocortical neurons as a result of reduction in a resting leak  $K^+$  conductance and enhancement of  $I_h$  [52, 56, 55, 51]. The depolarization of membrane potentials is of order 5 – 20 mV, which inactivates the low-threshold  $Ca^{2+}$  current and therefore inhibits burst-firing mode [75].

Similar effect can be simulated in the model. Transition between modes of generation shown in (fig. 3.24 c) and a) ) is obtained by simultaneous reduction of  $I_{LK_{TC}}$  and  $I_{LK_{RE}}$  conductance in modeled neural populations and shift of  $I_h$  activation function towards the more positive membrane potential. The depolarization of TC and RE membrane potentials is of correct order.

*From the model studies we see that a single loop formed by interconnected populations of RE and TC cells can oscillate either in spindle generating mode or in  $\delta$  mode.* Transition between these two modes occurs when the resting  $K^+$  conductances in RE and TC populations are increased and the activation function of  $I_h$  is shifted towards more negative membrane potentials. Altogether, these changes of model parameters result in membrane hyperpolarization in both populations. The progressive changes in resting membrane potential during the course of the sleep cycle can explain the typical relation between sleep spindle and SWA (fig. 2.5). This result agrees with the neurophysiological experiments on the cellular level. Steriade (1991) [74] reported that the sleep spindle and delta waves appear at different membrane potentials of thalamocortical cells. At resting potential around -60 mV thalamic cells display spontaneous or cortically elicited spindle oscillations, whereas at potentials more negative than -65 or -70 mV spindles progressively decrease in amplitude and the oscillation switch to delta frequency range.

Together, model and experimental results suggest that there are many loops of interconnected subpopulations of TC and RE neurons. Each of these loops can generate sleep spindle or  $\delta$  oscillations depending on the average resting membrane potential in each population. The positive association between spindles and slow waves in the early and late parts of the NREM sleep episodes may reflect an increasing number of loops entering the burst mode, with some of them exhibiting spindle oscillations while others are already in the slow wave mode. The negative association between spindle

amplitude and SWA in the middle part of the NREM episodes would then be a reflection of many loops being in the slow wave mode and only a few in the spindle mode.

**Different frequencies of sleep spindles in the model and the two types of sleep spindle — HFS and LFS — in real EEG.** Topographic study of sleep spindles distribution, presented in Chapter 2, revealed two types of sleep spindles: LFS occurring predominantly in frontal and HFS - in parietal derivations for all studied subjects. The patterns of occurrences of LFS and HFS were found different as well — high-frequency spindles occurred rhythmically with a period of 3.9 s whereas low-frequency spindles showed no specific rhythmicity (sec.: 2.4.2). Two kinds of sleep spindles differing in spectral and topographical characteristics were also observed in several human EEG studies (e.g. [45, 87]). In the animal studies, however, no such differentiation of sleep spindles was observed ([75, 13, 71]). Sleep spindles present in animals seem to correspond to HFS observed in human studies. Close analogies between them were found by Contreras et al. (1997) [13]. However, LFS found in humans and appearing predominantly in the frontal cortex may be difficult to observe in animals, in which association cortex is much less developed.

There are close reciprocal connections between the thalamic nuclei and specific regions of the cerebral cortex. Propagation of sleep spindle sequences in the cortex reflects orderly propagation in the anteroposterior axis of the thalamus [13]. Prefrontal cortex, where low-frequency spindles are observed, is connected mainly to the mediodorsal nucleus important for memory functions, whereas the central and posterior parts of cortex are mainly connected with thalamic nuclei more closely related with sensory inputs. Thalamic regions mostly communicating with prefrontal areas are more developed in humans than in animals. Therefore we may suspect that the "frontal sleep spindles generators" may somewhat differ from those observed for animals. According to present neurophysiological studies, the observed frequency of sleep spindles depends on the time required for one completion of the loop between thalamocortical cells and thalamic reticular neurons (McCormick and Bal, 1997 [56]).

In Chapter 3, we presented model of interacting TC and RE populations of neurons. For the physiological range of parameters the model is able to generate spindle oscillations with frequencies in the range 9 – 16 Hz. Parameters that control the frequency are: coupling strength (fig. 3.16) and leak  $K^+$  conductance in RE population (fig. 3.18).

Spindles with any frequency in the physiological range can be produced

depending on coupling strength and leak  $K^+$  conductance in RE population in the model. At the same time we observe two types of sleep spindles: LFS and HFS in human sleep EEG. *These suggest that perhaps one of the parameters is not uniformly distributed in a human brain. We hypothesize that the LFS and HFS spindles are generated in different RE-TC loops characterized by different coupling strengths.* A support for this hypothesis can be found in the work on squirrel monkey by Smith et. al. (1987) [69] showing, that different nuclei of thalamus are innervated with different densities by RE GABAergic (inhibitory) terminals. Furthermore, the authors observed that the density of the inhibitory axon terminals is higher in lateral and ventral than in medial dorsal nuclei. The lateral and ventral nuclei project generally to motor and sensory cortex and to parietal lobe that in humans is located in the region from which HFS are predominantly recorded. Medial dorsal nucleus projects mainly to prefrontal cortex that in humans is located in the region from which LFS are predominantly recorded.

The different coupling strength of TC-RE loops generating LFS and HFS can explain the difference in their periodicity. In sec 2.4.2 we show that HFS occur with a period of about 4s., while LFS do not show specific periodicity. In fig. 3.23 we see that for a certain range of coupling strengths the measure of periodicity is higher and for other range it is smaller. In the same ranges of parameters the frequency of generated spindles is respectively higher and lower (fig. 3.16).

All these experimental and model results indicate that possibly the different properties of LFS and HFS spindles recorded in EEG result from different density of RE GABAergic innervation of thalamus nuclei that are involved in their generation.

**Periodicity of sleep spindles** The periodicity of sleep spindle reoccurrence depends on the experimental conditions in which the intervals between successive spindles are measured. Periods of spindle reoccurrence observed in studies in vivo (sec. 2.4.2 and [75, 72]) are of the order 3–10 s. The intervals reported from experiments in vitro performed in thalamic slices are longer — of the order 10–20 s. (e.g. [48]).

The proposed model suggests a possible explanation of these results. In sec. 3.5.1 we showed that there are two possible ways to initiate a spindle in the model. With sufficient level of external noise, a spindle can be induced in a relatively short time after the previous one. In the absence of noise, a spindle can be initiated spontaneously but then the interval is longer (figs. 3.21 and 3.22). We can assume that the external noise — the input from other structures — is practically absent in slice preparation and is present in experiments in vivo.

**Relationship between LFS and HFS** In the animal studies, sleep spindles with different propagation velocities were observed, namely sleep spindles propagating slowly along the axis of thalamus and spindle waves that occur almost simultaneously in widely dispersed regions of cerebral cortex [56]. We have observed the simultaneous appearance of sleep spindles belonging to the same type, LFS or HFS, in different derivations. It is hard to attribute the time delay between HFS and LFS to different propagation times in anterior and posterior connections between cortex and thalamus taking into account this evidence. It seems that the constant time delay observed between LFS and HFS indicates some kind of weak coupling between loops generating them. Since in case of superimposed sleep spindles HFS tends to precede LFS we can assume that TC-RE loops generating high-frequency spindles from time to time drives the TC-RE loops generating low-frequency spindles. The mechanism of this relation is not known yet. We can only hypothesize that HFS oscillations may induce LFS oscillations either via intracortex connections or via reticular nucleus.

**Possible explanation of differences between sleep spindles of normal and insomniac subjects** Sleep spindles with frequencies above 14 Hz were reported to undergo some changes of their characteristics with the change of subjects' conditions. Landolt (1996) [50] reported that the age related reduction of SFA did not include the SFA with frequency above 14 Hz. The largest variations of SFA during both the menstrual cycle [25] and pregnancy [11] were present for the faster SFA, above 14 Hz. Melatonin has been recently found to enhance SFA around 14 Hz and to reduce the activity in the frequency band 15-16.5 Hz [23]. Werth (1997) [87] reported the different time-evolution of the high-and low-frequency spindles during the overnight sleep.

In our study of sleep spindles in insomniac subjects we also found that the biggest differences between normal and insomniac subjects concern HFS spindles and especially the sleep spindles with frequencies above 14 Hz (fig. 2.12). The statistically confirmed differences are:

1. higher average frequency of HFS spindles in channel Cz
2. shorter average interval between successive HFS spindles in insomniac subjects than in normals.

In model studies we tested the relation between model parameters and spindle frequency (sec:3.5.2) and between model parameters and intervals between successive spindles (sec:3.5.2). In the model, only one parameter

produces the differences of spindle parameters observed in insomniac subjects with respect to normals. This parameter is coupling strength between RE and TC population  $RE \rightarrow TC$ . Thus the model suggests that the differences in sleep spindles characteristics between normal and insomniac subjects may be due to different strength of inhibition of thalamic relay nuclei by reticular thalamic nucleus in these groups of subjects. This hypothesis could be tested by other neurophysiological methods. Further work is also needed to verify if the observed changes in properties of sleep spindles in insomniac subjects are one of the symptoms of insomnia or they are the long lasting effects of priori medications.

# Summary

Sleep EEG was analyzed by means of high-resolution time-frequency method (Matching Pursuit). Special attention was devoted to sleep spindles detection and evaluation. Following features of sleep spindles were observed:

1. Two types of sleep spindles - HFS and LFS were characterized and differences between them were evaluated by statistical tests. HFS differed from LFS in spectral characteristic, topographical distribution and rhythmicity of reoccurrence.
2. Superimposed sleep spindles were resolved. A constant time delay between the higher and the lower frequency component was found, which suggests some kind of coupling between their generators.
3. A number of differences in HFS characteristics were found between normal and insomniac subjects.

A model of thalamic system combining properties of a lumped and a single representative neuron type model was constructed. It includes the data on intrinsic ionic currents. It allows to compare directly model output with observables derived from the scalp EEG. The model accounts for a number of clinical and experimental observations:

1. waxing and waning of sleep spindles,
2. topographical differences in their spectra,
3. topographical differences in the slow rhythm of their reappearance in the scalp EEG,
4. differences in the rhythm of reappearance of spindles reported in vivo and in vitro.
5. The model also describes rhythms in awake and deep sleep EEG. Transition between different rhythms is achieved by physiologically justified changes in the model parameters.
6. The model suggests also an explanation of the differences between properties of HFS in normal and in insomniac subjects.

# Appendices: Formulas and parameters used in the model

# Appendix A

## The sigmoid function

We used the following form of sigmoid:

$$g(V) = \frac{1}{1 + e^{-s(V-E_{tr})}} \quad (\text{A.1})$$

where:

$s$  — slope,

$E_{tr}$  — average threshold for action potential generation.

In both population we used the same values of  $s = 0.6mV^{-1}$  and  $E_{tr} = -45$  mV.

$$\lambda_{TC} = \lambda_{RE} = 400Hz. \quad (\text{A.2})$$

# Appendix B

## Synaptic currents

Synaptic currents are modeled by transfer functions of the following form:

$$h(\tau) = A [\exp(-a\tau) - \exp(-b\tau)] \quad (\text{B.1})$$

**GABA synapse**  $A = -0.0003 \frac{\mu A}{cm^2}$ ,  $a = 0.15 \text{ ms}^{-1}$ ,  $b = 10 \text{ ms}^{-1}$ ,

**AMPA synapse**  $A = 0.0006 \frac{\mu A}{cm^2}$ ,  $a = 0.05 \text{ ms}^{-1}$ ,  $b = 2.5 \text{ ms}^{-1}$ .

# Appendix C

## Values of parameters used in TC population

All potentials are given in [mV], time constants in [ms] concentrations in [mM].

$I_{TC}$  — **Low threshold calcium current** We model low threshold calcium current in TC population as proposed by Wang et al. (1991) [85] and used by Destexhe et al. (1993) [19]

$$I_{TC} = g_{TC} m^3 h (V - E_T) \quad (C.1)$$

$$g_{TC} = 2 \frac{mS}{cm^2}, E_T = 120mV$$

$$\dot{m} = \frac{m_\infty(V) - m}{\tau_m(V)} \quad (C.2)$$

$$\dot{h} = \alpha_1(V)(1 - h - d - K(V)h) \quad (C.3)$$

$$\dot{d} = \alpha_2(V)(K(V)(1 - h - d) - d) \quad (C.4)$$

$$m_\infty(V) = \left[ 1 + \exp\left(-\frac{V + 65}{7.8}\right) \right]^{-1} \quad (C.5)$$

$$\tau_m(V) = 0.15 m_\infty(V) \left[ 1.7 + \exp\left(-\frac{V + 30.8}{13.5}\right) \right] \quad (C.6)$$

$$\alpha_1(V) = \frac{\exp\left(-\frac{V + 162.3}{17.8}\right)}{0.26} \quad (C.7)$$

$$\alpha_2(V) = \frac{1}{\tau_2(V)(K(V) + 1)} \quad (C.8)$$

$$\tau_2(V) = \frac{62.4}{1 + \exp\left(\frac{V + 39.4}{30}\right)} \quad (C.9)$$

$$K(V) = \sqrt{0.25 + \exp\left(\frac{V + 85.5}{81}\right)} - 0.5 \quad (C.10)$$

$I_h$  — **Hyperpolarization activated current** Destexhe and Babloyantz (1993) [18] proposed a model of hyperpolarization activated current that had two activating variables *slow*  $S$  and *fast*  $F$ . Destexhe et al. (1996) [20] proposed kinetic scheme of indirect regulation of  $I_h$  by calcium. It was assumed that  $Ca^{2+}$  binds to a regulating factor ( $P$ ) which itself binds to the open ( $O$ ) form of the channel and blocks its transition to the closed form ( $C$ ).



where:  $P_0, P$  — unbound and calcium-bound forms of regulating factor,  
 $C, O, O_L$  — closed, open, open-locked states of a channel,

$$k_1 = 2.5 * 10^7 mM^{-4} ms^{-1}$$

$$k_2 = 4 * 10^{-4} ms^{-1}$$

$$k_3 = 0.1 ms^{-1}$$

$$k_4 = 0.001 ms^{-1}$$

The current is proportional to the relative concentration of the open channels with the conductance of the locked state being twice of the unbound open state.

$$I_h = g_h(S_1 + 2S_2)(F_1 + 2F_2)(V - E_h) \quad (C.14)$$

where:  $S_1, S_2$  — open unbound and locked slow gates,  
 $F_1, F_2$  — open unbound and locked fast gates,  
 $g_h$  — model parameter,  
 $E_h = -43.0$  mV

The parameters of calcium kinetics were adjusted to give the average level of  $Ca^{2+}$   $2.4 * 10^{-4} mM$  and values of  $I_h$  variables similar to those presented in [19].

$$[\dot{C}a] = -0.0001I_T - 0.7[Ca] \quad (C.15)$$

$$[\dot{P}] = k_1(1 - [P])[Ca]^4 - k_2[P] \quad (C.16)$$

$$\dot{S}_1 = \alpha_S(V)(1 - S_1 - S_2) - \beta_S(V)S_1 + k_4S_2 - k_3S_1[P] \quad (C.17)$$

$$\dot{F}_1 = \alpha_F(V)(1 - F_1 - F_2) - \beta_F(V)F_1 + k_4F_2 - k_3F_1[P] \quad (C.18)$$

$$\dot{S}_2 = k_3S_1[P] - k_4S_2 \quad (C.19)$$

$$\dot{F}_2 = k_3F_1[P] - k_4F_2 \quad (C.20)$$

The activation rates of  $S$  and  $F$  are identical to those in the model introduced by Destexhe et al. (1993) [19].

$$\alpha_S(V) = \frac{H_\infty(V)}{\tau_{S_1}(V)} \quad (C.21)$$

$$\beta_S(V) = \frac{1 - H_\infty(V)}{\tau_{S_1}(V)} \quad (C.22)$$

$$\alpha_F(V) = \frac{H_\infty(V)}{\tau_{F_1}(V)} \quad (C.23)$$

$$\beta_F(V) = \frac{1 - H_\infty(V)}{\tau_{F_1}(V)} \quad (C.24)$$

$$H_\infty(V) = \left[ 1 + \exp\left(\frac{V + 68.9}{6.5}\right) \right]^{-1} \quad (C.25)$$

$$\tau_{S_1}(V) = \exp\left(\frac{V + 183.6}{15.24}\right) \quad (C.26)$$

$$\tau_{F_1}(V) = \frac{\exp\left(\frac{V + 158.6}{11.2}\right)}{1 + \exp\left(\frac{V + 75}{5.5}\right)} \quad (C.27)$$

$I_{LTC}$  — **Leak current**

$$I_{LTC} = g_{LTC}(V - E_{LTC}) + g_{LKTC}(V - E_{LKTC}) \quad (C.28)$$

where:  $g_{LTC} = 0.01 \frac{mS}{cm^2}$ ,  $E_{LTC} = -55mV$ ,  $E_{LKTC} = -100mV$

# Appendix D

## Values of parameters used in RE population

Currents  $I_{T_{RE}}$ ,  $I_{K(Ca)}$ ,  $I_{CAN}$  in equation 3.33 are based on a model developed by Destexhe et al. 1994 [21]. The formulas and parameters of the currents are given below. All potentials are given in [mV], time constants in [ms] concentrations in [mM].

$I_{T_{RE}}$  — **Low threshold calcium current.**

$$I_T = g_T m^2 h (V - E_T) \quad (D.1)$$

$$g_T = 1.75 \frac{mS}{cm^2}, \quad E_T = 120mV$$

Activating variable:

$$\dot{m} = \frac{m_\infty(V) - m}{\tau_\infty(V)} \quad (D.2)$$

$$m_\infty(V) = \left[ 1 + \exp\left(-\frac{V + 52}{7.4}\right) \right]^{-1} \quad (D.3)$$

$$\tau_m(V) = 0.44 + \frac{0.15}{\exp\left(\frac{V+27}{9}\right) + \exp\left(-\frac{V+102}{15}\right)} \quad (D.4)$$

Inactivating variable

$$\dot{h} = \frac{h_\infty(V) - h}{\tau_h(V)} \quad (D.5)$$

$$h_\infty(V) = \left[ 1 + \exp\left(\frac{V + 80}{5}\right) \right]^{-1} \quad (D.6)$$

$$\tau_h(V) = 22.7 + \frac{0.27}{\exp\left(\frac{V+48}{4}\right) + \exp\left(-\frac{V+407}{50}\right)} \quad (D.7)$$

$I_{K(Ca)}$  — **Calcium dependent potassium current.**

$$I_{K(Ca)} = g_{K(Ca)}m^2(V - E_{K(Ca)}) \quad (D.8)$$

$$g_{K(Ca)} = 10 \frac{mS}{cm^2}, E_{K(Ca)} = -90.0mV$$

$$\dot{m} = \frac{m_\infty([Ca]) - m}{\tau_m([Ca])} \quad (D.9)$$

$$m_\infty([Ca]) = \frac{48[Ca]^2}{48[Ca]^2 + 0.03} \quad (D.10)$$

$$\tau_m([Ca]) = \frac{1}{48[Ca]^2 + 0.03} \quad (D.11)$$

$I_{CAN}$  — **Calcium dependent nonspecific cation current**

$$I_{CAN} = g_{CAN}m^2(V - E_{CAN}) \quad (D.12)$$

$$g_{CAN} = 1 \frac{mS}{cm^2}, E_{CAN} = -20mV$$

$$\dot{m} = \frac{m_\infty([Ca]) - m}{\tau_m([Ca])} \quad (D.13)$$

$$m_\infty([Ca]) = \frac{20[Ca]^2}{20[Ca]^2 + 0.005} \quad (D.14)$$

$$\tau_m([Ca]) = \frac{1}{20[Ca]^2 + 0.005} \quad (D.15)$$

**The intracellular calcium** dynamics is determined by two contributions: the influx of  $Ca^{2+}$  which is proportional to  $I_{TRE}$  current and the efflux due to an active pump.

$$[\dot{Ca}] = -0.00052I_{TRE} - \frac{0.005[Ca]}{0.005 + [Ca]} \quad (D.16)$$

Parameters of the **RE leakage current** —  $I_{LRE}$  are:

$$E_L = -60mV,$$

$$g_L = 0.025 \frac{mS}{cm^2},$$

$$E_{LK} = -95mV.$$

# Bibliography<sup>1</sup>

- [1] D. Aeschbach and A.A. Borbèly. All-night dynamics of the human sleep EEG. *J. Sleep. Res.*, 2:70–81, 1993.
- [2] D. Aeschbach, D.J. Dijk, L. Trachsel, D.P. Brunner, and A.A. Borbèly. Dynamics of slow wave activity and spindle frequency activity in the human sleep EEG: Effects of midazolam and zopiclone. *Neuropsychopharmacology*, 11(4):237–244, 1994.
- [3] A. L. Bardou, P. M. Auger, P. J. Birkui, and J. L. Chasse. Modeling of cardiac electrophysiological mechanisms: from action potential genesis to its propagation in myocardium. *Critical Reviews in Biomedical Engineering*, 24(2–3):141–221, 1996.
- [4] C. Bassetti, J. Mathis, M. Gugger, K.O. Lovblad, and Ch.W Hess. Hypersomnia following paramedian thalamic stroke: a report of 12 patient. *Annals of Neurology*, 39(4):471–480, 1996.
- [5] K.J. Blinowska and P.J. Durka. The application of Wavelet Transform and Matching Pursuit to the time-varying EEG signals. In C.H. Dagli and B.R. Fernandez, editors, *Intelligent Engineering Systems through Artificial Neural Networks*, volume 4, pages 535–540. ASME Press, New York, 1994. ISBN 0-7918-045-8.
- [6] K.J. Blinowska, P.J. Durka, M. Kamiński, and W. Szelenberger. Methods of topographical time-frequency analysis of EEG in coarse and fine time scale. In F.H. Lopes da Silva, J.C. Principe, and L.B. Almeida, editors, *Spatiotemporal Models in Biological and Artificial Systems*, pages 1–8. IOS Press, 1996. ISBN 90 5199 304 8.
- [7] K.J. Blinowska, P.J. Durka, and W. Szelenberger. Time-frequency analysis of nonstationary EEG by Matching Pursuit. In *World Congress of Medical Physics and Biomedical Engineering*, Rio de Janeiro, Aug 1994.

---

<sup>1</sup>Author’s papers are cited in the text with boldface and superscript a: [.]<sup>a</sup>

- [8] A. Bové, A. Culebras and J.T. Moore, and R.E. Westlake. Relation between sleep spindles and hypersomnia. *Sleep*, 17(5):449–445, 1994.
- [9] R. Broughton, T. Healey, J. Maru, D. Green, and B. Pagorek. A phase-locked loop device for automatic detection of sleep spindles and stage 2. *Electroenceph. Clin. Neurophysiol.*, 40:657–77, 1976.
- [10] D.P. Brunner, D.J. Dijk, M. Munch, and A.A. Borbély. Effects of zolpidem on sleep and sleep EEG spectra in healthy young men. *Psychopharmacology*, 104:1–5, 1991.
- [11] D.P. Brunner, M. Munch, K. Biedermann, R. Huch, A. Huch, and A.A. Borbély. Changes in sleep and sleep electroencephalogram during pregnancy. *Sleep*, 17:576–582, 1994.
- [12] K. Campbell, A. Kumar, and W. Hofman. Human and automatic validation of a phase-locked loop spindle detection system. *Electroenceph. Clin. Neurophysiol.*, 48:602–605, 1980.
- [13] D. Contreras, A. Destexhe, T.J. Sejnowski, and M. Steriade. Spatiotemporal patterns of spindle oscillations in cortex and thalamus. *J. Neurosci.*, 17:1179–1196, 1997.
- [14] F.H. Lopes da Silva, P. Barts, E. van Heuschen, A. van Rotterdam, and W. Burr. *Perspectives in brain research*, chapter Models of neuronal populations, the basic mechanisms of rhythmicity. Progress in brain research. Elsevier, Amsterdam, 1976.
- [15] F.H. Lopes da Silva, A. Hoeks, H. Smiths, and L.H. Zetterberger. Model of brain rhythmic activity, the alpha-rhythm of the thalamus. *Kybernetik*, 15:27–37, 1974.
- [16] G. Davis. *Adaptive Nonlinear approximations*. PhD thesis, New York University, 1994.
- [17] A.C. Declerck, W.L.J Martens, and W. Wauquier. Sleep spindle detection and its clinical relevance. *Eur. Neurol.*, 25:56–60, 1986.
- [18] A. Destexhe and A. Babloyantz. A model of the inward current  $I_h$  and its possible role in thalamocortical oscillations. *Neuro Report*, 4:223–226, 1993.
- [19] A. Destexhe, A. Babloyantz, and T.J. Sejnowski. Ionic mechanisms for intrinsic slow oscillation in thalamic relay neurons. *Biophysical Journal*, 65(4):1538–52, 1993.

- [20] A. Destexhe, T. Bal, D.A. McCormick, and T.J. Sejnowski. Ionic mechanisms underlying synchronized oscillations and propagating waves in a model of ferret thalamic slices. *Journal of Neurophysiology*, 76(3):2049–2069, 1996.
- [21] A. Destexhe, D. Contreras, T.S. Sejnowski, and M. Steriade. A model of spindle rhythmicity in the isolated thalamic reticular nucleus. *Journal of Neurophysiology*, 72(2):803–817, 1994.
- [22] D.J. Dijk, B. Hayes, and A. Czeisler. Dynamics of electroencephalographic sleep spindles and slow wave activity in men: effects of sleep deprivation. *Brain Research*, 626:190–199, 1993.
- [23] D.J. Dijk, C. Roth, Landolt, E. Werth, M. Aeppli, P. Achermann, and A.A. Borbély. Melatonin effect on daytime sleep in man; suppression of EEG low frequency activity and enhancement of spindle frequency activity. *Neurosci. lett.*, 201:13–16, 1995.
- [24] M.E. Drake, Jr.A. Pakalnis, H. Padamadan, S.M Weate, and P.A. Cannon. Sleep spindles in epilepsy. *Clinical Electroencephalography*, 22(3):144–149, 1991.
- [25] H.S. Driver, D.J. Dijk, E. Werth, K. Biederman, and A.A. Borbély. Sleep and the sleep electroencephalogram across the menstrual cycle in young healthy women. *J. Clin. Endocrinol. Metab.*, 81:728–735, 1996.
- [26] P.J. Durka. *Time-frequency analyses of EEG*. PhD thesis, Warsaw University, August 1996.
- [27] P.J. Durka and K.J. Blinowska. Analysis of EEG transients by means of matching Pursuit. *Annals of Biomedical Engineering*, 23:608–611, 1995.
- [28] P.J. Durka and K.J. Blinowska. In pursuit of time-frequency representation of brain signals. In Metin Akay, editor, *Time frequency and wavelets in biomedical signal processing*, IEEE Press Series in Biomedical Engineering, pages 389–406. IEEE press, New Jersey, 1997. ISBN 0-7803-1147-7.
- [29] P.J. Durka and K.J. Blinowska. Matching pursuit parametrization of sleep spindles. In *Abstracts of 18th Annual International Conference of the IEEE EMBS, Amsterdam 31 Oct-3 Nov, 1997*. ISBN 90-9010005-9(CD-ROM) SOE 9609001, paper 163.

- [30] P.J. Durka, K.J. Blinowska, and J. Żygierewicz. Matching Pursuit - a method of evaluation and parameterization of non-stationary signals and transients. *Medical & Biological Engineering and Computing*, 34:429–430, 1996. Supplement 1, Part 1, The 10th Nordic-Baltic Conference on Biomedical Engineering, June 9-13, Tampere, Finland.
- [31] P.J. Durka, D. Ircha, J. Żygierewicz, and K.J. Blinowska. Recent advances in Matching Pursuit representation of brain signals. In P. Rabischong, J. Meli, and M. Nałęcz, editors, *Abstracts of 4th European Conference on Engineering and Medicine, Warsaw*, pages 105–106, 1997.
- [32] P.J. Durka, E.F. Kelly, and K.J. Blinowska. Time-frequency analysis of stimulus-driven EEG activity by Matching Pursuit. In *Abstracts of 18th Annual International Conference of the IEEE EMBS, Amsterdam 31 Oct-3 Nov, 1997*. ISBN 90-9010005-9(CD-ROM) SOE 9609001, paper 162.
- [33] P.J. Franaszczuk, G.K. Bergey, and P.J. Durka. Application of time-frequency transform analysis to hippocampal activity in mesial temporal seizures. *Epilepsia*, 37(5):144, 1996. Abstracts of 1996 American Epilepsy Society Annual Meeting.
- [34] P.J. Franaszczuk, G.K. Bergey, and P.J. Durka. Time-frequency analysis of mesial temporal lobe seizures using the Matching Pursuit algorithm. *Soc. Neurosci. Abstr.*, 22(1):184, 1996.
- [35] P.J. Franaszczuk, G.K. Bergey, P.J. Durka, and H.M. Eisenberg. Time-frequency analysis using the Matching Pursuit algorithm applied to seizures originating from the mesial temporal lobe. *Electroencephalogr. Clin. Neurophysiol*, 106:513–521, 1998.
- [36] F.A. Gibbs and E.L. Gibbs. *Atlas of Electroencephalography*. Addison Wesley Press, Cambridge, 2nd edn. edition, 1950.
- [37] D. Golomb, X.-J. Wang, and J. Rinzel. Synchronization properties of spindle oscillation in a thalamic reticular nucleus model. *Journal of Neurophysiology*, 72(3):1109–1126, 1994.
- [38] D. Golomb, X.-J. Wang, and J. Rinzel. Propagation of spindle waves in a thalamic slice model. *Journal of Neurophysiology*, 75(2):750–769, 1996.

- [39] M. Guazelli, I. Feinberg, M. Aminoff, G. Fein, T.C. Floyd, and C. Maggini. Sleep spindles in normal elderly: Comparison with young adult patterns and relation to nocturnal awakening, cognitive function and brain atrophy. *Electroencephalogr. Clin. Neurophysiol.*, 63:526–539, 1986.
- [40] N. Hagiwara and H. Irisawa. Modulation by intracellular  $Ca^{2+}$  of the hyperpolarization activated inward current in rabbit single sino-atrial node cells. *J.Physiol.Lond.*, 409:121–141, 1989.
- [41] A.L. Hodgkin and A.F. Huxley. A quantitative description of membrane current and its application to conduction and excitation in nerve. *J. Physiol. Lond.*, 117:500–544, 1952.
- [42] D.H. Hubel and T.N. Wiesel. . *J.Neurophysiol*, 26:994, 1963.
- [43] D.H. Hubel and T.N. Wiesel. . *J.Neurophysiol*, 28a:229, 1965.
- [44] J.R. Hughes. Development of sleep spindles in the first year of life. *Clinical Electroencephalography*, 27(3):107–115, 1996.
- [45] M. Jobert, E. Poiseau, P. Jahing, H. Schluz, and S. Kubicki. Pattern recognition by matched filtering: an analysis of sleep spindle and K-complex density under the influence of lormetazepam and zopiclone. *Neuropsychobiology*, 26:100–107, 1992.
- [46] E.G. Jones. *The Thalamus*. New York: Plenum, 1985.
- [47] E.R. Kandel, J.H. Schwartz, and T.M. Jessell, editors. *Principles of neural science*. Appleton & Lange, 1991.
- [48] M. Von Krosigk, T. Bal, and D.A. McCormick. Cellular mechanisms of a synchronized oscillation in the thalamus. *Science*, 261:361–364, 1993.
- [49] A. Kumar. The complex demodulation method for detection of alpha waves and sleep spindles of the human eeg in real-time. In *Proc. Int. Conf. on Adv. Signal Processing Techn.*, Lausanne, 1975.
- [50] H.P. Landolt, D.J. Dijk, P. Achermann, and A.A. Borbély. Effects of age on the sleep EEG: slow-wave activity and spindle frequency activity in young and middle-aged man. *Brain Research*, 738:205–212, 1996.
- [51] K.H. Lee and D.A McCormick. Abolition of spindle oscillations by serotonin and norepinephrine in the ferret lateral geniculate and perigeniculate nuclei in vitro. *Neuron*, 17:309–321, 1996.

- [52] K.H. Lee and D.A. McCormick. Modulation of spindle oscillations by acetylcholine, cholecystokinin and 1s,3r-acpd in the ferret lateral geniculate and perigeniculate nuclei in vitro. *Neuroscience*, 77(2):335 – 350, 1997.
- [53] J. Majkowski, editor. *Atlas elektroencefalografii*. Państwowy Zakład Wydawnictw Lekarskich, Warszawa, 1991.
- [54] S.G. Mallat and Z. Zhang. Matching pursuit with time-frequency dictionaries. *IEEE Trans. Sign. Process.*, 41:3397–3415, 1993.
- [55] D.A. McCormick. Neurotransmitter actions in the thalamus and cerebral cortex and their role in neuromodulation of thalamocortical activity. *Prog. Neurobiol.*, 12:337 – 388, 1992.
- [56] D.A. McCormick and T. Bal. Sleep and arousal: Thalamocortical mechanisms. *Annu. Rev. Neurosci.*, 20:185–215, 1997.
- [57] D.A. McCormick and J.R. Huguenard. A model of electrophysiological properties of thalamocortical relay neurons. *Journal of Neurophysiology*, 68(4):1384–1400, 1992.
- [58] R.S. Morison and D.L. Bassett. Electrical activity of the thalamus and basal ganglia in decorticate cats. *Journal of Neurophysiology*, 8:309–314, 1945.
- [59] V.B. Mountcastle. . *J.Neurophysiol*, 20:408, 1957.
- [60] P. L. Nunez. *Electric Fields of the Brain: The Neurophysics of EEG*. Oxford University Press, 1985.
- [61] P.L. Nunez. *Neocortical Dynamics and Human EEG Rhythms*. Oxford University Press, 1995.
- [62] D. Paré, M. Steriade, M. Deschênes, and G. Oakson. Physiological properties of anterior thalamic nuclei, a group devoid of inputs from the reticular thalamic nucleus. *Journal of Neurophysiology*, 57:1669–1685, 1987.
- [63] R.D. Pascual-Marqui, D. Lehmann, T. Koenig, K. Kochi, MC. Merlo, D. Hell, and M. Koukkou. Low resolution brain electromagnetic tomography (loreta) functional imaging in acute, neuroleptic-naive, first-episode, productive schizophrenia. *Psychiatry Research.*, 90(3):169–79, 1999.

- [64] J.C. Principe and J.R. Smith. Sleep spindle characteristics as a function of age. *Sleep*, 5:73–84, 1982.
- [65] A. Rechtschaffen and A. Kales, editors. *A manual of standardized terminology, techniques and scoring system for sleep stages in human subjects*. Washington:US Government Printing Office, 1968.
- [66] W. Scheuler, S. Kubicki, G. Scholz, and J. Marquardt. *Sleep 90*, chapter Two different activities in sleep spindle frequency band discrimination based on the topographical distribution of spectral power and coherence., pages 13–16. Pontenagel Press, Bochum, 1990.
- [67] P. Schimicek, J. Zeitlhofer, B. Anderer, and P. Saletu. Automatic sleep spindle detection procedure: aspects of reliability and validity. *Clinical Electroencephalography*, 25(1):26–29, 1994.
- [68] E. De Schutter and J. M. Bower. An active membrane model of the cerebellar Purkinje cell. *Journal of Neurophysiology*, 71(1):374–400, 1994.
- [69] Y. Smith, P. Séguéla, and A. Parent. Distribution of GABA-immunoreactive neurons in the thalamus of the squirrel monkey. *Neuroscience*, 22:579–591, 1987.
- [70] M. Steriade. *Electroencephalography: Basic Principles, Clinical Applications, and related Fields*, chapter Cellular Substrates of Brain Rhythms. William I& Wilkins, 1993.
- [71] M. Steriade and F. Amzica. Coalescence of sleep rhythms and their chronology in corticothalamic networks. *Sleep Res. Online*, 1:1–10, 1998.
- [72] M. Steriade, D. Contreras, and F. Amzica. Synchronized sleep oscillations and their paroxysmal developments. *TINS*, 17(5):199–208, 1994.
- [73] M. Steriade, L. Domich, and G. Oakson M. Deschenes. The deafferented reticular thalamic nucleus generates spindle rhythmicity. *Journal of Neurophysiology*, 57:260–273, 1987.
- [74] M. Steriade, R. Curró Dossi, and A. Nunez. Network modulation of a slow intrinsic oscillation of cat thalamocortical neurons implicated in sleep delta waves: cortically induced synchronization and brainstem cholinergic suppression. *J.Neurosci.*, 11:3200–3217, 1991.
- [75] M. Steriade, D.A. McCormick, and T. Sejnowski. Thalamocortical oscillations in the sleeping and aroused brain. *Science*, 262:679–685, 1993.

- [76] P. Suffczyński, J. P. Pijn, G. Pfurtscheller, and F. H. Lopes da Silva. *Handbook of Electroencephalography and Clinical Neurophysiology*, volume 6 of *Revised Series*, chapter Event-Related Desynchronization. Elsevier Science Ltd, 1999.
- [77] W. Szelenberger, K. J. Blinowska, J. Żygierewicz, P. J. Durka, and W. Androsiuk. High-frequency sleep spindles in primary insomnia. In *XI World Congress of Psychiatry, Abstracts Volume II*, page 113, August 1999.
- [78] W. Szelenberger, P.J. Durka, and K.J. Blinowska. Evaluation of sleep spindles by means of matching pursuit. In *X World Congress of Psychiatry*, Madrid, Aug 1996.
- [79] N. V. Thakor, JM Jr. Ferrero, J. Saiz, B. I.Gramatikov, and JM Sr. Ferrero. Electrophysiologic models of heart cells and cell networks. *IEEE Engineering in Medicine & Biology Magazine.*, 17(5):73–83, 1998.
- [80] J. Villablanca. *Basic Sleep Mechanisms*, chapter Role of the thalamus in sleep control: sleep-wakefulness studies in chronic diencephalic and athalamic cats. Academic Press, New York, 1974.
- [81] C. D. Wagner and P. B.Persson. Chaos in the cardiovascular system: an update. *Cardiovascular Research*, 40(2):257–64, 1998.
- [82] X.-J. Wang and J. Rinzel. Alternating and synchronous rhythms in reciprocally inhibitory model neurons. *Neural Computation*, 4:84–97, 1992.
- [83] X.-J. Wang and J. Rinzel. Spindle rhythmicity in the reticularis thalami nucleus: synchronization among mutually inhibitory neurons. *Neuroscience*, 53:899–904, 1993.
- [84] X.-J. Wang and J. Rinzel. Multiple dynamical modes of thalamic relay neurons: Rhythmic bursting and intermittent phase-locking. *Neuroscience*, 59(1):21–31, 1994.
- [85] X.-J. Wang, J. Rinzel, and M.A. Rogawski. A model of T-type calcium current and the low-threshold spike in thalamic neurons. *J.Neurophysiol*, 66:839–850, 1991.
- [86] A. Wauquier. Aging and changes in phasic events during sleep. *Physiol. Behav.*, 54:803–806, 1993.

- [87] E. Werth, P. Acherman, D.J. Dijk, and A.A. Borbèly. Spindle frequency activity in the sleep EEG: individual differences and topographic distribution. *Electroenceph. clin. Neurophysiol.*, 103:535–542, 1997.
- [88] H.R. Wilson and J.D. Cowan. Excitatory and inhibitory interactions in localized populations of model neurons. *Biophysical Journal*, 12:1–24, 1972.
- [89] L. H. Zetterberg, L. Kristiansson, and K. Mossberg. Performance of a model for a local neuron population. *Biol. Cybernetics*, 31:15–26, 1978.
- [90] L.H. Zetterberger. Stochastic activity in a population of neurons - system analysis approach. Report 153, Inst. Med. Physics TNO, Utrecht 1, 1973.
- [91] J. Żygierewicz. Identyfikacja wrzecion snu w zapisie EEG przy pomocy metody MP. Master’s thesis, Warsaw University, Warszawa, 1995.
- [92] J. Żygierewicz, K. J. Blinowska, P.J. Durka, W. Szelenberger, and S. Niemcewicz. Matching pursuit, a generalization of wavelet analysis: Topographic study of sleep spindles and slow wave activity by matching pursuit. *Brain Topography*, 11(1):78, 1998. 9<sup>th</sup> World Congress of International Soc. For Brain Electromagnetic Topography, New Orleans.
- [93] J. Żygierewicz, K.J. Blinowska, P.J. Durka, W. Szelenberger, Sz. Niemcewicz, and W. Androsiuk. High resolution study of sleep spindles. *Clinical Neurophysiology*, 110:2136–2147, 1999.
- [94] J. Żygierewicz, P. J. Durka, K.J. Blinowska, W. Androsiuk, and S. Niemcewicz. Time-frequency analysis of eeg sleep structures. In *Proceedings of Satell. Symp. of 20th Ann. Intern. Conf. Of IEEE Engn. Medicine, Beijing*, pages 191–192, 1998.
- [95] J. Żygierewicz, E. F. Kelly, K.J. Blinowska, P.J. Durka, and S.E. Folger. Time-frequency analysis of vibrotactile driving responses by Matching Pursuit. *Journal of Neuroscience Methods*, 81:121–129, 1998.
- [96] J. Żygierewicz, M. Skalski, K.J. Blinowska, P.J. Durka, and W. Szelenberger. Topographic characteristics of spindles in young and elderly during overnight sleep. *Electroenceph. Clin. Neurophysiol*, 103:176, July 1997. Special Issue: Abstracts of the 14th International Congress of EEG and Clinical Neurophysiology, Florence, August 24-29.

# List of author's papers

- [1] P.J. Durka, K.J. Blinowska, J. Żygierewicz. "Matching Pursuit — a method of evaluation and parametrisation of non-stationary signals and transients". *Med. & Biol. Eng. & Comput.* 34 Supp.1, 429 – 430, 1996; The 10th Nordic-Baltic Conference on Biomedical Engineering, June 9–13, Tampere, Finland
- [2] T. Paiva, K.J. Blinowska, J. Żygierewicz, M. Kamiński, A. Rosa, E. Guimaraes, "Topographical covariance structure of sleep EEG during stage 2: A comparison between stable and pre REM epochs" — *in Abstracts of 4th European Conference of Engineering and Medicine*, Warszawa, May 25–28, 1997.
- [3] J. Żygierewicz, M. Skalski, K.J. Blinowska, P.J. Durka, W. Szelenberger, "Topographic characteristics of spindles in young and elderly during overnight sleep", *Electroenceph. Clin. Neurophysiol.* 103:176, July 1997. *Special Issue: Abstracts of the 14th International Congress of EEG and Clinical Neurophysiology*, Florence, August 24–29.
- [4] P.J. Durka, D. Ircha, J. Żygierewicz, K.J. Blinowska, "Recent advances in Matching Pursuit representation of brain signals", *in Abstracts of 4th European Conference of Engineering and Medicine*, Warszawa (P. Rabischong, J. Meli and M. Nałęcz, eds.), pp. 105–106, 1997
- [5] W. Androsiuk, P.J. Durka, J. Żygierewicz, "Zastosowanie metody Matching Pursuit do automatycznej detekcji wrzecion snu i fal wolnych", *in abstracts of XXXIX Zjazd Psychiatrów Polskich* (Bydgoszcz–Toruń, 3–6.06.1998), p.5, 1998.
- [6] J. Żygierewicz, D. Ircha, E. F. Kelly, M. Niznikiewicz, K.J. Blinowska, P. J. Durka "Matching Pursuit In ERP Analysis — An Application To Vibrotactile Driving Responses" — *poster P4–30, XIIth International Conference on Event-Related Potentials of the Brain*, Boston Royal Hotel Cambridge, Massachusetts, USA July 19–23, 1998.

- [7] J. Żygierewicz, K.J. Blinowska, P.J. Durka, W. Szelenberger, S. Niemcewicz "Matching Pursuit, a generalization of wavelet analysis: Topographic study of sleep spindles and Slow Wave Activity by Matching Pursuit" *9th World Congress of International Soc. For Brain Electromagnetic Topography*, New Orleans, 1998, *Brain Topography*, 11(1):78, 1998.
- [8] J. Żygierewicz, E.F. Kelly, K.J. Blinowska, P.J. Durka, S. Folger, "Time-frequency analysis of vibrotactile driving responses by Matching Pursuit," *Journal of Neuroscience Methods*, 81:121–129, 1998.
- [9] J. Żygierewicz, P.J. Durka, K.J. Blinowska, W. Androsiuk, S. Niemcewicz "Time-Frequency Analysis of EEG Sleep Structures" *Proceedings of Satell. Symp. of 20th Ann. Intern. Conf. Of IEEE Engn. Medicine*, Beijing, pp. 191–192, 1998
- [10] W. Szelenberger, K. Blinowska, J. Żygierewicz, P. Durka, W. Androsiuk "High-frequency sleep spindles in primary insomnia" *XI World Congress of Psychiatry, Abstracts Volume II*, p. 113, August 1999,
- [11] J. Żygierewicz, K.J. Blinowska, P.J. Durka, W. Szelenberger, Sz. Niemcewicz, W. Androsiuk. "Time-Frequency Analysis of Sleep Spindles" *Abstracts of 5<sup>th</sup> Conference of ESEM, Barcelona*, pp. 161–162, 1999.
- [12] J. Żygierewicz, K.J. Blinowska, P.J. Durka, W. Szelenberger, Sz. Niemcewicz, W. Androsiuk. "High resolution study of sleep spindles" *Clinical Neurophysiology* 110:2136–2147, 1999.
- [13] J. Żygierewicz, P. Suffczyński, K.J. Blinowska. "Model generacji wrzecion snu", *XI Krajowa Konferencja Biocybernetyka i Inżynieria Biomedyczna*, Warszawa, grudzień 1999
- [14] J. Żygierewicz, K.J. Blinowska, P. Suffczyński, "A model of sleep spindle generation" — accepted for *2000 Computational Neuroscience Meeting*, Brugge, Belgium, 16–20 July, 2000